CONSIDERING RISKS IN POWER SYSTEM OPERATION AND THE CONSEQUENCES OF DIFFERENT ACCEPTED RISK LEVELS

REPORT 2017:375

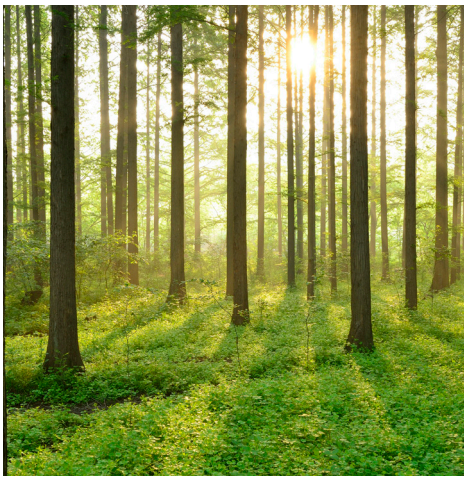

RISK OCH TILLFÖRLITLIGHETSANALYS

Energiforsk

Considering risks in power system operation and the consequences of different accepted risk levels

LARS ABRAHAMSSON

ISBN 978-91-7673-2017-375 | © ENERGIFORSK August 2017

Energiforsk AB | Phone: 08-677 25 30 | E-mail: kontakt@energiforsk.se | www.energiforsk.se

Foreword

The Risk analysis program was in its second phase (2011-2015), when this project initiated. One important issue concerning the power system is the risk of outages in the transmission system. An outage can lead to black-outs which have happened several times in both Sweden and in other systems all over the world. This type of problem causes large costs when it occurs which, fortunately, is not often. But it is also important to notice that one way to minimize these risks is to keep very high margins. This is possible but requires often large investment and maintenance costs since transmission lines are under-used or large amounts of power plants that are seldom used since they are only kept as margins for outages in other power plants. This means that it is important to have a good knowledge of the risk of power system stability problems in order to make a correct balance between risk of black-outs/other severe problems and the costs of continuously keeping too high margins in the operation.

The overall aim of this project is to improve the research in this area and consider that some situations can cause larger problems if they happen compared to other situations, i.e. that some situations have larger risks than others even if they would be equally likely to occur (e.g. 0,001% risk of plant outage and 0,001% risk of stability problem causing black-out). In addition to this, it is important to consider the evolution of the risks with time. As the operation points of the system changes, the risk exposure is consequently altered.

Lars Abrahamsson from the Royal Institute of Technology and later Luleå University of Technology, has been the project manager for the project. He has worked together with Lennart Söder who is professor in Electric Power Systems at KTH and Math Bollen who is Professor in Department of Engineering Sciences and Mathematic, LTU.

This report is summarized in Swedish, see report *2017_ 412 Risker i drift av elkraftsystem*.

Many thanks to the program board for good initiative and support. The program Board consisted of the following persons:

- Jenny Paulinder, Göteborg Energi (chairman)
- Lars Enarsson, Ellevio
- Jonas Alterbäck, Svk
- Hans Andersson, Vattenfall Distribution
- Kenny Granath, Mälarenergi Elnät
- Par-Erik Petrusson, Jämtkraft
- Magnus Brodin, Skellefteå Kraft Elnät
- Ola Löfgren, FIE
- Anders Richert, Elsäkerhetsverket
- Carl Johan Wallnerström, Energimarknadsinspektionen
- Susanne Olausson, Energiforsk (program manager)

The following companies have been involved as stakeholders in the project. A big thanks to all the companies for their valuable contributions.

- Ellevio AB
- Svenska kraftnät,
- Vattenfall Distribution AB,
- Göteborg Energi AB,
- Ellinorr AB,
- Jämtkraft AB,
- Mälarenergi Elnät AB,
- Skellefteå Kraft Elnät AB,
- AB PiteEnergi,
- Energigas Sweden,
- Jönköping Elnät AB,
- Boras Elnät AB,
- Industrial Electric Power Engineering Society, FIE

Stockholm, June 2017

Susanne Olausson
Energiforsk AB
Research area Electrical Networks, Wind and Solar electricity

Contents

List of Tables

List of Figures

Abbreviations

Alternating Current (AC)

Alternating current is a current that in ideal conditions can be described by a sinusoidal function over time. Pages: 27, 50

Automatic Voltage Regulator (AVR)

Automatic voltage regulators are used to control the voltage level outputs of generators. An AVR consists of several components such as diodes, capacitors, resistors and potentiometers or even microcontrollers, all placed on a circuit board. The AVR is mounted near the generator and connected with several wires to measure and adjust the generator. The AVR monitors the output voltage and controls the input voltage for the exciter of the generator. By increasing or decreasing the exciter voltage, the output voltage of the generator increases or decreases accordingly. The AVR calculates how much voltage has to be sent to the exciter numerous times a second, intending to stabilize the output voltage to a predetermined setpoint. Pages: 6, 28, 29, 62, 63, 75–77, 87

Central Processing Unit (CPU)

A central processing unit is is the electronic circuitry within a computer that carries out the instructions of a computer program by performing the basic arithmetic, logical, control and input/output operations specified by the instructions. Page: 118

Corner Point (CP)

Here, a corner point means a point in (net) load space which lies on at least two different surfaces. Pages: 36, 73

Corrective Security Constrained Optimal Power Flow (CSCOPF)

Corrective security constrained optimal power flows is a subset of the SCOPF problems, in which corrective actions (when applicable) are planned for to take action after the occurrence of a contingency. Pages: 52–55

Cumulative Distribution Function (CDF)

Cumulative distribution function, $F_X(x)$, of a real-valued random variable, X, evaluated at x, is the probability that X will take a value less than or equal to x, $P(X \leq x)$. In the case of a continuous distribution, it gives the area under the PDF from minus infinity, $-\infty$, to x. Cumulative distribution functions are also used to specify the distribution of multivariate random variables. Pages: 31, 58, 59, 122

Direct Current (DC)

Direct current is a current that in ideal conditions can be described by a constant function over time. Pages: 27, 50

ElectroMotive Force (EMF)

The electromotive force is the voltage developed by any source of electrical energy such as a battery or dynamo. It is generally defined as the electrical

potential for a source in a circuit. A device that supplies electrical energy is called an electromotive force. EMFs convert chemical, mechanical, and other forms of energy into electrical energy. Pages: 28, 62, 64, 65

Expected Security Cost Optimal Power Flow (ESCOPF)

Expected security cost optimal power flows is a subset of the CSCOPF problems since a distinction is being made between the post-contingency control variables and the pre-contingency control variables. ESCOPFs are more specifically defined than CSCOPFs in the way that that the ESCOPFs include the probabilities of the studied contingencies and the costs of the corrective actions in the model, and the objective function can and should thus consider the expected (operational) costs. Pages: 55, 56

First Order Necessary Condition (FONC)

The first order necessary conditions, or the Karush-Kuhn-Tucker (KKT) conditions, are first-order necessary conditions for a solution in nonlinear programming to be optimal, provided that some regularity conditions are satisfied. Allowing inequality constraints, the KKT approach to nonlinear programming generalizes the method of Lagrange multipliers, which allows only equality constraints. In some cases, the necessary conditions are also sufficient for optimality. In general, the necessary conditions are not sufficient for optimality and additional information is necessary. OPF problems are in exact form and in the general case not convex, so there exist no simple sufficient conditions for them to be solved to global optimality. Pages: 22, 33–35

General Algebraic Modeling System (GAMS)

General algebraic modeling system is one (of a number of existing) algebraic modeling systems particularly designed for optimization, but it can also solve systems of equations. Pages: 64, 74, 107, 116, 121

Generalized Reduced-Gradient (GRG)

The generalized reduced-gradient method is a numerical method for solving optimization problems. Particularly, it is a generalization of the reduced gradient method by allowing nonlinear constraints and arbitrary bounds on the variables. Page: 33

High Voltage Direct Current (HVDC)

A high-voltage, DC electric power transmission system uses direct current for the bulk transmission of electrical power, in contrast to the more common alternating current (AC) systems. Pages: 25, 118

Hopf Bifurcation (HB)

A Hopf bifurcation is a critical point where a system's stability switches and a periodic solution arises. An HB is a local bifurcation in which a fixed point of a dynamical system loses stability, as a pair of complex conjugate eigenvalues (of the linearization around the fixed point) cross the complex plane imaginary axis. Under reasonably generic assumptions

about the dynamical system, a small-amplitude limit cycle branches from the fixed point. HBs are one of the bifurcation types "common" enough in power systems to be considered in various studies. HBs are not considered in this study, but the the developed models are extendable to future HB consideration. Pages: 25, 28–30, 44, 75, 87, 88, 112, 116, 117, 119, 120

Immediate instability point (IIP)

Immediate instability point: sometimes used in the literature as a synonym to SLL. Page: 26

Institute of Electrical and Electronics Engineers (IEEE)

Institute of Electrical and Electronics Engineers: a professional association, formed in 1963 from the amalgamation of the American Institute of Electrical Engineers and the Institute of Radio Engineers. Pages: 8, 22, 64, 69, 74–76, 79, 80, 93, 103, 122

Linear, Interactive, and Discrete Optimizer (LINDO)

LINDO (Linear, interactive, and discrete optimizer) is a solver for linear programming, integer programming, nonlinear programming, stochastic programming and global optimization. Pages: 35, 64, 87, 88, 117

Luleå University of Technology (LTU)

LTU is abbreviated in Swedish from Luleå Tekniska Universitet. Page: 125

MATrix LABoratory (MATLAB)

MATLAB is a multi-paradigm numerical computing environment and fourth-generation programming language. A proprietary programming language developed by MathWorks, MATLAB allows matrix manipulations, plotting of functions and data, implementation of algorithms, creation of user interfaces, and interfacing with programs written in other languages. Page: 88

MegaVoltAmpere (MVA)

Megavoltampere is a unit of apparent power. Pages: 6, 61, 77, 80

MegaWatt (MW)

Megawatt is a unit of (active) power. Page: 61

MegaWatt-hour (MWh)

Megawatthour is a unit of energy. Page: 51

NonLinear Programming (NLP)

Nonlinear programming is a name for optimizing (continuous) nonlinear problems. Page: 64

Operational Limit (OL)

Operational Limit: a point in (net) load space on the border between the allowed operation region and an undesired but not directly unstable operation region. Pages: 19–22, 25, 30, 39, 107–112, 114

Optimal Power Flow (OPF)

Optimal power flows is a group of optimization problems, in which the laws of Kirchhoff are considered as part of the constraints; possible control actions are typically power production, power consumption, activation/deactivation (unit commitment) of units, etc.; and in which the objective function can be to minimize losses, production costs, or something else. Pages: 49, 51, 56, 63, 65, 72, 73, 112

OvereXcitation Limiter (OXL)

The overexcitation limiter in an AVR is a circuit that allows signals below a specified input level to pass unaffected while attenuating the peaks of stronger signals that exceed this threshold. This is used in order to save the generating unit from undesired thermal overheating. Underexcitation limiters also exist. Pages: 28, 29, 63

Power/Voltage-curve (PU-curve)

P denotes active power and U denotes voltage level in this case – it is a common way of illustrating voltage as a function of active power in a node. Pages: 26, 29, 33, 35, 44, 121

PQ (PQ)

A node/bus in which (net) load is described by (net) consumption of active power (P) and reactive power (Q), respectively. Pages: 28, 77

Preventive Security Constrained Optimal Power Flow (PSCOPF)

Preventive security constrained optimal power flows is a subset of the SCOPF problems, in which the operational plan is made such that it will be resilient for any of the imagined possible contingencies that can take place within the planning period. Page: 53

Probabilistic Optimal Power Flow (POPF)

In probabilistic optimal power flows, the stochastic variables representing the uncontrollable (net) loads are modeled by their PDFs. POPFs are thus obviously a subset of OPFs. Pages: 32, 55, 56

Probability Density Function (PDF)

In probability theory, a probability density function is a function, $f_X(x)$, whose value at any point x can be interpreted as providing a relative likelihood of the outcome x of the random variable X. The reader should however note that the absolute likelihood for a continuous random variable X to take on any particular value is 0. In a more precise sense, the PDF is used to specify the probability of the random variable X falling within a particular domain of values, that is $X \in [x_1, x_2], x_1 < x_2, \{x_i\}_{i\in\{1,2\}} \in \mathbb{R}$. This probability is given by the integral of the PDF over that domain. The

probability density function is nonnegative everywhere, and its integral over the entire space is equal to one. Moreover, for a PDF $f_X(x)$, $F_X(x) = \int_{-\infty}^{x} f_x(y)\,dy$, which is the CDF. Pages: 56, 59, 110

PU (PU)

A node/bus in which (net) load is described by (net) consumption of active power (P) and voltage level (U), respectively. Pages: 75–77, 103

Quasi-steady State Simulation (QSS)

Using quasi-steady state simulations for detecting instabilities, c.f. Section 2.3.2.4, can be seen as the opposite of the direct method, c.f. Section 2.3.2.1. Instead of finding a particular operational limit, one studies if the system remains stable in the present operation point also after some contingency by making a dynamic time-domain simulation. The quasi-steady state assumption is that $\dot{y} = 0$, c.f. Eqs. (1) and (2). More concretely that means that it is implicitly assumed that frequency stability will not be an issue after the contingency. The QSS assumption speeds up the simulations significantly. Pages: 33, 35

Royal Institute of Technology (KTH)

KTH is abbreviated in Swedish from Kungliga Tekniska Högskolan. Pages: 18, 19

Saddle Node Bifurcation (SNB)

Saddle node bifurcation: a bifurcation type that in power systems represents voltage and angle instabilities. Pages: 6, 8, 22, 25–29, 34, 35, 39, 42, 44, 59, 64, 66, 71–74, 80, 83, 84, 86–91, 93, 112, 115–117, 119, 120, 125

Security Constrained Optimal Power Flow (SCOPF)

Security constrained optimal power flows is a subset of the OPF problems, in which contingencies are considered in one way or the other in the constraints of the OPF. Pages: 32, 46, 51–56, 60, 112–114

Singularity Induced Bifurcation (SIB)

Singularity induced bifurcations are less common in power systems, but they do occur. In this study they are not explicitly considered, but might be considered in future work. A bit simplified, they occur when one eigenvalue tends to infinity through a rapid sign change while another one tends to zero (also making a sign change). Thus, the system Jacobian seems stable, while the individual eigenvalues are not. Pages: 30, 124, 125

Specially Ordered Set of type 1 (SOS1)

Specially ordered set of type 1 is a variable of special type that can be used for some optimization problem solvers. At most one variable within a Specially Ordered Set of type 1 (SOS1) can take on a non-zero value. That non-zero value is nonnegative. Page: 122

Specially Ordered Set of type 2 (SOS2)

Specially ordered set of type 2 is a variable of special type that can be used for some optimization problem solvers. At most two variables within a Specially Ordered Set of type 2 (SOS2) can take on non-zero values. The two non-zero values have to be in adjacent elements. Page: 107

Stability Limit (SL)

Stability Limit: a point in (net) load space on the border between a stable operation region and an unstable operation region. Pages: 19–22, 25, 27, 60, 72, 87, 107–111, 115

Static VAR (VoltAmpere Reactive) Compensator (SVC)

A Static VAR (voltampere reactive) compensator is a set of electrical devices for providing fast-acting reactive power on high-voltage electricity transmission networks. Unlike a synchronous condenser which is a rotating electrical machine, a static VAR compensator has no significant moving parts (other than internal switchgear). Prior to the invention of the SVC, power factor compensation was the preserve of large rotating machines such as synchronous condensers or switched capacitor banks. Note that there are other, more modern static VAR compensators, such as STATCOM (STATic synchronous COMpensator), so the name is a bit misleading. Page: 59

Stochastic Optimal Power Flow (SOPF)

Stochastic optimal power flow: a term that can have many meanings. In this report, the term is given a special meaning which is explained in Section 2.7.5. With the meaning of the term SOPF used in this report, it is a subset of the category of chance constrained OPFs. Pages: 20–22, 40, 50, 51, 55–60, 64, 107, 108, 111, 113, 114, 118–120, 122, 123, 125

Switching Loadability Limit (SLL)

Switching loadability limit: a point in (net) load space for which a switching (for example of control modes or in terms of system configuration) takes place such that the system ends up "beyond" a bifurcation without passing it. Pages: 19, 25, 26, 28, 29, 33–35, 44, 64, 72, 87, 119, 121, 125

Thyristor Controlled Series Capacitors (TCSC)

Thyristor controlled series capacitors (according to [1] Thyristor Control Series Capacitance) is a technique that is primarily used to reduce transfer reactances, most notably in bulk transmission corridors. The result is a significant increase in the transient and voltage stability in transmission systems. Page: 59

Transmission System Operator (TSO)

A transmission system operator is an entity entrusted with transporting energy in the form of natural gas or electrical power on a national or regional level, using fixed infrastructure. The term is defined by the European Commission. The certification procedure for Transmission System Operators is listed in Article 10 of the Electricity and Gas Directives of

2009. In electrical power business, a TSO is an operator that transmits electrical power from generation plants over the electrical grid to regional or local electricity distribution operators. The United States has similar organizational categories: independent system operator (ISO) and regional transmission organization (RTO). Pages: 25, 32, 46–48, 50, 54, 57, 108, 118, 122, 123

Union for the Coordination of the Transmission of Electricity (UCTE)

Union for the coordination of the transmission of electricity, was one of the predecessors to ENTSO-E (the European Network of Transmission System Operators for Electricity). Nordel was another one of the predecessors to ENTSO-E. ENTSO-E represents 42 electricity TSOs from 35 countries across Europe. Page: 48

Voltage Source Converter (VSC)

A voltage source converter, is a converter type using transistors which, in contrast to thyristors that only can be turned on by control actions, can be both turned on and off by control actions. Thus VSCs have two degrees of freedom instead of one. Therefore, VSCs can be self-commutated. In self-commutated converters, the polarity of the DC voltage is usually fixed, and being smoothed by a large capacitance it is intended to be kept constant. This explains the name "voltage source". Because of the improved controllability, the harmonic performance is improved. Moreover, VSCs don't need to rely on synchronous machines in the AC system for their operation. Page: 118

Abstract

This report presents the results of a postdoctoral project with the same name as the title of the report. Methods and models for identifying and illustrating individual operational limit surfaces have been developed during the project. A discussion about the usability of the surface representations is followed by graphical images justifying the use of such representations. A theoretical and project background is presented. Thereafter possible ways forward are presented. The long-term goal of the work is to be able to optimally do the re-dispatch of the tertiary control given stochastic power production and consumption, where different risk levels will be accepted for different system operational limits depending on their different severities in terms of consequences related to their violation.

1 Introduction

This document is among other things an inclosure with technical details associated to a more brief and less technical report [2] about this project written in Swedish.

1.1 Background to the Project

1.1.1 Project Motivation

With increased shares of uncontrollable renewable power production, such as wind power and solar power, the power production will become harder to predict and control with time. Also, in the future, with so-called *smart homes*, and with hourly measurements of electricity prices and consumed energy, one can also expect consumption to be more price sensitive, and thus more time variant [3, 4]. Moreover, the production units are expected to in the future be larger in numbers, smaller in size, and spatially more outspread. With this combination of changed structure and increased uncertainties, the number of contingency situations of relevance to a system operator increases, since the most important lines, transformers and production units will be different for different production and consumption levels. This increased uncertainty motivates stochastic models of power production and generation, combined with a generalized consideration of component contingencies.

A research project was initiated at Royal Institute of Technology (KTH) to, among other things, address the above mentioned issues. That project developed, among other things, optimization models that minimize the re-dispatch costs of the power system for the coming 15 minutes (in different countries, the time frames are different, confer to Section 2.5). In the optimization, estimations of the stochastic nature of power system loads and generation levels are used. These models minimize the re-dispatch costs under the constraint of keeping the risk levels of violating any of the operational limits of the system below some predefined limits [5–9]. Some of the results and experiences from that research was to a large extent underlying work to and motivation to the initiation of this project.

The idea for this project was that the 15 minute-ahead re-dispatch planning could be done more elaborately by considering the individual risks associated to the different operational limits and their different degrees of severity. That would for example allow accepting higher risks of operation limit violations leading to less severe consequences, and conversely, a more conservative view on risks for violating operation limits causing more severe consequences to the power system and its users, c.f. Section 4.2.2. This idea differs from the approach in the underlying work, where the accepted risk levels are the same – regardless of severity associated to each different (type) of operation limit violation. Risk in this case means the probability of something unwanted to happen – such as: completely losing (black out), harming, or reducing the reliability or the functionality of the power system or components in it. By accepting different risk levels for different levels of severity, the re-dispatch costs can be reduced without necessarily operating the system as a whole in a riskier way.

Differences between this project and the underlying work will be treated further in Section 1.1.2 which follows.

1.1.2 Project differences to the underlying work

At the former Electric Power Systems department at KTH, models describing the envelope of the operation limits of a power system have been developed for the determination of the optimal operation of power systems with large shares of renewable power production, considering stochasticity in production, loads and possible contingencies [5–9]. Further details can be found in summarized form in Sections 2.7.5.2 and 2.7.5.3.

1.1.2.1 Two categories The project of this report was created as a sort of spin-off project from [6] considering things of both academic and industrial interest that could not be prioritized within that project. In this underlying work; (as seems to be common in the literature) all different sorts of operational limits of the power system have been treated as equally risky. In reality, that however is not the case. The operational limits can be subdivided into two main categories:

Category one Operational limits that, with high probability, cause instability to the system, denoted Stability Limits (SLs) for simplicity, confer Section 2.2.1. These can indeed be subdivided into further subcategories, but that is left as a topic for future work.

Category two Secondly, there are the less severe operational limits: For simplicity, let Operational Limit (OL) denote operational limits that are not necessarily stability limits, confer Section 2.2.2. An example of commonly considered and relevant OLs is (long-term thermal) overloading of one or more components (including lines). It follows naturally that also OLs as a category can be further subdivided, just like the SLs can.

The severity of an overloading (such as described for the OL category above) depends on the time of overloading, the degree of overloading, ambient temperature, and possible cooling systems. The consequences of violating an official (often long-term) thermal OL will lie in the continuous range from "nothing", through degraded lifetime and earlier future replacement or repair of equipment, to damaged equipment, or, more likely, to units eventually being disconnected by protection systems. An overloaded line that is not disconnected in time by the protection system will tend to sag because of material heating, and eventually hit/touch an object and likely result in a fault. After the occurrence of a fault, other protection systems might cause an interruption.

A disconnection is a discontinuous event (here, in the context of this report, it would be treated as a contingency induced by a long term OL violation) that, in turn, always leads to a different, and most likely increased, risk level of the system. An example of a significant step increase of the severity level is to suddenly end up beyond an SL in load space with respect to the stable region. Typically in such a case, the SL would be a voltage instability limit (that is, the disconnection would be considered a contingency-induced Switching Loadability Limit (SLL), confer Section 2.2.1.2). It is reasonable to assume that also other SLs could be induced by such a disconnection as well.

1.1.2.2 Accepting Different Risk Levels This project is about how to, in the optimal re-dispatch, be able to distinguish between different sorts of

operational limits, that is between various sorts of OLs or SLs, how to handle them individually, and their respective associated risk levels and degrees of severity.

The models of the underlying work are not considering consequences of violating an operational border. Ideas of how that could be implemented are presented in this report, including the depth of the operational limit violations.

1.2 Project aim and scope

The project has (in alignment with the underlying work) been limited to aiming for work with chance-constrained Stochastic Optimal Power Flows (SOPFs) where the power system has been simplified conceptually and computationally by reducing the model size by working in (net) load space rather than in state space. The operational limit surfaces are simplified as polynomials in load space. It is of importance that these surface approximations can be expressed in comparatively simple and in closed-form, and it is explained why in Sections 2.3 and 2.4. The project is also limited to the usage of general algebraic optimization tools which facilitate usage of a variety of available up-to-date and off-the-shelf solvers.

The work behind this report can be subdivided into three main parts:

- The first part explains the societal, technical, and theoretical backgrounds for the project and the studies made. This part is laying out the foundation needed for choosing and developing the types of methods and models used. In particular the methods and models needed for detecting and properly representing a number of individual OLs and SLs to be used in stochastic optimal re-dispatch tertiary control.

- The second part presents the actual assumptions made, model choices and modifications, and methods used for detecting a number of individual OLs and SLs. The aim was to use a general algebraic optimization tool for that, among other reasons in order to be able to ensure access to a large variety of professional solvers from the market.

- The third part regards the actual numerical studies in finding a number of individual OLs and SLs, approximating them by polynomials in load space, and illustrating them graphically. For the possibility of graphically illustrating them, a test system with three (net) load buses was chosen. Plotting surfaces of more than three dimensions is complicated. The third part also contains comparatively detailed implementable algebraic optimization models, that in different steps goes further from the underlying work towards the goal of managing different accepted risk levels depending on the severities of the OLs and SLs, and on the re-dispatch costs associated in reducing these risks.

1.3 Approach

The approach to address the three main parts of the work introduced in Section 1.2 has been to:

- For the first part, the work regarded studies of literature. Initially the study was focused on the underlying work and their references, but with

time the studies broadened. The studies were needed for obtaining background and related knowledge in order to find feasible ways forward handling OLs and SLs individually with different severities and probabilities (risk levels) – instead of treating every aspect of risky operation in an amalgamated way.

- For the second part, assumptions had to be made, in order to make the power system models simplified, but still useful for the aim of the project. Thereafter, the optimization model for finding and identifying the operational limit surfaces in a systematic and reliable manner was developed. An articulated intention of the author has been to present the models and theory in a more comprehendible way than typically encountered in the literature. This is done in order to broaden the audience for the topic. The models for approximating the OL and SL surfaces were for example presented using a notation that clearly and explicitly writes out all partial derivatives, making the approximation models comprehensible for most engineers.

- The third part contains numerical studies of finding, identifying, approximating, and graphically illustrating the approximations of the closest OL and SL surfaces to a given point of operation. The graphical representation was done in order to facilitate presentation and analysis of the results. The third part also contains a proposed outline for the continuation of the work in regards to applying the developed individual surface approximations to optimal re-dispatch in a chance-constrained SOPF. That outline will be summarized in the listing at the end of this section. Finally, in the third part, based upon the insights given from the literature studies, a proposed improvement in managing margins for conservative solutions was given for usage in future re-dispatch studies.

In regards to the proposed outline in how to use these surfaces with the aim of managing risks for violating different OL and SL surfaces, three mutually independent steps that had to be numbered/named somehow, were proposed in relation to an idealized, but not implementable approach presented in Section 4.2.1. The idealized approach is not implementable, given, among other things, the desired scope of using general algebraic optimization tools, SOPFs, and chance-constraints.

Step 1 After determining one aggregated SL surface and the individual OL surfaces one can assign different allowed maximal accepted probabilities (risk levels) α of violation of these surface limits. Typically, the value of α should be significantly smaller for an SL than the value of α for an OL. A proposal how such an approach could be implemented is presented in Section 4.2.2.

Step 2 Another way forward can be to for SL consider the measures, called corrective actions, needed to be taken to keep the (remains) of the system stable after the occurrence of a certain SL. These actions are associated to different costs. For SLs, discretization of different levels of needed corrective actions is used to estimate the expected monetary costs related to SLs of the ideal model Eq. (212) by weighting the corresponding with

risk levels. For OLs, the monetary costs of different depths of their violations can be estimated – a discretization as well. A proposal how such an approach could be implemented is presented in Section 4.2.3. In the proposed approach, the cases of damaged or disconnected equipment due to an OL has not been addressed, but the model could be extended to handle such by the inclusion of such supplementary "post-contingency" distance functions.

Step 3 A different approach proposal is presented in Section 4.2.4. There, on the other hand, the (net) load space is discretized, and the expected costs for each sample in (net) load space can be computed beforehand (preprocessing), whereas the values of the costs function between the samples needs to be interpolated.

1.4 Results and contributions

The main contributions from this report are:

- The creation of an algebraic general optimization model for finding operational limits (OLs and SLs) in a given power system. A method associated to the model has been presented that can find the $n \leq m$ closest operation limit surfaces in relation to the present operation point of the power system for a given number m. If, after applying the method, it turns out that $n < m$, it is because there are no more than n surfaces to be found. The proposed approach, compared to for example approaches based upon First Order Necessary Conditions (FONCs) or Lagrangian approaches, is less sensitive and dependent on initial values of variables and has a lower probability of finding local optima.

- In the numerical study finding the 7 closest surfaces of the IEEE 9-bus test system [10, Appendix C.1] considering thermal line limits as OLs and one single SNB (because of limiting assumptions) as an SL, it was noticed that for larger distances in load space from the present operation point, the second order Taylor approximation of surfaces might not be accurate enough. It needs however to be considered if, under which circumstances, and to which probability so large changes in net load actually will take place within the intended 15 minute time frame.

- An alternative surface margin approach, for creating a conservative representation of the operation limits, compared to the one proposed in [6], has been proposed, but not investigated further.

- A number of stepwise more advanced and enhanced SOPF model approaches have been proposed for further work.

- Models and theory have been presented with a notation indented to be as simple and comprehendible as possible.

- As a spinoff of the literature review for this project, some ambiguities in terminology in the field were discovered. An effort has been made to straighten out some of them.

1.5 Structure of the report

The report starts with this introductory section, followed by a theoretical background, given in Chapter 2. The content of that chapter is aimed at putting the work of, and the models used for this project in its context for a researcher or an experienced engineer in the field of electric power systems. For people familiar with the theoretical background, that section can be skipped without losing too much information about the particular work done in this project.

In Chapter 3, the assumptions made, the methods developed and used, and the adapted and developed models used for the numerical study are located. The results of the numerical study are presented in Section 4.1. System data and parameters used in the numerical study are gathered in Section 4.1.1.

The study results are presented and analyzed in Chapter 4, which is subdivided into two major parts: Section 4.1 presenting the numerical results obtained from some of the studies done; and Section 4.2 presenting non-numerical findings such as proposing detailed conceptual models and motivated steps how to proceed the work towards a SOPF making optimal re-dispatch considering the varieties of accepted risk levels in a power system. Section 4.2 also includes other findings that open up for new research questions. Section 4.3 discusses some preliminary methodological findings with regards to operational limit surface margins.

Finally, the report ends with a quite lengthy discussion in Chapter 5 and finalizes with a summary of the conclusions, presented pairwise as *findings* and *recommendations* in Chapter 6.

2 Theoretical Background

2.1 Dynamic Power System Modeling

2.1.1 Generally

Let us recall that a dynamically modeled electric power system can be represented by the equations

$$\dot{x} = f(x, y) \tag{1}$$

$$0 = g(x, y) \tag{2}$$

where the vector x represents the set of state variables associated to equipment and units in the power system with dynamic time constants large enough not too be easily neglected, $\dot{x}$ the corresponding time derivative of x, and where the vector y represents state variables associated electric equipment and units with significantly smaller time constants that can be neglected for this type of study. Equipment with very small time constants, can often be modeled statically since the transients they give rise to fade out very fast. Thus, $\dot{y}$ is assumed to be zero in these studies. Analogously, the functions $f(\cdot)$ and $g(\cdot)$ represent the system constraints related to parts of the system with dynamic behaviour, and the parts of the system that for the types of studies made within this project can be modeled statically, respectively. At steady state,

$$\dot{x} = 0, \tag{3}$$

an equality that is assumed to hold also on the border to instability or the other system operational limits sought for. This assumption is valid for slowly varying changes in load, and when post-contingency transients have died out, see Section 3.1.1.

Sometimes, mid-term dynamics are considered, [11], but they are not considered in this report. In such a study, the system could be modeled as

$$\dot{x} = f(x, y, z) \tag{4}$$
$$0 = g(x, y, z) \tag{5}$$
$$\dot{z} = h(x, y, z) \tag{6}$$

where z denoted the set of mid-term dynamic state variables, and $\dot{z}$ its corresponding time derivatives.

2.1.2 Small signal analysis models

For small perturbations in the state variables x and y, the system equations Eq. (1) and Eq. (2) can be represented by a linearization around a point (x_0, y_0) to

$$\begin{aligned} \begin{bmatrix} \dot{\Delta x} \\ 0 \end{bmatrix} &= \begin{bmatrix} f_x(x_0, y_0) & f_y(x_0, y_0) \\ g_x(x_0, y_0) & g_y(x_0, y_0) \end{bmatrix} \begin{bmatrix} \Delta x \\ \Delta y \end{bmatrix} \\ &= [J] \begin{bmatrix} \Delta x \\ \Delta y \end{bmatrix} \end{aligned} \tag{7}$$

in which J denotes the system Jacobian. From Eq. (7) one can derive

$$\begin{aligned} \dot{\Delta x} &= \left(f_x - f_y (g_y)^{-1} g_x \right) \Delta x \\ &= A \Delta x \end{aligned} \tag{8}$$

in which A defines the dynamic Jacobian of the system.

2.1.3 Simplified notation

For the stability analysis to follow in Section 2.2.1, a simplified notation is needed. Let

$$\begin{aligned} \begin{bmatrix} \dot{x} \\ 0 \end{bmatrix} = \begin{bmatrix} f(x, y) \\ g(x, y) \end{bmatrix} = \Bigg\{ z = \begin{bmatrix} x \\ y \end{bmatrix}, F(z) = \begin{bmatrix} f(z) \\ g(z) \end{bmatrix} = \\ = \begin{bmatrix} f(x, y) \\ g(x, y) \end{bmatrix} \Bigg\} = F(z) \end{aligned} \tag{9}$$

and in equilibrium

$$0 = F(z) \tag{10}$$

which in turn can be rewritten as

$$0 = F(z, \lambda) \tag{11}$$

when explicitly considering the net-load "parameters" as variables. Note that net-load λ can in turn be subdivided into

$$\lambda = \begin{bmatrix} u \\ \zeta \end{bmatrix} \tag{12}$$

in which u represent the control variables of the Transmission System Operator (TSO) for the tertiary control, and ζ represent the uncontrollable and stochastically modeled net loads. Note further, that u and ζ might exist in the same power system bus – depending on the coarseness of the power system model.

2.2 Operational Limits

The main focus with this project is to, as mentioned in Section 1.1, study the ability to distinguish between different sorts of undesired operating situations and their severities in optimal power flow models considering the operational risk. As also mentioned in Section 1.1, there are two principal kinds of operation limits:

1. The ones which physically cannot be violated, SLs, confer Section 2.2.1. Technically, SLs are either bifurcation points or switching instabilities. For the latter, the very point of bifurcation is never passed because of operation mode switching.

2. The operational constraints that can be violated for some time and to some extent, but may damage components in the power system eventually.

Examples of the former type are SNBs, Section 2.2.1.1; Hopf Bifurcations (HBs), Section 2.2.1.3; and SLLs, Section 2.2.1.2.

Examples of the latter type are power transfer limits, allowed voltage levels, etc., confer Section 2.2.2.

2.2.1 Stability Limits (SL)

This section treats the mathematical descriptions of a selection of important stability limits, in this report denoted SL, that in contrast to OL will put the power system at risk into more or less immediate (with respect to the time frame this project considers) insecure operation of the power system.

Confusion exists in terminology regarding the descriptions of voltage instabilities. Because of that, the intention in this report is to rather use the term "bifurcation" when applicable. In the case of SLL (confer Section 2.2.1.2), it is for example not possible. The term voltage security occurs also in the literature, even in [6, 12, 13], but that term seems more general than voltage instability. Sometimes, in order to simplify the mathematical models, some implicit hedging takes place when doing voltage security, meaning just imposing some upper and lower bounds on some voltages in the system based upon experience and heuristics. The latter phenomenon in briefly treated in [14, Section 3.2] as belonging to *Class B*.

According to [12, p. 9] and [15] voltage instabilities are load driven. If voltage instabilities are long term [12, p. 8], they are caused by the electrical distances between generation and load, and thus they depend upon the network structure. Short-term voltage instabilities can on the other hand be hard to distinguish from short-term angular instabilities [12, p. 9], but it seems like by definition it is an angle instability if it is generator driven, and a voltage instability if it is load driven. Since many loads, including High Voltage Direct Current (HVDC) connections, are dynamically controlled, it makes the distinction even harder [12, p. 9]. It is also verified that in practice it is very hard to distinguish between voltage and angle instabilities [15].

From the mathematical point of view, a voltage instability can be represented by a bifurcation or by an SLL, that is, the switching (of control modes or in terms of system configuration) such that you end up "beyond" a bifurcation, confer Section 2.2.1.2. Also SLLs are given many different names, often involving the word "bifurcation" which is actually false because the system never passes such a point [16]. The term "limit induced bifurcation" is for example used in [17, 18]. The term "saddle limit-induced bifurcation" (and not "saddle-limit induced bifurcation" as wrongly cited in [16]) is used in [19]. Another synonym for SLL that has been identified in the literature is Immediate instability point (IIP) in [20]. SLLs were called "voltage collapses related to control limits" in [13, Chapter 4.3.5.1]. The term SLL will be used in this report, as well as it has been in [6, 9, 16]. The term "switching loadability limit", without the abbreviation SLL, seems to have been introduced in [21]. Breaking points or switching (control) modes of operation that lead to harmless changes in the operation of the power system are not given any names in this report.

Even in [14] the unclarities of categorizations of stabilities can be found. There, transient instability is discussed as something essentially different than voltage stability. It is an impossible separation of stabilities, since voltage instabilities can be both long-term and short-term [12]. Because of the ambiguity in the literature to classify different stabilities. In this report the terminology is restricted to the technical/mathematical actual properties of the system, and not in investigating what causes the instability in detail, neither where in the system the instability occurs or which variable causes it.

2.2.1.1 SNB

2.2.1.1.1 Generally From bifurcation theory [22], it is known that SNBs occur when the system Jacobian, J, becomes linearly dependent, that is, when (at least) one of its eigenvalues becomes zero.

Typically, and true locally in the neighbourhood of the SNB point (confer the illustration in [12, p. 24] of a set of Power/Voltage-curves (PU-curves); voltage instability has occurred when an increased amount of load for (at least) one location results in an increased voltage for (at least) one node (or the reverse).

Typically, as illustrated on [12, p. 24], increasing the net-load of the power system beyond the SNB point, the system has no longer any feasible long-term steady-state solution. At such a point, load shedding, rapid generation increase, or similar emergency measures need to be taken in order to save the power system from voltage collapse.

In [15] it is shown that SNB points can exist for both high loads and low loads in some systems; a drop in load can also result in the system passing the SNB limit.

It is worth noting here that in [6, p. 107] it was observed that A is the Schur complement [23] of the block g_y in the J matrix,

$$\begin{aligned} A &= J/g_y \\ &= f_x - f_y \left(g_y\right)^{-1} g_x \end{aligned} \tag{13}$$

and for such the determinant property of Schur complements

$$\begin{aligned}\det(J) &= \det(g_y)\det(J/g_y)\\ &= \det(g_y)\det\left(f_x - f_y\left(g_y\right)^{-1}g_x\right)\\ &= \det(g_y)\det(A)\end{aligned} \tag{14}$$

gives that anytime either g_y or A is singular, J will also be singular.

2.2.1.1.2 When g_y is singular Since power in Alternating Current (AC) as well as Direct Current (DC) systems is quadratically dependent on voltage, there are mathematically (and physically) for each possible load flow situation two possible voltages in a node for each level of power consumption. For the simplified case of an AC power system with power source $E\angle 0$, impedance $0 + jX$, load $P + jQ$, and voltage over the load $U\angle\theta$ [12, Chapter 2.3], the voltage over the load is related to the load following

$$U = \sqrt{\frac{E^2}{2} - QX \pm \sqrt{\frac{E^4}{4} - X^2P^2 - XE^2Q}}, \tag{15}$$

and as can be seen, Eq. (15) has two unique solutions except for the case when

$$\frac{E^4}{4} - X^2P^2 - XE^2Q = 0, \tag{16}$$

for which there is only one solution,

$$U = \sqrt{\frac{E^2}{2} - QX}, \tag{17}$$

corresponding to when J is singular. If

$$\frac{E^4}{4} - X^2P^2 - XE^2Q < 0, \tag{18}$$

the system is loaded beyond its capacity and there are no (real) solutions to Eq. (15). The lossy case, with R nonzero would be slightly more complicated, but conceptually the same. When reaching the situation Eq. (16) and the load starts to decrease, there is no longer any guarantee that a reduced active load P will result in an increase voltage U over the load. That is a point beyond the point of voltage instability (or in other words, beyond the SNB point).

Recall the simplified notation of Eq. (10) which will be used when working with SLs. According to [1, 22] the system is at an SNB when Eqs. (19) to (22); that is when the system is in equilibrium, Eq. (19), and the system Jacobian, sometimes denoted J and sometimes F_z throughout this report depending on the context, has a unique zero eigenvalue, and the transversality conditions Eqs. (21) and (22)

$$F = 0 \tag{19}$$

$$vF_z = F_z u = 0 \tag{20}$$

$$vF_\lambda \neq 0 \tag{21}$$

$$vF_{zz}uu \neq 0 \tag{22}$$

hold at that point. Note that uniqueness is not guaranteed by Eq. (20) alone, only existence. In [6, Chapter 4.4] the terms "nondegeneracy" and "transversality" conditions are used, which are defined slightly differently than Eqs. (21) and (22). Since, in [6, Chapter 4.4], another, more compact, notation is used, it is hard to judge by simple visual inspection whether or not these conditions are the same as the transversality conditions of Eqs. (21) and (22). In addition, another slightly different definition of the transversality conditions can be found in [12, equations (5.39c) and (5.39d)], where the counterparts to Eqs. (21) and (22) are of higher dimensions; matrix instead of vector, and 3-tensor instead of scalar, respectively.

In some of the literature, for instance in [1], is it claimed that Eq. (21) guarantees normalization of v. It is clear to the author of this report that it guarantees the avoidance of the trivial solution of $v = 0$, but normalization is not clearly explained or motivated in [1] and logically it should not be the case generally.

Another peculiar claim stated in [1] with a reference to [24] is that systems with constant F_λ, for power systems with constant load models (that is PQ (PQ) load models), are expected to bifurcate through a saddle node (that is a saddle node bifurcation, an SNB, since Eq. (21) is generally satisfied. This is however a bit contradictory to many other studies in the field, for example in [6], where constant load models are used and HBs have been found. This could possibly be an interpretation issue.

It is also said in [1], referring to [22, the 1986 issue of], that "local saddle-node bifurcations are generic, i.e., they are expected to occur in nonlinear systems with one slow varying parameter, as opposed to other types of 'singular' local bifurcations such as transcritical and pitchfork, which require certain specific symmetries in the system to occur".

Lots of information is given by analyzing the SNB point in scrutiny; following [1] the sign and the sizes of Eqs. (21) and (22) will give information about how the system bifurcates locally. This could probably be utilized in future work, confer Chapter 5 in order to estimate the costs of an SNB to occur, depending on what causes it and under which conditions. Also the eigenvectors may give valuable information.

In the literature studied, it seems not to be a focus of the authors to confirm the zero eigenvalue uniqueness. Neither has that been a focus within the work summarized in this report. In practical power system operation, multiple zero eigenvalues of the Jacobian might not occur at all, or at least have extremely low probabilities of occurrence. That could however be a topic to determine through numerical studies and/or further literature read-through and review.

2.2.1.2 SLL When equipment and units in the power system have the ability to switch (for example between different modes of operation), immediate voltage instability may occur. Such immediate voltage instability is here denoted SLL and is dependent on what happens after the switching has taken place.

This kind of mode switching occurs typically when the excitation Electro-Motive Force (EMF), E'_f, has reached its upper limitation voltage and the AVR switches from *AVR control mode* into *OvereXcitation Limiter (OXL) control*

mode. Note that in some cases, under-excitation will also be an important issue. Mathematically, switching from one control mode to another means that Eqs. (1) and (2) may change in dimensions and/or content. In the particular case of a generator i equipped with an AVR, operating in AVR control mode, Eq. (119) constitutes one of the rows of $f(\cdot)$ for that particular generator i. Then, at the same time, Eq. (123) will not be a part of $g(\cdot)$ for that i. The opposite applies when generator i is in OXL mode. Moreover, the variable $E'_{f,i}$ will be one element in x when generator i is in AVR control mode, and one element in y when it is in OXL control mode. In reality, at the very point of switching both constraints would be active.

It may happen that for a certain loading of the system, $\left(P_D^0, Q_D^0\right)$, the eigenvalues of the corresponding system Jacobian, J^0, will not be close to zero. But for a small perturbation in net system load, $\Delta P_D, \Delta Q_D$, one or many units may have switched mode of operation such that the system is now represented by a different set of Eqs. (1) and (2). Also here, for the new load

$$\left(P_D^1, Q_D^1\right) = \left(P_D^0, Q_D^0\right) + \left(\Delta P_D, \Delta Q_D\right) \tag{23}$$

the new system jacobian, J^1, might be far from having zero-valued eigenvalues. This does however not give any information of whether or not the system has entered a voltage-unstable mode.

Simply studying the eigenvalues of J does not give any information whether Eq. (18) is the case or not. Therefore, after a unit in the power system has made a switching between modes of operation, one needs to study whether

$$\frac{\partial U}{\partial P} < 0 \tag{24}$$

or not. If Eq. (24) holds, the unit's switching did not result in an SLL, whereas if Eq. (24) does not hold, the unit switching did result in an SLL. This is explained somewhat differently, but with graphical illustrations in [6].

Remark: As can be seen on the illustration on [12, p. 24], also for the upper part of the PU-curve, there are areas and situations where Eq. (24) doesn't hold, in such cases it would be likely that the study of the second order derivatives would be of use. In [15] it is explained that there might be one SNB limit for high loads, and one for low loads. It is still not clear to the author of this report how in such systems an SLL would be identified after a unit switching. This is out of the scope of this report and left for possible future studies, confer Chapter 5.

2.2.1.3 Hopf Bifurcation (HB) It is also known from bifurcation theory that when the dynamic Jacobian of the system, A, has paired eigenvalues of the kind $0 \pm i \cdot \nu$, the system has reached a HB. The paired imaginary eigenvalues gives rise to an (increasing [11]) oscillatory behaviour of the power system and not an immediate voltage collapse. Thus, one can conclude that HBs are less severe than SNBs. Something to bear in mind for future work, and discussed somewhat further in Chapter 5.

It is stated in [25] "... that HBs ... are not possible in purely ac lossless systems with second-order generator models". And naturally, they cannot exist in systems modelled without dynamics.

Sometimes when only transient bifurcations are of interest, and only the matrix A from Eq. (8) is considered, it is implicitly assumed that the grid itself never reaches a bifurcation, that is, that g_y is nonsingular. In [1] it is stated that in its references [26, 27] (on [28] wrongly crediting L. H. Fink as their author) it should be explained under which conditions one can expect g_y to be nonsingular. That is however left as out of the scope of this project. In such cases however, it is explained [1] that the conditions Eqs. (19) to (22) stated for $F(x, y, \lambda)$ can be applied for $f\left(x, y^{-1}(x, \lambda), \lambda\right)$. As a contrast to the above, in [29] the cases when only g_y singularity is of importance for studying power system bifurcations are treated.

By natural reasons, since the frequency is assumed to be stable, there are no transients for the mathematical model describing the grid, $g(x, y)$, so HB cannot occur because of properties in g_y.

HB can occur also for mid-term dynamics [11], but such are not treated in this report.

2.2.1.4 Other bifurcations occurring in power systems Singularity Induced Bifurcations (SIBs) are explicitly mentioned in [12, Chapter 5.3.2], [13, Appendix 2.B] and in [11]. Simply, they occur when one eigenvalue μ_i of J passes through ± 0 as another eigenvalue μ_j passes through $\pm\infty$ like $c_i \cdot t$ and $\frac{-c_j}{t}$ respectively for a parameter $t : -\epsilon \to \epsilon, \epsilon > 0$, and for constants $\{c_i, c_j\} \in \mathbb{R}^+$, such that the entire system remains stable. The practical impacts of SIB needs to be further determined, confer Chapter 5.

A thorough description of other bifurcations occurring in power systems can be found [26, 27]. Consideration of such may be an issue for future work, confer Chapter 5.

2.2.2 Operational limits that are not necessarily stability limits (OL)

Operational limits that are not necessarily stability limits, OL, can as mentioned in Section 1.1 and in [6] treat different things. Typically thermal overload is of importance.

This report (as [6]) and its numerical study has limited itself to thermal transfer limits of lines. It is known to the author that thermal overloads are actually caused by the currents, I, flowing in the lines. And for comparatively constant voltages, U, the transfer limits in terms of currents, $I^{\max}$ can be modeled as transfer limits in terms of apparent power, $|S|^{\max}$, for which

$$|S|^{\max} = I^{\max} \cdot U. \tag{25}$$

By some reason, maybe under the assumption that the reactive power transfers are small related to the active power transfers, the thermal transfer limits of lines in [6] were modeled as active power transfer limits. In order to align this report with that approach, active power transfer limits have been chosen here as well. Modifying the study to transfer limits in terms of currents I or apparent power $|S|$ would be comparatively straight-forward, but left out of this work. In line with the numerical model of Chapter 3, the active power transfer limit is in the optimization program identifying the various operational limit surfaces defined as Eqs. (140) and (141).

Another example of operational constraints that are not necessarily critical to the operation of the entire system is voltage level operational constraints.

Voltage constraints are set in order to avoid damage of equipment. It is in this project however assumed that tap changers on the distribution-side of the transformers connecting to the different distribution grids will be able to handle such. This project studies phenomena in the transmission grid. Discussions of the validity of assuming constant loads because of tap changers making voltage-sensitive loads on the distribution side see no voltage level changes can be found in [11, Section 4].

2.3 Representing Operation Limits as surfaces in load space

An operational limit surface is defined by the mathematical equations describing it in Section 2.2. As explained in Section 2.3 there are many reasons for working with surface representation in load space in the kinds of problems treated in this project. In the below, ways of finding and identifying these surfaces/limits will be treated, as well as ways of approximating them.

Since some work already has been done treating power system operation in (net) load space with respect to operational limits represented by surfaces, this was a natural step to take. Representing nodes of generation and consumption in the power system as dimensions in (net) load space, the dimension of the problem can be significantly decreased by getting rid of all the state variables. Following the research line of [6], assume that second order polynomials have been chosen to represent the various operation limits in load space. Other alternatives exist, and should not be totally rejected for future studies of the topic. One example of alternatives is using hyper plane approximations instead [30], but then, quite naturally, many more surfaces are needed in order to maintain the same accuracy as given by a second order polynomial. There are always trade-offs regarding computation between how large a mathematical program should be compared to how complex.

At any case, working with second order polynomials, the stochastic nature of the uncontrollable net loads can be modelled and approximated by the use of multivariate Edgeworth expansions [9]. Since these typically approximate Cumulative Distribution Functions (CDFs), the approach can be easily applied to chance-constrained optimization problems. But it also leaves some challenges that need to be addressed; confer Section 4.2.

2.3.1 Identifying the most important point

For the moment, assume i.i.d. (identically and independently distributed) stochastic variables of all parameters in load space. Such an assumption is probably made when no other models are available, and no other information of the system is available. Then, the most likely point in load space to encounter an operation limit is the point in load space with the shortest Euclidean distance from the present (assumed stable) point to the operation limit in question. For simplicity and for illustrative purposes, the Euclidean approach is anyhow used in the model presented in Section 2.3.2 and in the numerical examples of Section 4.1.

In reality however, the case is more complicated. Firstly, the net loads of the stochastic and uncontrollable loads are often dependent (at least correlated). Particularly, weather phenomena affecting production are geographically dependent. Also consumer loads are dependent on each other and with the weather.

Moreover, it is reasonable to assume the expected control actions taken (automatic as well as by the TSO) to be dependent upon these stochasticities.

So the most probable point in load space to be at when encountering an operation limit is not by necessity the closest one in Euclidean terms. Therefore, the concept of *most important point* was introduced in [6] and after some development and improvements ended up in the approach of [9]. In the latter approach, the most important point is estimated in three steps:

- Firstly, a Security Constrained Optimal Power Flow (SCOPF) (see Section 2.7.2) is solved considering the most relevant contingencies and the stochastic variables are assigned their expectation values. The SCOPF solution gives the expectation values u^* of the control variables u.
- Secondly, the control variables are modeled as normal variables (confer Chapter 5) with covariances defined by linearizing u around the SCOPF solution as a function of the stochastic uncontrollable net loads ζ that also seems to be needed to be modeled as normally distributed.
- Thirdly, now that a stochastic approximation model of all of λ (recall that Eqs. (12) and (111)) has been achieved, this joint distribution function of the net load at the end of the control period can be used as *importance function*.

Note that steps 1 and 2 in the above list are describing the Probabilistic Optimal Power Flow (POPF) procedure/method of Section 2.7.4.

Finding the most important point to approximate the surface around will thus be done by replacing Eq. (137) with $f_\Lambda(\lambda)$. Note that here, at least the ζ-part of λ could be possible to be described with its actual stochastic model, and not with the previously used normal distribution approximation of the actual distribution. The reason why all this is done is of course to make sure that the surface approximation of Section 2.3 is made around a point close to where the power system is most likely to be operating within the upcoming 15 minute period of study. Taylor approximations are quite accurate close to the points around which they are approximated, but less so further away from that point. By the same reason, using normal distributions in the POPF part of the procedure would not do much harm. In addition, for higher accuracy, a stochastic variable can be approximated as close as desired to the original distribution by a series of normal distribution approximations.

This approach is attractive as long as the distribution functions of the net loads are unimodal. It is left for future research, Chapter 5, to determine under which conditions that is a valid assumption, and for which practical cases it would not be.

2.3.2 Finding and identifying the surfaces

In [6] and its references a description of methods of identifying the operational limit surfaces can be found. Generally, the methods available are:

- Direct methods
- Optimization methods
- Continuation methods

- Quasi-steady State Simulations (QSSs).

In the following, these methods will be described by a brief theoretical literature review aiming at motivating the approach decided for in this project.

Of the above mentioned four methods, only optimization methods and continuation methods can, in a straight-forward manner, be used to find the closest (or more generalized; the most important) operational limit surface(s). It will be explained why in the below.

2.3.2.1 Direct Methods Direct methods solve a system of equations in such a way that it results in a unique solution. The problem is arranged such that a particular operational limit will be violated, and the right number of system parameters are fixed or interrelated such that the problem gets a unique solution.

One of the main challenges working in this project was the confusion in the use of terminologies. In order to simplify future studies in the field it is important to mention alternative names and denotations of the same concept and phenomenon. A popular synonym to *Direct Methods* is *Point of Collapse methods* [12, 25, 31–33]

One drawback with direct methods is that they are unable to find voltage collapses related to control limits [13, Chapter 4.3.5.1] (what in this report is denoted SLL, Section 2.2.1.2), particularly generators reaching reactive power limits [32] cannot be detected using this technique.

In [13, Chapter 4.3.5.1] it is a bit falsely claimed that using the direct method is the same as minimizing the increase in load such that the power flow constraints are fulfilled [13, equation (4.20)]. It is true that the FONCs of that problem are fulfilled for the solution of the direct method problem, but it it more luck than skill since power flows are strongly nonlinear and non-convex to their nature. Would that optimization actually be done with an appropriate solver, the most likely solution would be the zero solution of load increase, given that the initial load was feasible. In problems like this, in order to achieve optimum, also second order conditions and other measures needs to be taken. That is one of the reasons algebraic modeling and off-the shelf solvers have been used within this project.

2.3.2.2 Continuation Methods Continuation methods is based upon incremental increases of loads in predefined load increase directions. The load is incrementally increased until an operational limit is reached. This approach will lead to a large number of comparatively easily solved load flow problems. The main challenge how to handle load increments close to problem singularities has been solved in [6] and its succeeding work, and before that in among others [12, Chapter 9.3.2]. (Initially) the tangent vector is used to follow the PU-curve. As the solver approaches the bifurcation point, the step size is decreased. At the very point of the bifurcation, the right eigenvector to the system Jacobian and the tangent vector to the PU-curve are equal [29].

The benefit with using continuation methods is that they are both reliable and informative, but they may be very computationally costly [13, Chapter 4.3.5.2].

According to [1], continuation methods are equivalent to solving [13, equation (4.20)] with Generalized Reduced-Gradient (GRG) methods. That can however

not be totally the case, following the similar discussion in the last paragraph of Section 2.3.2.1. If however, the objective function would have opposite sign, it would be closer to the truth, because in [13], λ denotes the scalar parametrization of load increases. That paper, [1] also uses continuation methods.

In [6], continuation methods are used, and load increases in a large number of randomized directions are used in the process of finding the aggregated operational limit surface sought for.

2.3.2.3 Optimization Methods Optimization methods typically aim at finding any, or a specific (kind of) operational limit violation. The objective is for example set to find such a limit violation as close as possible to the present operation point of the system. Distances are typically defined as some norm of the load-change in load space.

Some approaches parameterize the direction in load space of the load increase in order to simplify the problem. If however aiming at finding the generally closest point to a limit surface with that approach, one needs to try a great variation of load increase directions. That approach has similarities with the continuation methods of Section 2.3.2.2.

Another, generalized, but more computationally burdensome approach is to allow a free (or at least freer) direction of load increase in load space. Then only one optimization is needed per surface to be sought for. It is a trade-off between a few "semihard" and vast numbers of very simple problems to solve (note the similarity with the continuation method of Section 2.3.2.2). The latter, generalized, approach is used in this project.

The optimization methods found in the literature are less generalized than the one presented in Section 3.4. In for example [13, equation (4.20)], the change in load is minimized, but no actual constraint is ensuring singularity. There, they rely completely on *only* looking for an SNB, and that the FONCs might lead you there. In [12, Chapters 7 and 9] load maximization is discussed. But that can only be done with the scalar parameterized definition of λ, since for a general load increase direction you might end up infinitely far away from the present operation point. Particularly, in [12, Chapter 9] the load change is maximized with respect to the load flow equations. That method can find an SNB, given that the direction of load increase is predefined in a relevant direction, but the method cannot be used generally to find any operation limit surface of interest.

It is also confirmed in [34] that for unknown directions of load increase, one needs to minimize the distance to the surface when finding it, not maximize it. This is in accordance to the approach used in this report.

A common critique against the classically used optimization methods is that they similarly to the direct methods do not necessarily consider the path from the present load point to the operation surface. That property makes optimization methods faster than continuation methods [12, Chapter 9.3.3]. The critique is base on the risk that control actions along the path might be missed. With the optimization approach proposed in Section 3.4 however, that drawback will be eliminated since the model simultaneously considers all the possible closest operational limits – including those induces by control actions.

Besides the need of identifying SLLs for example, within the scope of this project, there are not obvious needs for having the whole solution path, or

the path of load increase to the operational limit. Without the equilibrium assumption of Section 3.1.1 holding, the solution path indeed becomes relevant, but then the temporal resolution of a typical continuation method would be too coarse anyway. For such cases, other approaches are needed.

According to [12, Chapter 9.3.3], the lagrange multipliers associated to the power system equality constraints at the point of solution of the optimization problem looking for an SNB are also the left eigenvector of the system Jacobian.

Another example of existing optimization methods strongly relying on the FONCs to indicate optimality is [1]. It is clear that the presented approach there relies heavily on local optima where, naturally, initial points for the algorithm will be crucial. With the approach presented in Section 3.4 in this report, initial guesses are far less crucial because of the generalized approach the usage of off-the-shelf solvers. A solver like Linear, Interactive, and Discrete Optimizer (LINDO) [35, 36] is efficient, and typically its local solver reaches the global optimum. Such a solver has however not studied power systems at university level, so it still relies on initial guesses of voltages on the "correct" side of the PU-curve. Also in [1], the optimization model is tailored for a predefined direction of load increase and a scalar parameter representing the load increase, which in turn is maximized for finding the SNB surface. Those models discussed seem however also to be sensitive to initial guesses of variables, and only designed for finding SNBs, and not operation limits in general.

Minimum distances to SNB only is also studied in [34, 37].

2.3.2.4 Quasi-steady state simulation (QSS) Quasi-steady state simulation can be seen as the opposite of the direct method. Instead of finding a particular operational limit, one studies if the system remains stable in the present operation point also after some contingency (e.g. disconnection of some unit or line). The quasi-steady state assumption is in line with Eqs. (1) and (2), [12, Chapter 6.4] by assuming that $\dot{y} = 0$. That means that it is implicitly assumed that frequency stability will not be an issue after the contingency. After that a "common" time-domain simulation takes place. The QSS assumption speeds up the simulations significantly.

2.3.2.5 Other Methods In [13, Chapter 4.3.6] the method of *multiple power flow solutions* is mentioned. It is a bit complicated, and expectedly faster than using the continuation method, but continuation methods better take into account where in load space you started, and the direction in which you are going. Therefore, they cannot consider system control limits (that is SLL). In general, the method seems very approximative, but fast, and maybe necessary for computers of older times, or for very detailed models of large systems.

2.3.3 Approximating the surfaces

For each operational limit point found using the methods presented in Section 3.4, a second order approximation to the operation limit surface has be done according to theory presented in [6]. It is done slightly differently depending on the kind of operation limit being approximated.

This Chapter is a summary of how the surface approximations used for the numerical example in Section 4.1. Surface types not considered in Section 3.4

and its corresponding numerical results of Section 4.1 are omitted from this summary.

2.3.3.1 Introduction In this section, it is assumed that the surface has been found, and also the point on it, denoted λ_c, around which the approximation will be done. The descriptions are very similar to the ones of [6], but with the aim of a less abstract approach making it easier for the intended reader of this report to apprehend.

Another difference to the approach of [6] is that since in this project each surface is intended to be treated individually, the consideration of Corner Points (CPs) is not expected to be an issue.

2.3.3.2 General Theory

2.3.3.2.1 First order approximation of the surface For first order approximations of an operational limit, the tangent plane of the surface expressed in load space needs to be determined. This is done differently for different particular limits, but as soon as the surface normal in load space coordinates, $N(\lambda) = n_\Sigma(\lambda)$, is found, the orthonormal base, C, for the tangent plane can be determined. A first order approximation of each operation limit found, can be done in load space around the found point λ_c, following

$$\Gamma^{\lambda_c^1}(x_c) = \lambda_c + Cx_c, \tag{26}$$

where Γ represents the (hyper)plane in load space that approximates the operational limit, λ_c is the point in load space which the approximation is made around, C is the base matrix to the tangent plane of the operational limit surface at that point, and x_c is any point in $\mathbb{R}^{|\mathbf{\Lambda}|-1}$ (representing points in the tangent plane of the surface). An illustration of a 1^{st} order surface approximation can be found in Fig. 1.

The boldfaced $\mathbf{\Lambda}$ used in the paragraph above denotes the set of of net-load buses which has the cardinality $|\mathbf{\Lambda}| = |\mathbf{L}| + |\mathbf{G} \setminus s|$ since, as can be seen in Eqs. (124), (125), (130) and (131), the controlled generation and the uncontrolled (net-)consumption are modelled differently.

2.3.3.2.2 Second order approximation of the surface For second order approximations of an operational limit, the curvature of the surface expressed in load space needs to be determined. Adapting to the notation of [6], let Σ_{x_c} be a surface in $\mathbb{R}^{|\mathbf{\Lambda}|}$, which approximation is denoted Γ_{x_c}. Then, denote the normal to this surface, at the point λ_c, $n_\Sigma(\lambda_c)$. Then the tangent hyperplane is denoted $T_\lambda\Sigma$, and the orthonormal base matrix C of $T_\lambda\Sigma$ consists of $\Lambda - 1 = |\mathbf{\Lambda}| - 1$ unit vectors $u_i, i \in \{1, 2, ..., \Lambda - 1\}$. Then define the mapping N that assigns a unit normal to Σ pointing in the direction away from the stability domain on each point λ on Σ as the *Gauss map*, $N : \Sigma \to \mathbb{S}^{\Lambda-1}$,

$$N(\lambda) = n_\Sigma(\lambda) \in \mathbb{S}^{\Lambda-1}, \forall \lambda \in \Sigma, \tag{27}$$

from which the changes in the normal along the surface can be formalized.

Another mapping, the *Weingarten map* [6], dN_λ at $\lambda \in \Sigma$ is also essential; it is defined as the map from the tangent hyperplane $T_\lambda\Sigma$ to itself, giving the

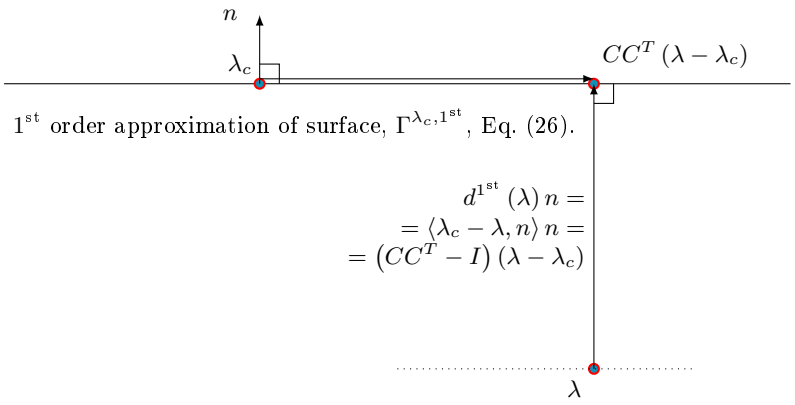

Figure 1: The first order approximation of the surface, and distance from load point λ to hyperplane approximation of surface.

derivative of the Gauss map for changes in load λ along the operational limit surface Σ. Changes in the unit normal vector is by nature changes in directions orthogonal to the normal vector, and therefore the derivative of the normal vector express movements in $T_\lambda\Sigma$. For infinitesimally small movements (load changes) along Σ, these movements will be in the tangent plane of it, $T_\lambda\Sigma$. Thus the mapping is from the tangent plane to itself. Moving in the direction of the normal would imply leaving the surface. The Weingarten map, $dN_\lambda(x_c), \forall x_c \in T_\lambda\Sigma$ can be represented by a $(\mathbf{L}-1)\times(\mathbf{L}-1)$, symmetric, real-valued matrix, dN_λ operating on vectors x_c. The matrix $dN_{\lambda,i,j}$, has by definition columns j representing the derivatives of the Gauss map along the unit basis vectors u_j, whereas the rows i in it represents the changes of the normal in direction u_i for an infinitesimal movement du in the u_j direction along $T_\lambda\Sigma$. Thus, a first order approximation of the normal can be expressed as

$$N(\lambda + du_j) = N(\lambda)_l + C_{l,i} dN_{\lambda,i,j} du_j. \tag{28}$$

for which $l \in \mathbf{\Lambda} = \mathbb{R}^L$, and $\{i,j\} \in T_\lambda\Sigma = \mathbb{R}^{L-1}$.

For a second order approximation, it is needed to define the *second fundamental form*, $\mathrm{II}_\lambda(x_c)$, of Σ at a point λ on Σ, to simply be the negative inner product of the Weingarten map $dN_\lambda x_c$ and the displacement x_c, that is $-\langle dN_\lambda x_c | x_c \rangle$, or simpler $-x_c^T dN_\lambda x_c$. It is worth noting here that the surface Σ is the real surface and Γ is its corresponding approximation.

For simplicity, let the surface Σ be represented by points λ in load space, for which $f(\lambda) = 0$. Then the inwards-pointing unit normal to that surface in load space is $-\frac{\nabla f}{\|\nabla f\|}$, and the Weingarten map is $C^T f_{\lambda,\lambda} C x_c$, where $f_{\lambda,\lambda}$ represents the hessian of f at λ. It can be proven that the second fundamental form for any point of displacement x_c in the tangent plane at λ is 2 times the length of the inner product $\langle \sigma(x_0) - \lambda | N \rangle$, where $\sigma(x_0)$ is a second order Taylor expansion Γ^{λ_c} of the surface Σ at λ. Thus, the geometrical interpretation of the second order fundamental form is that up to a factor of $\frac{1}{2}$ it measures the distance (see Fig. 2) from the tangent plane to the second order Taylor expansion of the surface Σ. In turn, the second order approximation of Σ at λ can be expressed

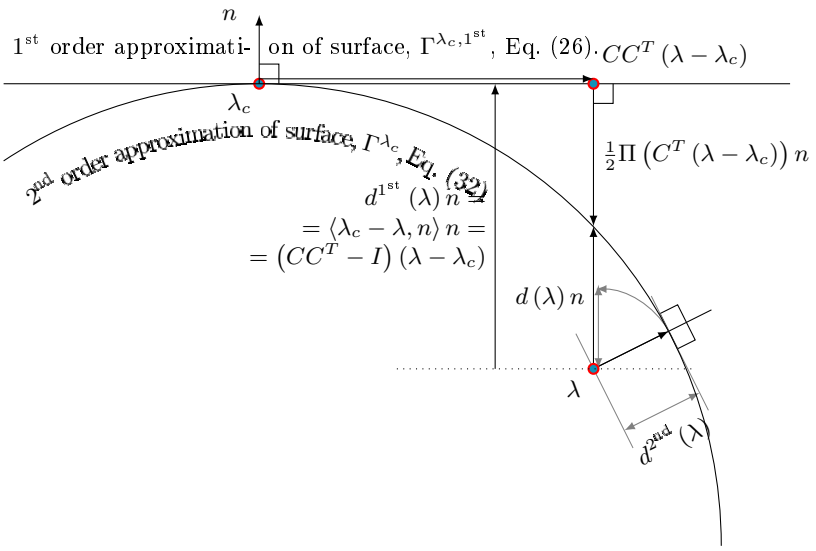

Figure 2: The first and second order approximations of the surface, and three different distance functions from load point λ to approximation of surface.

as

$$\Gamma^{\lambda}(x_c) = \lambda + Cx_c - \frac{1}{2}x_c^T dN_\lambda x_c n_\Sigma(\lambda_c) \tag{29}$$

that is, as a function of x_c in the tangent hyperplane $T_\lambda\Sigma$. In practice, however, it is easier to differentiate N with respect to λ_i, rather than to $x_c \in T_\lambda\Sigma = \mathbb{R}^{\Lambda-1}$, so in this project

$$\Gamma^{\lambda}(x_c) = \lambda + Cx_c - \frac{1}{2}x_c^T C^T \frac{dN_\lambda}{d\lambda} Cx_c n_\Sigma(\lambda_c) \tag{30}$$

will be used. In order to simplify notation, let

$$\Pi_{\lambda_c}(x_c) = -\langle dN_{\lambda_c}(x_c), x_c\rangle = -x_c^T dN_{\lambda_c} x_c = -x_c^T C^T \frac{dN_\lambda}{d\lambda} Cx_c \tag{31}$$

such that Eq. (30) becomes

$$\Gamma^{\lambda_c}(x_c) = \lambda_c + Cx_c + \frac{1}{2}\Pi_{\lambda_c}(x_c)\, n_\Sigma(\lambda_c) \tag{32}$$

for a briefer denotation later on in the report.

2.3.3.3 Thermal line transfer limits

2.3.3.3.1 The surface normal For all kinds of thermal and other operational constraints, the method and the mathematical theory behind is conceptually the same. In this report, however, only thermal operational limits of power transmission lines are considered. And in this report, they are expressed as active power constraints. When such an operational limit has been reached, the constraint Eq. (140) is active, as

$$-G_{i,j}(U_i)^2 - (U_iU_j)\left(-G_{i,j}\cos(\theta_{i,j}) - B_{i,j}\sin(\theta_{i,j})\right) \le P_{i,j}^{\lim} \tag{33}$$

for some specific line $\{i,j\} \in \mathbf{B}$. The normal to the OL surface associated to this thermal limit at the point of net load $\left[\begin{array}{cc} P_{G,g} & P_{D,1,l} \end{array} \right]^T$ in coordinates in active power net-loads in load space is n_i^{OL} as a contrast to the previously used more general notation $n_\Sigma(\lambda)$. The normal n_i^{OL} needs to be determined as a first step towards approximating the operational limit surface. Let us first denote the left-hand side of Eq. (33) as $L^{i,j}$, denoting that the line is limited for power flowing from bus i to bus j. Moreover, let following Section 2.1.3

$$z = \left[\begin{array}{c} x \\ y \end{array} \right] \tag{34}$$

for which $f(x,y)$ and $g(x,y)$ can be simplified to

$$F(z) = \left[\begin{array}{c} f(x,y) \\ g(x,y) \end{array} \right], \tag{35}$$

and let the load vector, λ, represent the active (net-)loads in load space,

$$\lambda = \lambda_i = \lambda_{g,l} = \left[\begin{array}{c} u_g \\ \zeta_l \end{array} \right] = \left[\begin{array}{c} P_{G,g} \\ P_{D,1,l} \end{array} \right], i \in \mathbf{\Lambda}, g \in \mathbf{G}, \text{and } l \in \mathbf{L} \tag{36}$$

for which in turn $f(x,y,\lambda)$ and $g(x,y,\lambda)$ can be simplified to $F(z,\lambda)$. Since the load at the OL thermal limit, $\lambda = \lambda_1$, is not an SNB, the system Jacobian, J, or from now on also F_z, is nonsingular, the implicit function theorem implies that there is a smooth function Φ, defined in a neighbourhood of λ_1 with

$$\Phi(\lambda_1) = z_1 \tag{37}$$

$$\Phi(\lambda) = z \tag{38}$$

$$F(\Phi(\lambda), \lambda) = 0 \tag{39}$$

$$F_z \Phi_\lambda + F_\lambda = 0 \tag{40}$$

for λ in a neighbourhood of λ_1, where more explicitly for this case study

$$F_\lambda = \frac{\partial F}{\partial P_D} \tag{41}$$

$$F_{\lambda,i,j} = 1, \qquad i = 2\mathbf{g}^{\mathrm{ns}} + 2\mathbf{g} + l^j, \qquad j \in \{1,2,...,L\} \tag{42}$$

$$F_{\lambda,i,j} = \frac{Q_{D,0,l^j}}{P_{D,0,l^j}}, i = 2\mathbf{g}^{\mathrm{ns}} + 2\mathbf{g} + \mathbf{b} + l^j, j \in \{1,2,...,L\} \tag{43}$$

for which l^j denotes the jth element in the set $\mathbf{L}$.

By the above reasoning, the (unscaled) normal vector $n^{\mathrm{OL,unsc}}$ of the thermal operation limit Eq. (33) at λ_1 can be obtained by

$$n^{\mathrm{OL,unsc}} = \left. \frac{\partial L^{i,j}(\Phi(\lambda))}{\partial \lambda_i} \right|_{\lambda=\lambda_1} = L_z^{i,j}(\Phi(\lambda_1)) \Phi_\lambda(\lambda_1) \tag{44}$$

in which

$$L_{z_k}^{i,j}(\Phi(\lambda_1)) = \left. \frac{\partial L^{i,j}(z)}{\partial z} \right|_{z=\Phi(\lambda_1)}, \tag{45}$$

in particular

$$L_{z_k}^{i,j} = -U_i U_j (+G_{i,j} \sin(\theta_{i,j}) - B_{i,j} \cos(\theta_{i,j})), k = 2\mathbf{g}^{\mathrm{ns}} + 2\mathbf{g} + i \tag{46}$$

$$L_{z_k}^{i,j} = -U_i U_j \left(-G_{i,j}\sin\left(\theta_{i,j}\right) + B_{i,j}\cos\left(\theta_{i,j}\right)\right), k = 2\mathbf{g}^{\mathrm{ns}} + 2\mathbf{g} + j \tag{47}$$

$$L_{z_k}^{i,j} = -2G_{i,j}U_i - U_j \left(-G_{i,j}\cos\left(\theta_{i,j}\right) - B_{i,j}\sin\left(\theta_{i,j}\right)\right), k = 2\mathbf{g}^{\mathrm{ns}} + \\ + 2\mathbf{g} + \mathbf{b} + i \tag{48}$$

$$L_{z_k}^{i,j} = -U_i \left(-G_{i,j}\cos\left(\theta_{i,j}\right) - B_{i,j}\sin\left(\theta_{i,j}\right)\right), k = 2\mathbf{g}^{\mathrm{ns}} + 2\mathbf{g} + \mathbf{b} + j, \tag{49}$$

and

$$\Phi_\lambda = -F_z^{-1} F_\lambda. \tag{50}$$

Normalizing $n^{\mathrm{OL,unsc}}$ of Eq. (44) such that its 2-norm length is 1, and such that it points in the direction away from the stability domain can be done by

$$b = \left|n^{\mathrm{OL,unsc}}\right|_2 \tag{51}$$

$$c_l = \mathrm{sgn}_l \left(P_{D,1,l} - P_{D,0,l}\right) \tag{52}$$

$$a_l = \frac{c_l}{b} \tag{53}$$

$$n_l^{\mathrm{OL}} = a_l n_l^{\mathrm{OL,unsc}}. \tag{54}$$

2.3.3.3.2 A remark on generalization The observant reader has seen that ever since Eq. (41), λ has been reduced only to the uncontrollable loads ζ_l, and not any longer considering the entire net-load space. That is actually what is done in the numerical example of Section 4.1, since more than three dimensions are hard to visualize in print. In the general case, when the surfaces are not obtained for visual inspection, but rather for later usage in the SOPF (see Section 2.7.5), λ needs also to include u.

When considering also the controllable generation, Eqs. (41) to (43) are not valid any longer. Instead

$$F_\lambda = \begin{bmatrix} \frac{\partial F}{\partial P_G} \\ \frac{\partial F}{\partial P_D} \end{bmatrix} \tag{55}$$

$$F_{\lambda,i,j} = -1, \qquad i = 2\mathbf{g}^{\mathrm{ns}} + 2\mathbf{g} + g^{\mathrm{ns},j}, \qquad j \in \{1, 2, ..., G^{\mathrm{ns}} = |\mathbf{G} \setminus s|\} \tag{56}$$

$$F_{\lambda,i,j} = 1, \qquad i = 2\mathbf{g}^{\mathrm{ns}} + 2\mathbf{g} + l^j, \qquad \begin{matrix} j \in \{G^{\mathrm{ns}} + 1, G^{\mathrm{ns}} + 2, ... \\ ..., G^{\mathrm{ns}} + L = G^{\mathrm{ns}} + |\mathbf{L}| = \Lambda\} \end{matrix} \tag{57}$$

$$F_{\lambda,i,j} = \frac{Q_{D,0,l^j}}{P_{D,0,l^j}}, \; i = 2\mathbf{g}^{\mathrm{ns}} + 2\mathbf{g} + \mathbf{b} + l^j, \; \begin{matrix} j \in \{G^{\mathrm{ns}} + 1, G^{\mathrm{ns}} + 2, ... \\ ..., G^{\mathrm{ns}} + L = G^{\mathrm{ns}} + |\mathbf{L}| = \Lambda\} \end{matrix} \tag{58}$$

for which $g^{\mathrm{ns},j}$ denotes the jth element in the set $\mathbf{G} \setminus s$, and l^j denotes the jth element in the set $\mathbf{L}$. In Eq. (44), L_z would be the same as before, whereas Φ_λ would be different depending on Eq. (50) using the new F_λ of Eq. (55). Moreover, b of Eq. (51) would be recomputed, and

$$c_i = \mathrm{sgn}_i \left(\lambda_{i,1} - \lambda_{i,0}\right) \tag{59}$$

$$a_i = \frac{c_i}{b} \tag{60}$$

$$n_i^{\mathrm{OL}} = a_i n_i^{\mathrm{OL,unsc}}. \tag{61}$$

2.3.3.3.3 The Weingarten Map and its necessary associated components For a second order approximation of the surface, the derivative of the

normal is needed. Differentiating Eq. (54) with respect to λ gives by insertion of Eq. (44)

$$\begin{aligned}\frac{dN}{d\lambda} &= \frac{dn_l^{\mathrm{OL}}}{d\lambda_n} = \frac{d}{d\lambda_n} a_l \left(\frac{\partial L^{i,j}}{\partial z_m} \frac{\partial \Phi_m}{\partial \lambda_l} \right) = \\ &= a_l \left(\frac{\partial^2 L^{i,j}}{\partial z_o \partial z_m} \frac{\partial \Phi_m}{\partial \lambda_l} \frac{\partial \Phi_o}{\partial \lambda_n} + \frac{\partial L^{i,j}}{\partial z_m} \frac{\partial^2 \Phi_m}{\partial \lambda_n \partial \lambda_l} \right) + a_{l,\lambda} L_z^{i,j} \Phi_\lambda\end{aligned} \tag{62}$$

for which the $a_{l,\lambda}$-term is nonzero but can here be unconsidered since the application of $\frac{dN}{d\lambda}$ in this project is Eq. (30), and since $C^T \perp N$, that term will be zeroed out anyway later on in the calculations. The remaining part of $\frac{dN}{d\lambda}$ is denoted $\left(\frac{dN}{d\lambda}\right)_1$. Thus, dN can be computed as

$$dN = C^T \left(\frac{dN}{d\lambda} \right)_1 C = a_l C^T \left(\frac{\partial^2 L^{i,j}}{\partial z_o \partial z_m} \frac{\partial \Phi_m}{\partial \lambda_l} \frac{\partial \Phi_o}{\partial \lambda_n} + \frac{\partial L^{i,j}}{\partial z_m} \frac{\partial^2 \Phi_m}{\partial \lambda_n \partial \lambda_l} \right) C \tag{63}$$

in which $\frac{\partial^2 L^{i,j}}{\partial z_o \partial z_m}$ can be determined as

$$L_{z_o,z_m}^{i,j} = \frac{\partial^2 L^{i,j}}{\partial z_o \partial z_m}, \tag{64}$$

which only nonzero elements are:

$$\begin{aligned}L_{z_o,z_m}^{i,j} &= -U_o U_m \left(+G_{o,m} \cos\left(\theta_{o,m}\right) + B_{o,m} \sin\left(\theta_{o,m}\right) \right), \{o = m\} = \\ &= \{2\mathbf{g}^{\mathrm{ns}} + 2\mathbf{g} + i, 2\mathbf{g}^{\mathrm{ns}} + 2\mathbf{g} + j\}\end{aligned} \tag{65}$$

$$\begin{aligned}L_{z_o,z_m}^{i,j} &= -U_o U_m \left(-G_{o,m} \cos\left(\theta_{o,m}\right) - B_{o,m} \cos\left(\theta_{o,m}\right) \right), \{o, m\} = \\ &= \{(2\mathbf{g}^{\mathrm{ns}} + 2\mathbf{g} + i, 2\mathbf{g}^{\mathrm{ns}} + 2\mathbf{g} + j), (2\mathbf{g}^{\mathrm{ns}} + 2\mathbf{g} + j, 2\mathbf{g}^{\mathrm{ns}} + 2\mathbf{g} \\ &\quad + i)\}\end{aligned} \tag{66}$$

$$\begin{aligned}L_{z_o,z_m}^{i,j} &= -U_o \left(+G_{o,m} \sin\left(\theta_{o,m}\right) - B_{o,m} \cos\left(\theta_{o,m}\right) \right), \{o, m\} = \{(2\mathbf{g}^{\mathrm{ns}} + \\ &\quad + 2\mathbf{g} + i, 2\mathbf{g}^{\mathrm{ns}} + 2\mathbf{g} + \mathbf{b} + j), (2\mathbf{g}^{\mathrm{ns}} + 2\mathbf{g} + \mathbf{b} + j, 2\mathbf{g}^{\mathrm{ns}} + 2\mathbf{g} + i)\}\end{aligned} \tag{67}$$

$$\begin{aligned}L_{z_o,z_m}^{i,j} &= -U_m \left(+G_{o,m} \sin\left(\theta_{o,m}\right) - B_{o,m} \cos\left(\theta_{o,m}\right) \right), \{o, m\} = \{(2\mathbf{g}^{\mathrm{ns}} + \\ &\quad + 2\mathbf{g} + i, 2\mathbf{g}^{\mathrm{ns}} + 2\mathbf{g} + \mathbf{b} + i), (2\mathbf{g}^{\mathrm{ns}} + 2\mathbf{g} + \mathbf{b} + i, 2\mathbf{g}^{\mathrm{ns}} + 2\mathbf{g} + i)\}\end{aligned} \tag{68}$$

$$\begin{aligned}L_{z_o,z_m}^{i,j} &= -U_o \left(-G_{o,m} \sin\left(\theta_{o,m}\right) + B_{o,m} \cos\left(\theta_{o,m}\right) \right), \{o, m\} = \{(2\mathbf{g}^{\mathrm{ns}} + \\ &\quad + 2\mathbf{g} + j, 2\mathbf{g}^{\mathrm{ns}} + 2\mathbf{g} + \mathbf{b} + j), (2\mathbf{g}^{\mathrm{ns}} + 2\mathbf{g} + \mathbf{b} + j, 2\mathbf{g}^{\mathrm{ns}} + 2\mathbf{g} + \\ &\quad + j)\}\end{aligned} \tag{69}$$

$$\begin{aligned}L_{z_o,z_m}^{i,j} &= -U_m \left(-G_{o,m} \sin\left(\theta_{o,m}\right) + B_{o,m} \cos\left(\theta_{o,m}\right) \right), \{o, m\} = \{(2\mathbf{g}^{\mathrm{ns}} + \\ &\quad + 2\mathbf{g} + j, 2\mathbf{g}^{\mathrm{ns}} + 2\mathbf{g} + \mathbf{b} + i), (2\mathbf{g}^{\mathrm{ns}} + 2\mathbf{g} + \mathbf{b} + i, 2\mathbf{g}^{\mathrm{ns}} + 2\mathbf{g} + j)\}\end{aligned} \tag{70}$$

$$\begin{aligned}L_{z_o,z_m}^{i,j} &= +G_{o,m} \cos\left(\theta_{o,m}\right) + B_{o,m} \sin\left(\theta_{o,m}\right), \{o, m\} = \{(2\mathbf{g}^{\mathrm{ns}} + 2\mathbf{g} + \\ &\quad + \mathbf{b} + j, 2\mathbf{g}^{\mathrm{ns}} + 2\mathbf{g} + \mathbf{b} + i), (2\mathbf{g}^{\mathrm{ns}} + 2\mathbf{g} + \mathbf{b} + i, 2\mathbf{g}^{\mathrm{ns}} + 2\mathbf{g} + \\ &\quad \mathbf{b} + j)\}\end{aligned} \tag{71}$$

$$L_{z_o,z_m}^{i,j} = -2G_{o,m}, \{o = m\} = \{2\mathbf{g}^{\mathrm{ns}} + 2\mathbf{g} + \mathbf{b} + i\}, \tag{72}$$

which are computed by by partially differentiating Eqs. (46) to (49); and in which $\frac{\partial^2 \Phi_m}{\partial \lambda_n \lambda_l}$ needs to be determined. That determination is done by differenti-

ating Eq. (40) with respect to λ,

$$\begin{aligned} 0 &= \frac{d}{d\lambda}\left(F_z\Phi_\lambda + F_\lambda\right) = \\ &= \frac{d}{d\lambda}\left(\frac{\partial F_i}{\partial z_m}\frac{\partial \Phi_m}{\partial \lambda_l} + \frac{\partial F_i}{\partial \lambda_l}\right) \\ &= \frac{\partial^2 F_i}{\partial z_o \partial z_m}\frac{\partial \Phi_m}{\partial \lambda_l}\frac{\partial \Phi_o}{\partial \lambda_n} + \frac{\partial F_i}{\partial z_m}\frac{\partial^2 \Phi_m}{\partial \lambda_n \partial \lambda_l} = \\ &= \{\text{to be specific}\} = \\ &= \frac{\partial^2 F_i}{\partial z_o \partial z_{m_2}}\frac{\partial \Phi_{m_2}}{\partial \lambda_l}\frac{\partial \Phi_o}{\partial \lambda_n} + \frac{\partial F_i}{\partial z_{m_1}}\frac{\partial^2 \Phi_{m_1}}{\partial \lambda_n \partial \lambda_l} \end{aligned} \tag{73}$$

in which it may be noted that since the components of $F_{z,\lambda}$ and $F_{\lambda,\lambda}$ are zero for constant load models, they can be ommitted. From Eq. (73),

$$\frac{\partial^2 \Phi_{m_1}}{\partial \lambda_n \partial \lambda_l} = -\left(\frac{\partial F_i}{\partial z_{m_1}}\right)^{-1}\frac{\partial^2 F_i}{\partial z_o \partial z_{m_2}}\frac{\partial \Phi_{m_2}}{\partial \lambda_l}\frac{\partial \Phi_o}{\partial \lambda_n} \tag{74}$$

can be deduced. And then dN in Eq. (63) can be computed by using Eqs. (46) to (50), (53), (65) to (72) and (74).

2.3.3.4 SNB surfaces

2.3.3.4.1 Revisiting the definition of SNB The conditions for an SNB is

$$F\left(z_1, \lambda_1\right) = 0 \tag{75}$$

$$F_z\left(z_1, \lambda_1\right) u = 0 \tag{76}$$

$$v F_z\left(z_1, \lambda_1\right) = 0 \tag{77}$$

$$v F_\lambda\left(z_1, \lambda_1\right) \neq 0 \tag{78}$$

$$\sum_{\forall i,j,k} v_i \frac{\partial^2 F_i}{\partial z_j \partial z_k} u_j u_k \neq 0 \tag{79}$$

where u and v denote the right- and left-hand eigenvectors, respectively. Moreover, (z_1, λ_1) is the point in state and load space where the bifurcation occurs.

2.3.3.4.2 The surface normal The surface normal vector of an SNB surface, Σ^{SNB} for changes in loads $d\lambda$ on Σ^{SNB} can be derived by the following. In order to be on Σ^{SNB}, Eq. (75) must hold. For an infinitesimal change in load, $d\lambda$, such that $\lambda_1 + d\lambda \in \Sigma^{\text{SNB}}$,

$$F\left(z_1 + dz, \lambda_1 + d\lambda\right) = 0 \tag{80}$$

holds, like

$$F_z\left(z_1, \lambda_1\right) dz + F_\lambda\left(z_1, \lambda_1\right) d\lambda = 0 \tag{81}$$

does. Multiplying Eq. (81) by the v vector in Eq. (77) from the left-hand side, considering that also Eq. (77) must hold in order to be on Σ^{SNB}, gives

$$v F_\lambda d\lambda = 0 \tag{82}$$

for which it can be seen that $vF_\lambda\left(z_1,\lambda_1\right)$ constitutes a normal to Σ^{SNB} expressed in load space λ coordinates, since small movements in λ on the surface are tangent to the surface. Thus vF_λ must be normal because of the orthogonality. The unit normal,

$$n^{\mathrm{SNB}}\left(\lambda_1\right)=avF_\lambda \tag{83}$$

is by definition pointing in the direction away from the stability domain by adjusting the sign and the value of the nonzero scalar $a\in\mathbb{R}$.

2.3.3.4.3 The Weingarten Map and its necessary associated components From Eq. (83), the derivative of the normal with respect to λ

$$\frac{dN}{d\lambda}=\frac{dn^{\mathrm{SNB}}}{d\lambda}=\frac{d}{d\lambda}\left(avF_\lambda\right)=a\left(v_\lambda F_\lambda+vF_{\lambda\lambda}+vF_{\lambda z}\Phi_\lambda\right)+a_\lambda vF_\lambda \tag{84}$$

can be obtained, in which $F_{\lambda\lambda}$ and $F_{\lambda z}$ are known to be zero in this report because of the linear dependencies of loads in F, and for which a_λ can be ignored since $C^T\perp vF_\lambda$ (since vF_λ is normal to the tangent plane) and it is rather dN than $\frac{dN}{d\lambda}$ that will be applied here. Thus,

$$dN=C^Tav_\lambda F_\lambda C=aC^Tv_\lambda F_\lambda C \tag{85}$$

in which v_λ is unknown. Differentiating Eq. (77) with respect to λ gives

$$\begin{aligned}v_\lambda F_z+vF_{z\lambda}+vF_{zz}\Phi_\lambda=\left\{F_{z\lambda}=0,\text{ for constant loads}\right\}=\\ v_\lambda F_z+vF_{zz}\Phi_\lambda=0\end{aligned} \tag{86}$$

which, regarding $F_{z\lambda}$ being zero because of the linear dependencies of the load, together with Eq. (40) in Eq. (85) gives

$$\begin{aligned}dN=&\\ &=-aC^Tv_\lambda F_z\Phi_\lambda C\\ &=aC^TvF_{zz}\Phi_\lambda\Phi_\lambda C\\ &=aC^Tv_i\frac{\partial^2F_i}{\partial z_j\partial z_k}\frac{\partial\Phi_j}{\partial\lambda_l}\frac{\partial\Phi_k}{\partial\lambda_m}\end{aligned} \tag{87}$$

for which v and F_{zz} are known, but Φ_λ needs to be determined. Since F_z is singular in $\left(z_1,\lambda_1\right)$, the Eq. (50) approach is not applicable here.

In order to attain an invertible matrix when solving for Φ_λ, Eqs. (76) and (77) are used to obtain

$$vF_zu=0 \tag{88}$$

$$\frac{d}{d\lambda}vF_zu=0 \tag{89}$$

$$\begin{aligned}v\left(F_{zz}\Phi_\lambda+F_{z\lambda}\right)u+v_\lambda F_zv+wF_zu_\lambda=\left\{F_{z\lambda}=0,\text{ for constant loads}\right\}=\\ vF_{zz}\Phi_\lambda u+v_\lambda F_zv+wF_zu_\lambda=\left\{\text{Eqs. (76) and (77)}\right\}=\\ vF_{zz}\Phi_\lambda u=0\end{aligned} \tag{90}$$

from which Eq. (89) together with Eq. (40) makes up the matrix equation

$$\begin{aligned}\begin{bmatrix}F_z\\ vF_{zz}u\end{bmatrix}\Phi_\lambda+\begin{bmatrix}F_\lambda\\ vF_{z\lambda}u\end{bmatrix}=\\ \begin{bmatrix}\frac{\partial F_i}{\partial z_j}\\ v_i\frac{\partial^2F_i}{\partial z_j\partial z_k}u_k\end{bmatrix}\frac{\partial\Phi_j}{\partial\lambda_l}+\begin{bmatrix}\frac{\partial F_i}{\partial\lambda_l}\\ v_i\frac{\partial^2F_i}{\partial z_k\partial\lambda_l}u_k\end{bmatrix}=0\end{aligned} \tag{91}$$

from which Φ_λ can be solved. The added row $vF_{z\lambda}u$ compensates for F_z being of rank (confer to Section 3.4.6.2) $2 \cdot \left(2 \cdot g^b - 1 + b^b\right) - 1$. The observant reader might note that the case of multiple zero eigenvalues is not considered, and therefore out of the scope of this report. Now that Φ_λ has been determined, dN of Eq. (87) can be computed.

2.3.3.5 Discussion of challenges related to Switching and Contingencies

2.3.3.5.1 Switching and SLL surface representation Exactly how SLL surfaces would be treated within the scope of the aims of this project is however still not cleared out and is an issue for future studies, confer Chapter 5. Unlike for example an SNB surface, the SLL surface is not to its nature such that it will be found eventually in almost any load increase direction. As explained in for example [6, Chapter 5.3.5], an SLL surface is only defined for when the switching of the controllers in the power system leads to a harmful point of operation. Typically, the SLL surface is at its endpoint tangential (except in very rare cases [6, Chapter 5.3.5] and [5,8]) in load space to an SNB surface, whereas SLLs intersects other surfaces (such as SLL-SLL, SLL-HB, etc.) transversally [6, Chapter 5.3.5].

2.3.3.5.2 Post-contingency instability surfaces For some combinations of contingencies and operation points, the risk will be that the previously stable and feasible operation point will be lying beyond a bifurcation, and the load flow problem becomes unsolvable. It can be assumed that for such rare cases some automatic control actions would kick in and shed loads, curtail production and/or activate very fast production in the most cost efficient way. In such a case one needs to find the most important point the enables solvability, and from there on, find the further optimal control actions that to a certain level of risk guarantees that solvability will be maintained for the rest of the period. A similar issue to this, but less generalized is discussed in [12, p. 331].

Smaller contingencies could possibly result in a solvable system, but with some loads operating at the "wrong side" of the PU-curve. This would be a contingency that practically results in an SLL-similar situation. This is probably a case that needs to be further studied in the future. In this case, the control actions would probably be to immediately get the system back to the right side of the nose in the PU-curve.

The costs associated to these should needs to somehow be accounted for in the continued research line of this project.

2.4 Distances to surface approximations

Given that the approximations of the operation limit surfaces for the pre-contingency case and all the relevant post-contingency cases are determined, the need for a distance function emerges. The purpose with this *distance function* is to estimate the distance from the current point of operation in load space of the power system to each of the approximations of the operation limit surfaces.

2.4.1 The distance to the first order approximation of the surface

The distance $d^{1^{\text{st}}}(\lambda)$ in Figs. 1 and 2 denotes the distance between the first order approximation (a (hyper)plane) of the surface, evaluated around the load λ_c in load space to an operation point λ in load space. This distance is both the shortest Euclidean distance between load λ and hyperplane $\Gamma^{\lambda_c,1^{\text{st}}}$, and the distance between load λ and $\Gamma^{\lambda_c,1^{\text{st}}}$ in the direction of the surface normal evaluated at λ_c. From Fig. 1

$$d^{1^{\text{st}}}(\lambda) = CC^T(\lambda - \lambda_c) \tag{92}$$

in which Eq. (92) is being derived.

2.4.2 Approximating the distance to the second order approximation of the surface

The distance function presented in this section is as discussed in this report as well as in [9] an approximation of the actual shortest distance. Even though the exact numerical distance measure is sometimes lower and sometimes higher than the actual shortest distance to the surface approximation, it obeys the property that is it negative for points in load space beyond the operational surface limit, and positive on the secure side of the operational limit.

The distance $d(\lambda)$ in Fig. 2 used in [6,9] is developed and used because of its attractive tradeoff between increased accuracy compared to the usage of $d^{1^{\text{st}}}(\lambda)$ of Section 2.4.1 and its relative simplicity compared to the usage of for example $d^{2^{\text{nd}}}(\lambda)$ of Section 2.4.3. The three different distance functions $d^{1^{\text{st}}}(\lambda)$, $d(\lambda)$, and $d^{2^{\text{nd}}}(\lambda)$ are depicted in Fig. 2. The distance function $d(\lambda)$ is defined as

$$\begin{aligned} d(\lambda) &= \left\langle \Gamma\left(C^T(\lambda - \lambda_c)\right) - \lambda, n \right\rangle = \\ &= \left\langle \lambda_c - \lambda + CC^T(\lambda - \lambda_c) + \frac{1}{2}\Pi_{\lambda_c}\left(C^T(\lambda - \lambda_c)\right) n, n \right\rangle = \\ &= \left\{ CC^T x_c \perp n, \langle n, n \rangle = 1 \right\} = \\ &= \langle \lambda_c - \lambda, n \rangle + \frac{1}{2}\Pi_{\lambda_c}\left(C^T(\lambda - \lambda_c)\right), \end{aligned} \tag{93}$$

which gives the signed distance from a point λ in load space in the direction of the normal n evaluated at λ_c to the second order approximation of the surface.

In the example illustrated in Fig. 2, one can see that $d(\lambda)$ is the shortest distance from λ to the first-order approximation of the surface (that is, to the tangent hyperplane) minus the correction term $\frac{1}{2}\Pi_{\lambda_c}\left(C^T(\lambda - \lambda_c)\right)$ representing the distance between the second order approximation of the surface and the first order approximation (the hyper plane) in the negative direction (recall the sign convention of Eq. (31)) of the normal n.

Another way of describing $d(\lambda)$ is that it measures the distance from λ to Γ^{λ_c} in the direction of the normal of Σ at λ_c, n_{λ_c}.

The corrective term $\frac{1}{2}\Pi(x_c)$ is evaluated at the point $x_c = C^T(\lambda - \lambda_c)$ in the tangent hyperplane which is the projection point of λ onto it. This projection point can be expressed in load space coordinates as $CC^T(\lambda - \lambda_c)$. With the definition of Eq. (93), the distance has a sign convention such that points λ in load space within the approximation of the surface results in positive distances, whereas points in load space outside the approximation surface results in negative distances.

2.4.3 The distance to the second order approximation of the surface

It should be noted from Fig. 2 that for second order approximations of the surface and large curvature, and for points λ in the load space, located comparatively far away from λ_c, the distance function $d(\lambda)$ overestimates the distance from λ to the approximation of the surface. Overestimating the distance to the surface might result in putting the system at a higher level of risk than desired.

The illustration in Fig. 2 shows an actual distance $d^{2^{\text{nd}}}(\lambda)$ that in the particular case illustrated is slightly more than half the size of the estimated distance $d(\lambda)$. It is possible, however not clarified, that from a practical point of view a point like λ in Fig. 2 is associated to a comparatively low probability of occurrence, since λ_c is chosen because it is the most probable point $\lambda \in \mathbf{\Lambda}$ on Σ in line with Section 2.3.1.

To compute $d^{2^{\text{nd}}}(\lambda)$ is numerically comparatively simple, but since the distance function in this approach needs to be possible to express algebraically in closed form, its determination is a challenge, but probably not an impossibility. Its determination is out of the scope of this report however. The computational benefits of $d(\lambda)$ compared to $d^{2^{\text{nd}}}(\lambda)$ are treated in [9].

Distances are overestimated also for surfaces with oppposite sign of the curvature. Such λ would however be expected to be even less likely to occur or be planned for than the λ of Fig. 2, since they are located beyond λ_c in terms of the n direction.

For the same sign of the curvature as in Fig. 2, an overestimation of the distance would occur as well for loads λ outside the surface. Overestimating the distance to get back into the feasible/safe region would result in either the TSO activating too many expensive production bids on the tertiary control market, or to excessive load shedding or uncontrollable production curtailment. Last, but not least, the SCOPF program would not "see" that there is a shorter (and probably cheaper) way in load space to bring the system back to the right side of the surface border again.

2.4.4 The distance to the actual surface

The actual surface is plotted in Fig. 3 with, $d^{\text{real}}(\lambda)$ the real distance to the real surface. The purpose with the figure is to illustrate how complex the reality can be.

2.5 Different levels of bulk power system control

2.5.1 Operating Period

In power energy markets, balance responsible players trade power on many time frames [6, Chapter 2.2]. A bit summarized, one can say that before each operating period, consumers and producers agree upon how to keep the energy balance during that operating period. In [6, page 1], referring to [38,39] it is said that the *operating periods* can vary in length for different power systems from 5 minutes up to 1 h. In the Nordic system, Nordel, the operating period is 1 h. Within this operating period, it is the responsibility of the system operator, the TSO, to make sure that power balance is kept in real time. Before each operating period, the balance responsible players can submit regulating bids to the balancing market [6, 40]. These bids can then be activated if and when

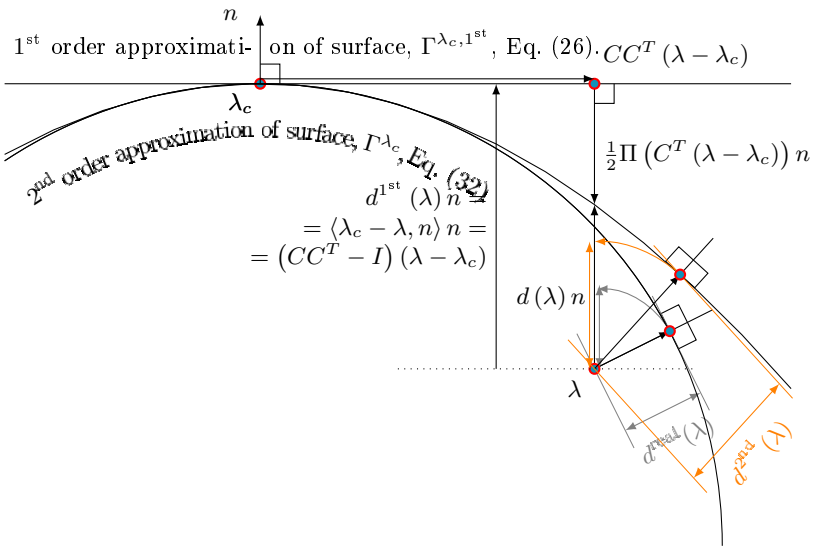

Figure 3: The first and second order approximations of the surface, the actual surface, and four different distance functions from load point λ to approximation of surface.

needed by the TSO in order to keep the power balance within the operating period.

2.5.2 Control actions within the Operating Period

The below terms are often used in power system operation. Since the definitions may vary in different systems and countries, and over time, they are briefly explained in the below.

In France, for example, 3 different time windows of power system control exists; 1, 5, 20 minutes [14]: Within 1 minute (probably primary control), no action is possible, however constant loads might not be a valid assumption. Within 5 minutes, some corrective action such as predefined topology changes (probably secondary control). Within 20 minutes; redispatching of generation, or the starting up fast units can take place (would possibly be categorized as tertiary control) can take place.

Most of the inspiration of this section is taken from [6].

2.5.2.1 Primary Control Primary control is done by a predefined subset of the generators in the power system in order to counteract deviations in frequency after (net) load changes or changes in system configuration. Typically, these generators are paid for doing so. For a measured change in system frequency, a corresponding change in active power production takes place. For a reduction in frequency, the production is increased. Conversely, for an increase in frequency, the production needs to be reduced. This is done until the system frequency ceases to change, that is until the balance between production and consumption is restored; or until the primary control reserves are depleted.

Generators participating in the primary control should leave capacity during normal operation to be able to do the control actions they are obliged to. Primary control is automatized using predefined controls.

Before this takes place, also a physical "primary control" takes place related to the physical inertia in the machinery in the system. The inertial response is strictly speaking not part of the frequency control schemes, but its role is important in the study of frequency stability.

2.5.2.2 Secondary Control Secondary control acts after the primary control in order to restore the frequency to nominal, and to relieve the generators of the primary control reserve back to having the unused amount of capacity they are obliged to. Secondary control is automatized using predefined controls.

Secondary control can also include the objective of restoring power flows on lines which are contracted to lie on a certain level or within certain limits. Also this is different in different countries. If, to which extent, and how the secondary control is affected by increased levels of uncertainty in the system is out of the scope of this report.

2.5.2.3 Tertiary Control Tertiary control is as the name suggests acting after the secondary control in the systems where secondary control is implemented. Tertiary control is not automatized, but regards manual activation of the power reserves by the system operator. Typically it is done on the balancing market, where producers can submit regulating bids. In the Nordic system, the operators can activate them, chosen depending on price and location. A bid activated by the TSO should according to [6], referring to [41, Chapter 4.4], in the Nordic system be executed within 15 minutes. In Union for the Coordination of the Transmission of Electricity (UCTE) the tertiary control is used to relieve and support secondary control reserves.

In Nordel (the Nordic system), tertiary control acts on the same time scale as secondary control in UCTE (within 15 minutes).

The tertiary control will be used throughout this work to refer to the manual activation of balancing bids. The new methods for re-dispatching generation proposed in [6] and its following publications, aims to improve parts of the tertiary control in terms of a more cost-efficient usage of the system having a higher awareness of the risk levels the system is exposed to. In Section 2.7, a review of the operation tools for generation dispatching typically used will be presented, aiming at putting the previous work by [6, 9] and their associated work in a context, and at introducing the needs for the project of this report.

2.6 The Load Margin Concept and its relation to the approach of the project

The term "load margin" is widely used and often refers to the amount of load increase in a certain direction that would cause a voltage collapse [13, Chapter 4.3.2]. That is what you get when you maximize the load in a certain direction under the constraints that the load flow equations and other relevant constraints are satisfied. The term can also be defined as the amount of power transferred between two areas when studying transfer capability between areas. It is straightforward to generalize the idea of load margin to any parameter that

can be varied until the system reaches voltage collapse. The term as such is straightforward, well accepted, and easily understood [13]. Moreover, it can be used for static as well as dynamic load models, and is under certain conditions independent of the details in the dynamic models of the system [13, Chapter 4.3.5].

In order to make a concrete study, one has to specify the concept of the load margin. Here, the load margin is concretized by the distance function Eq. (137) in Section 3.4.2, which measures how much the (net) loads of the system can change and still maintain a secure operation of the power system. In reality, one can only predict and never know for sure where the most critical load changes will take place, and that is why this general approach has been chosen. As explained in Section 1.1 some operation limits are more risky in terms of secure system operation than others, that is why why each operational limit surface is assigned its own associated distance function Eq. (93) within this project. The distance functions depend on the stochastic variables modeling the uncontrollable parts of the net load as well as on the controllable net generation. The proposed distance function approximates the Euclidean distance in load space to its corresponding surface. Different distances (that is, load margins) can thus be computed for each point of system operation and in each possible direction of net load change. And since different directions of net load change will be assigned different probabilities, the stochastic modeling will affect the strategic choices for risk minimization through tertiary control generation re-dispatch.

2.7 Optimal Power Flow with respect to short-term production planning

In this part of the report inspiration, and sometimes quotes from [6,14] has been taken. A historical and theoretical background in optimization-based generation re-dispatching is presented, leading to the motivation of the approach presented in Section 1.3.

Many of the approaches treated in this section and its subsections implicitly assumes quasi-statical load flows for systems in equilibrium before the load change brings the system into an instability. The issue is treated among other assumptions in Section 3.1

In the following, the system operator's perspective is taken. In the context of tertiary control, the control variables will (typically) be the output power of the participating generators and the objective function the overall operating costs associated with the generation redispatch. The parameters are quantities that are considered given before the problem is solved, and can be, for example, the active and reactive power loads.

Note that some consumers can also participate in frequency control schemes by accepting to reduce or increase their consumption on request of the system operator. In this case, these loads are included in the control variables and not in the parameters. The optimal solution will give the feasible optimal redispatch of the generation which minimizes the chosen objective function [6].

From Section 2.7.1 up until Section 2.7.5.1, Optimal Power Flows (OPFs) are treated generally, in which bifurcations rarely are and/or have been considered. The main reasons of that are likely two:

1. It is far more computationally demanding, and was probably not realistic until the mid nineties.
2. It can often be a practical obstacle in finding dynamic models, load models, and line models, accurate enough for the existing real-world systems to study.

Bifurcations and other instabilities were introduced in Section 2.2.1. In Section 2.7.6 some examples from the literature of optimization in power systems considering bifurcations are treated briefly. In Section 2.3, surface representations of operational limits are treated, including how to represent and use them in reduced-size load space. That chapter is followed by Section 2.4 defining the distances from any point λ in load space to each of the corresponding surface representations obtained. These distances are to be used in the SOPF in load space of Section 2.7.5.2.

With that in mind, the reader can easily approach Section 2.7.5.2 in which the usage of SOPF in the style of for example [6, 9] is explained and presented. The intended usage of these SOPF models by the TSO are briefly explained in Section 2.7.5.3. With that theory in mind, the results presented in Section 4.2 should be digestible for the reader.

2.7.1 Classic OPF

The optimization problem of generation dispatching has, as most optimization problems, two main components: an objective function to minimize or maximize (such as the production cost) and some constraints which the solution must satisfy. These constraints include equality constraints (such as AC or DC power flow equations) ensuring that the solution corresponds to a physical equilibrium point (confer Section 3.1.1) of the system, and inequality constraints representing operational limits (such as minimum and maximum generation capacity, maximum active power transfers on certain transmission lines or lower and upper bounds for bus voltages) [6]. An optimal power flow problem can in general have many different objectives, but with respect to short-term production planning, a typical design (slightly modified with respect to [42]) is

$$\min_{u,x} C(x, \lambda, u) \tag{94}$$

$$\text{s.t. } f(x, \lambda, u) = 0 \tag{95}$$

$$g(x, \lambda, u) \leq 0 \tag{96}$$

where x denotes state variables (following the notation in the stability analysis parts of this report x here is equivalent to z there), λ denotes the uncontrollable parameters, and u the control variables (in the dynamic parts of this report λ denotes all net loads in load space, and then λ consists of both ζ denoting the uncontrollable parameters and u the controllable ones). Moreover, C denotes the cost function (typically) related to activation of production bids in the tertiary control, f denotes the power flow equations, and g various operational constraints.

2.7.2 SCOPF (considering the $N-1$ criterion)

When considering post-contingency stability boundaries, post-contingency corrective actions must be taken into account, because they will change the system

state. Not taking into account post-contingency corrective actions would underestimate the loading margins [6, p. 93]. Such automatic control actions include the primary and secondary control, automatic tap-changing transformers, etc.

Grid operation planning with respect to uncertainties is often today, and has commonly been done, using the so-called $N-1$ criterion. Historically, and to some extent still toady, the predictions of future loads have been comparatively accurate, and the power generation has been fully controllable and therefore comparatively predictable. The $N-1$ criterion is a rule saying that the grid should manage (at least) 1 relevant simultaneous contingencies in 1 of the N most important lines, transformers, and production units. In classical power system configurations, the production units are comparatively large in size and small in number. In addition to the comparatively accurate estimates of the future consumption, the most important lines and transformers are as well easily identifiable.

Typically, post-contingency actions (automatized or not) such as load shedding, uncontrollable production curtailment, and rapid increase in power production are costlier per MegaWatt-hour (MWh) than what preventive (pre-contingency) re-dispatch bids are per MWh, but if the probability of an instability to occur is very small it might be economically justified to take that risk.

Quite naturally, a number of issues make the SCOPF much more computationally challenging than the OPF problem: the significantly larger problem size, the (possible) need to handle more discrete variables describing control actions (e.g. the start up of generating units and network switching) and the variety of corrective control strategies in the post-contingency states [14].

An implicit assumption of the conventional SCOPF formulation is that, after the occurrence of a contingency, the system will not lose stability and (with or without post-contingency corrective actions) will reach a viable steady-state (confer Section 3.1.1). The validity of this assumption depends on the system dynamics which are not modeled in the conventional SCOPF. Therefore, the SCOPF problem is often formulated in a conservative way by imposing strong constraints on the amount of usable post-contingency controls and the target feasible region [14]. According to [14], and quite logically, this may lead both to sub-optimality and an undetected risk of instability.

The drawbacks with SCOPF, and the need for other approaches in the future clearly justified by [14]: *While this classical formulation is indeed very useful, it does not cover anymore in a fully satisfactory way the needs encountered in today's operation and operational planning environments. Indeed, due to the increasing penetration of renewable and other uncontrollable generation sources, the set of contingencies should now also incorporate (possibly large) variations in power injections in addition to equipment failures. The operators and planners must anticipate second stage decisions to deal with these "injection pattern contingencies" which span complex continuous spaces and are highly dependent on system conditions and on real-time information gathered about exogenous variables such as weather forecasts and market prices.*. The research line of improved SOPFs in alignment with the description of Section 2.7.5 is clearly valid within this scope.

2.7.2.1 CSCOPF According to [14], and in line with the prerequisites of this project about expecting a more uncertain and risky future, already today, corrective actions are necessary in many places in the world in order to manage the $N-1$ criterion. Contributing reasons behind this trend is in practice pressure from market forces since corrective control is more cost-efficient than preventive scheduling [14]. Not allowing corrective control and still ensuring the fulfillment of the $N-1$ criterion would in practice result also in higher investment costs (and binding of capital) in the grid. Note that also load shedding and production curtailment are parts of the possible corrective control actions in a practical sense.

The corrective SCOPF (in this report, among others) denoted Corrective Security Constrained Optimal Power Flow (CSCOPF), is in [14] denoted the *conventional SCOPF*, and typically looks like

$$\min_{x_k,u_k} C_0\left(x_k,u_k\right), \qquad k\in\{0,1,...,c\} \tag{97}$$

$$f_k\left(x_k,u_k\right)=0, \qquad k\in\{0,1,...,c\} \tag{98}$$

$$g_k\left(x_k,u_k\right)\leq 0, \qquad k\in\{0,1,...,c\} \tag{99}$$

$$f_k^s\left(x_k^s,u_0\right)=0, \qquad k\in\{1,2,...,c\} \tag{100}$$

$$g_k^s\left(x_k^s,u_0\right)\leq 0, \qquad k\in\{1,2,...,c\} \tag{101}$$

$$|u_k-u_0|\leq \hat{\Delta u}_k, \; k\in\{1,2,...,c\} \tag{102}$$

in which the uncontrollable net loads are not explicitly mentioned since they are not variables, where x_k denotes the state variables, and u_k the control variables. Moreover, f_k denotes the load flow equations, g_k the operational limits, and index k the pre- and considered post-contingency situations of which $k=0$ denotes the pre-contingency situation and $k\geq 1$ the considered post-contingency situations. The short-term time-span between the occurrence of a contingency and the moment in time when the control actions are fully executed is not explicitly given in this problem formulation. The time-span is however implicitly considered in how the constant $\hat{\Delta u}_k$, representing the maximal changes in the control variables during this short time-span, for each contingency, is defined. Moreover, f_k^s and g_k^s denote the constraints that needs to be met during this short-term time period. Typically constraints like f_k^s and g_k^s can be fewer than f_k and g_k, and the demands on the system lower than for long-term feasible operation. Similarly, x_k^s denote the post-contingency state variables used in f_k^s and g_k^s during this short-term period of time. Also note that for $k>0$, the constraints f_k and g_k are different, and in alignment with the background for this project, especially some of the operational constraints on g_k might be looser constrained than for $k=0$. In addition, f_k will be redefined for $k>0$ contingent upon how each contingency k affects the system configuration. Finally, c denotes the number of considered contingencies.

Extending the above problem with many small "short-term" states, and even different control actions u_k^s for each such time step will lead to a more realistic but complex problem, confer Section 2.7.7.

Note that the solution to Eqs. (97) to (102) is the solution to a medium-term contingency problem. In the long term, the problem needs to meet up to the same security constraints as in the pre-contingency case.

Typical examples of the operational limits g_k are [14] bounds on the generators' active and reactive power output, ratio of controllable transformers,

reactance of shunts as well as operational limits on the branch currents and voltage magnitudes. In this *conventional SCOPF* model, bifurcations are rarely considered.

In practice and traditionally, the conventional SCOPF has been problematic in the sense that control actions needed to be computed beforehand, for each contingency, based upon prognoses of the expected point of operation [14]. Today, with faster computers, continuously updated stochastic prognoses and automatized decision support as proposed in [6] and further treated in Section 2.7.5.3, many of these drawbacks can however be eliminated. In [14] the intended planning period is of the "day-ahead" type, whereas in this project the aim is within the 15 minutes (in France 20 minutes) ahead time frames of tertiary control.

2.7.2.2 $N-k, k \in \mathbb{N} \setminus \{1\}$ Following the CSCOPF model above, it would be straightforward to consider an $N-k, k>1$ criterion, by for $k=2$ "simply" letting the number of contingencies grow to $c + \frac{c \cdot (c-1)}{2}$. This emphasizes even further why by purely computational reasons one needs to treat many small and combined contingencies differently (confer Section 3.1.2) than with the classical approach.

Other approaches to SCOPF with $N-k$ are indeed possible, for instance involving binary variables to the trade-off of smaller problem sizes. This is the classical trade-off in optimization between size and complexity. Which approach, that in the end, results to be the computationally most efficient one is very case-dependent and out of the scope of this report.

2.7.2.3 PSCOPF The "preventive" SCOPF [43] (denoted Preventive Security Constrained Optimal Power Flow (PSCOPF)) is a particular formulation of the SCOPF that does not consider the possibility of corrective actions in post-contingency states, other than those that take place automatically (e.g. active power of generators participating in frequency control, automatic tap-changers, capacitor and reactor bank switching, secondary voltage control, etc.) [14]. Therefore, in the PSCOPF the values of the non-automatic control variables u are thus the same in all system states. Common sense and inspection of the equations Eqs. (97) to (102) gives that the PSCOPF will result in a higher operation cost than the CSCOPF.

2.7.2.4 SCOPF drawbacks When solving a SCOPF, the uncontrollable loads are given values which, according to the system operator, reflects the operating conditions for which the study is done. Hence, if SCOPF is used for re-dispatching generation within the next fifteen minutes (as for tertiary control), the parameters can be set to their expected values in the next fifteen minutes. These expected values can be obtained by forecasts [6]. There are four main shortcomings associated with the *conventional SCOPF* approaches:

1. **Shortcoming** They do not consider the probabilities of the contingencies to happen [6]. According to [14] it is equivalent to treating all contingencies as equiprobable.

   Analysis *Point 1* means that the optimal solution from a SCOPF is feasible in the sense that no constraints are violated for any contingency,

irrespective of the possibly low probability of which these contingencies happen. That will probably lead to a costlier operation plan than necessary and foreseen. The reader should bear in mind that typically, by Eq. (102) the control actions u_0 are constrained by the control actions u_k even if they are not considered in the cost function Eq. (97).

2. **Shortcoming** They do not consider the costs of the corrective actions. (And they cannot, since this is contingent upon *Point 1.*) In [14] is is claimed that this implies assuming that the likelihood of their use is so small that on the long run their costs will remain negligible. That does however contradict the fact that in the CSCOPF formulation, Eq. (102), the preventive controls are actually contingent upon the planned post-contingency control actions.

   Analysis *Point 2* implies two things: *First*, since the costs for corrective actions are unconsidered, the choice between very expensive fast power generation and load shedding cannot be considered. *Secondly*, it also implies that the tradeoff between surely imposed costs by the preventive part, u_0, of the SCOPF and the to low probabilities imposed costs by the corrective parts $u_k, k \geq 1$ cannot be considered.

3. **Shortcoming** They consider only a small amount of operating conditions since they only consider expectation values of uncontrollable but varying outcomes.

   Analysis *Point 3* means that most of the possible outcomes will not be considered. Moreover, using expectation values may actually for certain (many practical) problems result in infeasible problems. While *point 1* indicates that the system is operated in a too conservative way, the shortcoming of *Point 3* typically underestimates the risk exposure of the system by disregarding the variations in stochastic parameters. It has been shown in [6, Chapter 2.4] that with large amounts of wind power, the net load forecast errors will increase in the sense that the variance of these forecast errors will increase. Hence, the uncertainty faced by the system operator will increase. Following [6], it is stated in [44] that new tools must be developed in order to account for this uncertainty. Today, system operators hedge against risks associated with uncertainty usually by having some operational margins hedging for the most probable changes of uncontrollable net loads. Considering uncertainties directly when computing the optimal decisions would allow a more flexible and efficient use of the system resources.

4. **Shortcoming** They also do not model the social and economic costs of brownouts and blackouts that may result from the failure (e.g. never executed activated bids) of, delayed, or purposely neglected corrective actions.

   Analysis *Point 4* implies that the entire remaining system should be maintained operable at any cost. If considering the brownout/blackout cost, in the for illustrative purposes simplified case of $c = 1$, the TSO has two main choices:

(a) To accept that to a low probability $p_k = p_1 = 1 - p_0$, there will be a brownout/blackout with a high cost. But, on the other hand, to a high probability of p_0, the operation cost will be $C_0(x_0, u_0) \ll C_0(x_0, u_0, x_1, u_1)$ since Eq. (102) does not need to be met here.

(b) To consider the brownout/blackout cost with its associated probability p_1 be too high to be acceptable, so that the cost $C_0(x_0, u_0, x_1, u_1)$ is being preferred.

It will be seen that Expected Security Cost Optimal Power Flow (ESCOPF) of Section 2.7.3 addresses the shortcomings of *Point 1, 2, and 4*, whereas POPF of Section 2.7.4 addresses (to some extent) the shortcoming of *Point 3*. The SOPF modeling approach of Section 2.7.5 is able to address all the *Point 1 – 4* shortcomings presented above.

One alternative way of addressing *Point 3* in the shortcoming list above is to cleverly sample outcomes of stochastic variables associated to the uncontrollable loads. Drawbacks with this is the extreme growth of the problem sizes when considering mutually dependent stochastic distributions with long tails. When assessing the risk of secure operation of the power system, also very unlikely but very severe possible outcomes needs to somehow be considered. This approach is however excluded in this study in line with the approach presented in Section 1.3.

2.7.3 ESCOPF

The CSCOPF problem of Eqs. (97) to (102) can be modified to the ESCOPF [45, 46] problem

$$\min_{x_k, u_k} \sum_{\forall k} p_k C_k(x_k, u_k) \qquad k \in \{0, 1, ..., c\} \tag{103}$$

$$f_k(x_k, u_k) = 0 \qquad k \in \{0, 1, ..., c\} \tag{104}$$

$$g_k(x_k, u_k) \leq 0 \qquad k \in \{0, 1, ..., c\} \tag{105}$$

$$f_k^s(x_k^s, u_0) = 0 \qquad k \in \{1, 2, ..., c\} \tag{106}$$

$$g_k^s(x_k^s, u_0) \leq 0 \qquad k \in \{1, 2, ..., c\} \tag{107}$$

$$|u_k - u_0| \leq \Delta\hat{u}_k \quad k \in \{1, 2, ..., c\} \tag{108}$$

in which p_k would denote the probability for contingency p_k to occur, where p_0 denotes the probability of nothing to happen (that is, staying in the pre-contingency state for the entire period planning for), in order to describe a ESCOPF problem. It is a CSCOPF in the sense that the optimal setting of post-contingency control variables is allowed to be different from that of the pre-contingency control variables. The difference with the classical corrective SCOPF (the CSCOPF) formulation presented above is that the ESCOPF model includes the probabilities of the studied contingencies and the costs of the corrective actions in the objective function which represents the expectation value of the costs within the planning period [6].

Note that (like in the CSCOPF Eq. (102)) the pre- and post-contingency costs are interdependent since the pre-contingency setting of the control variables u_0 cannot be too far from any of the post-contingency settings of the same

variables, $|u_k - u_0|$. If constraints like Eq. (108) are completely physical, they reflect ramp rates of controllable production. If, on the other hand, they try to heuristically impose stability margins, it is another story. Also note, that generally, u_k could also be binary variables indicating reconfigurations, shedding and curtailment that would complicate solvability of the problem significantly.

Hence, ESCOPF addresses the *Point 1, 2* and *Point 4* in the list of shortcomings mentioned in Section 2.7.2.4 by considering the probability associated with all contingencies and the cost of the post-contingency control actions. However, it does not address the third shortcoming [6, Chapter 2.5.4].

2.7.4 POPF

In POPF), the stochastic variables representing the uncontrollable loads are modeled by their probability density functions (Probability Density Functions (PDFs)).

The aim of a POPF is to obtain (estimations of) the PDFs of all variables in the problem [6, 47]. Probabilistic optimal power flows are usually [6] solved in the following way [6, p. 40]:

- First, the optimal settings of the control variables are obtained by solving a classical SCOPF or OPF with, for example, the expected value of the uncertain parameters.
- Then, the system is linearized around this optimal solution in order to express the variables as linear functions of the parameters. This allows the computation of cumulants or moments of the other variables from those of the parameters. Finally, using the cumulants of moments, an approximation of the PDF is calculated, for example using the Gram-Charlier expansion [47–50].

This procedure can be compared to the determination of the importance function presented in [9] and summarized in Section 2.3.1.

By considering the PDFs of the parameters, POPF takes into account the uncertainty which the system is subjected to, thus addressing the third shortcoming mentioned in Section 2.7.2.4.

2.7.5 SOPF

2.7.5.1 Generally The term *stochastic optimal power flow* is used for different meanings and embraces many different sorts of approaches. What in this report is denoted SOPF is actually a subset of the category of chance constrained optimal power flow problems. It will soon be obvious why.

SOPFs address all the four shortcomings of Section 2.7.2.4. While a POPF computes (an approximation of) the PDF of the optimal setting of the control variables in order to assess the effect of uncertainty on this optimal solution, a SOPF includes the uncertainty in the optimization problem itself. When considering the stochastic distributions of the parameters, rather than expectation values or a set of outcomes of them, the constraints must be changed from being deterministic to being probabilistic. Moreover, the probability of violating the deterministic constraints is almost surely nonzero [6]. Probabilistic mean in this context that the focus is set on the probabilities of meeting the constraints in the

optimization problem. Note that there might be alternative approaches, but the alternatives are anyhow unknown to the author and probably mathematically as well as computationally very complicated.

Work on SOPF includes according to [6] the references [49, 51–54]. A (very) general formulation of a SOPF (according to the above definition) problem is

$$\min_{x,u} E\left(C\left(x,\lambda,u\right)\right) \tag{109}$$

$$\text{s.t. } P\left(f_i\left(x,\lambda,u\right)\leq 0\right)\geq 1-\alpha_i \tag{110}$$

where α_i are parameters with small nonnegative numbers representing the maximally allowed probabilities of violating the constraints f_i.

In [51], a SOPF was formulated where the objective function was to maximize the power transfer over a set of buses under the constraints that the probabilities that the transfers across some bottlenecks violate their respective limits are kept low [6]. It can be seen in [6, Chapter 2.5.3], that similar constraints (although deterministic) are taken into account by the Swedish TSO.

2.7.5.2 SOPF in load space In [6] and its successors, the general SOPF approach of Section 2.7.5.1 is concretized in the steps that follows.

First, let the decision variables, u, be only "preventive". Not "preventive" in the sense that after a certain set of bids have been activated at time t_0, no more bids can be activated for the following 15 minutes period, $t^{15\text{ min}}$. Rather "preventive" in the sense that another set of bids can be activated at any time t_1, after solving a new updated optimal dispatch problem slightly before $t_1 > t_0$, where $t_1 < t_0 + t^{15\text{ min}}$ may hold. If the bids activated in t_0 are not yet fully activated, they needs to be specifically considered in the updated problem. Automatic control will work independently of TSO actions/decisions. The updated optimal dispatch problem can typically be solved continuously, or be triggered by, for instance, the occurrence of a contingency, a significantly updated contingency probability forecast, major changes in (net) load, or updated (net) load forecasts. The bids activated at t_1 will however not surely be fully implemented until 15 minutes after activation of the bids, $t_t + t^{15\text{ min}}$ (given the implicit assumption that the bids are executed in time).

The above approach is both reflecting reality, and making the problem to solve mathematically easier, since any stochastic influence is no longer explicitly found in the objective function Eq. (112).

Secondly, assume that the problem has moved over to load space. Thus, state variables are no longer of concern, only control variables u, and the stochastic variables Z with outcomes ζ representing the uncontrollable net loads in the system. To be clear, here

$$\lambda = \left[\begin{array}{c} u \\ \zeta \end{array}\right] \tag{111}$$

in line with the [6, Chapter 8] notation. At this moment the slightly less general SOPF model looks like

$$\min_{u} C\left(u\right) \tag{112}$$

$$\text{s.t. } \sum_{\forall i} p_i P\left(\zeta \notin D_i\left(u\right)\right)\leq \alpha \tag{113}$$

where p_i denotes the probabilities for the pre-contingency and the post-contingency situations, and where $D_i(u)$ denotes the operation domain inside all the operational limits.

With the above approach, balancing bids are activated at minimal cost, the uncertainty in the in the uncontrollable loads are considered in the optimization problem, a certain level of system security considering the aggregated system operation boundary is ensured, and the selected most important contingencies and their probabilities of occurrence are considered.

One contribution with the approach of [6] in contrast to the one of [51] besides working in load space instead of state space is this unified and aggregated boundary. For the aim of this project however, one "step back" will be taken, separating the aggregated boundary again into different ones, since now the different severities of each boundary is to be considered. More of that in Section Section 4.2. Using the word of [6] "... the main difference in our approach is that there is a single constraint, i.e. that the problem is solved so that the probability that any constraint is violated stays below a predefined threshold (as opposed to the probabilities that each constraints is violated stay below a predefined threshold). Thus, the formulation in (8.1) (Author remark: [6, equation (8.1)]) can be used to get an optimal generation re-dispatch which ensures a given overall level of system security ...".

In practice however, that approach needs to be further concretized and less general in order to be implementable. The domain Eq. (113) needs to expressed in closed form in order to useful in an optimisation program formulation. Thus, thirdly, let the domain D_i be described by Eq. (115) in the SOPF formulation

$$\min_{u} C(u) \tag{114}$$

$$\text{s.t.} \sum_{\forall i} p_i P\left(\min_{j \in J_i} d_{i,j}(u, \zeta) < 0\right) \leq \alpha \tag{115}$$

where J_i denotes the set of operation limit surfaces in contingency i, and where d denotes the distance function introduced in Section 2.4.2. In the context of this project, j denotes different surfaces representing different limits with different severities, whereas in the context of [6,9], j represents each of the small surface patches that all together make up the unified operation limit surface D_i.

As explained in Section 2.4.3 and [9], the actual minimum distance can be complicated to determine, thus the approximation of the distance to the second order approximation of the surface is used as d in Eq. (115).

The probability is still not in closed form. That can however be achieved with yet another approximation. In [9] it is explained that Edgeworth expansions can be used for this purpose. For the decision variables u, "normal" Taylor polynomial approximation can be done of the d function, whereas for ζ, Edgeworth is used. The benefit with Edgeworth series is that they represent the CDFs $P(X \leq x)$ for a stochastic variable X. Thus, as soon as the CDF of $d(u, \zeta)$, $P(D \leq d)$ has been determined, Edgeworth is very useful for evaluating a polynomial approximation of that probability. In the case of Eq. (115), $P(D \leq 0)$ will be used.

2.7.5.3 Usage of load space SOPF in practice As indicated in Section 2.7.5.2, the proposed practical usage of SOPF for tertiary control implies

making new "preventive" SOPFs and when needed, also activate new balancing bids as the net loads and the forecasts change during operation of the system.

The separation of the computer work into two *phases* is proposed in [6, p. 141]: *Phase 1* is the most computationally burdensome, and thus most time-consuming, and cannot be expected to be done in real-time operation. In this phase, the second-order approximations of the pre- and post-contingency surfaces are computed. Recall that these approximations are computed around the *most important points*. In *Phase 2*, the SOPF is solved. The SOPF can be solved in real-time, provided that the surfaces used are from *Phase 1*, and thus based upon forecasts that are older and thus less accurate than those present at the time of the SOPF being solved. For this phase, the more recent and accurate forecasts can be used to update the chance-constraints Eq. (115).

Since the time constants of the two phases are different, one can imagine the surface approximations of *Phase 1* to be to be updated by the computer(s) in the background with a periodicity of time T_1, in order to keep the surface approximations as accurate as possible. The SOPFs solved in *Phase 2* will always use the most recent update of the surface approximations available in the database.

On [6, p. 142], two main alternatives of practical usage of the SOPF of *Phase 2* is proposed:

The first alternative is denoted *monitoring and acting*, and the second is denoted *repeatedly acting*. In the first alternative, *monitoring and acting*, by using the most recent forecasts and measurements of net loads, the probability that the system would be operated outside D_i of Eq. (113) can be computed. This can typically be done with short even time intervals, at the most with a few second in between. If the computed probability exceeds α or by risk-averseness an even smaller number $k \cdot \alpha, k \in [0, 1]$, a SOPF can be solved and the resulting solution might lead to a new set of balancing bids being activated. In the second alternative, *repeatedly acting*, a SOPF can be solved (regardless of "needed" or not) with a periodicity of a few minutes (5 minutes is proposed in [6, p. 142]). According to [6, p. 142], [55] states that this approach is used in Texas today, but using deterministic models.

2.7.6 Optimizing power system security deterministically, but considering bifurcations

In order to give a fair picture and background to the field; it should be stated that lots of work has been done maximizing the power system security in various manners considering bifurcations more or less explicitly. For this project however, when stochasticity in uncontrollable net loads are to be considered, that path of research is closed since modeling actual load flow constraints and bifurcation detection constraints considering PDFs or CDFs would be a very complex and nontrivial task, as also explained in Section 2.3. Some examples below:

In [56, 57] the distance to the SNB surface is increased by shunt compensation, in [58] it is done by Static VAR (VoltAmpere Reactive) Compensator (SVC), [1]. System loadability is also increased by optimizing the SVC and Thyristor Controlled Series Capacitors (TCSC) location, dimension, and control in [59, 60].

In [1] itself, the distance to the instability is maximized for a predefined

direction of load increase by optimizing location and sizing of reactive shunt and/or series compensation. Since the aim of study in [1] is optimal grid design, that study considers completely different time scales than this project considers.

2.7.7 Beyond the scope of this project

The methods above, while addressing the shortcomings of SCOPF, give an optimal generation re-dispatch for one point in time only. However, since the system operator is responsible for maintaining the balance between production and consumption within the operating period, it seeks at optimizing power system operation not only at one point in time but throughout the whole operating period (confer Section 2.5.1). Hence, not only the cost of the decisions must be taken into account but also the expected costs of taking these decisions for the rest of the hour.

Decision taken by solving the SOPF problem is only optimal for the point in time it considers, and that the expected costs for the rest of the operating period arising from this decision are not considered. Considering these expected costs would require developing other tools. This is left as future work.

The expected changes in future power systems discussed in Section 1.1 suggest that larger (in theory uncountable) contingency sets should be considered to model the uncertainty between successive decision stages [14]. It is also very likely that a two-stage reduction of the optimization problem will no longer be sufficient. Instead, [14] suggests that one might have to define multistage frameworks, where the couplings between decisions and uncertainties induced by adverse scenarios over longer time horizons could be modeled better. In the end, considering the problem formulation of such studies, the trend leads to two complementary and intertwined directions of research. One regards optimal control problem formulations taking into account the uncertainties affecting power system operation. The other regards planning and decomposing the temporal control horizon and into successive decision making stages. These problems could, again following [14], be addressed in principle using two different frameworks, namely the robust optimal control framework [61] and multistage stochastic programming [62]. That is however out of the scope of this project and left for the future to be considered.

3 Assumptions, and Models Used in this Project

3.1 Main assumptions

3.1.1 Equilibria

The main basic assumption for the detection of the operational limit surfaces is the existence of equilibrium, in mainly three aspects:

1. Equilibrium at the present point of operation (pre-contingency).
2. Equilibrium reached in the post-contingency cases, at least for the cases when the post-contingency equilibrium point after automatic control actions lies within the stable region with respect to the SL surface(s).
3. Equilibrium in the sense that transients die out faster than the net-loads change over time. Since the aim of this project is treating uncontrollable

net-loads stochastically, this can in a non-stringent way be rephrased, taking two possible examples, as:

(a) "the expected transient time constant should be smaller than the expected time constant of the net-load causing the transients", or more conservatively

(b) "the probability, that a transient time constant should be smaller than the time constant of the change in net-load causing it, should be greater than or equal to $1 - \beta$, where β is a small nonnegative number."

The practical reason for making this assumption is that without it, there would be a need for significantly more complicated models. Then, the exact path in load space of the system from last previous equilibrium point would be needed to be studied. Such would increase computational workload and computer time significantly. The issue is discussed partly in Section 2.7.2 as well, but without explicitly treating *Point 3* above. Particularly the stochastic complication on the net-loads is not treated. Without the equilibrium assumption, the quasi-static load flow models used would not be sufficient.

For slowly (in the case of this report; compared to transient generator dynamics) varying loads (often denoted "parameters" in the literature, in order to emphasize their non-variable behaviour from the instabilities' points of view), it can be assumed that the system always reaches equilibrium in the transient and sub-transient sense after a change in (net-)load. In other words: For each incremental change in net load of the system, for each small unit of time, it can be assumed that transients die out before the next incremental change. This assumption validates the treatment of the uncontrollable loads and the tertiary controlled loads as parameters for the transient time scales.

Note that being in equilibrium in the transient sense is not any protection against creating an transiently instable situation when driving the system into a bifurcation in the non-g_y (that is, the A-matrix of Eq. (13)) parts of the system Jacobian.

Implicitly, the third aspect above, *Point 3*, of the equilibrium assumption means that if considering mid-term dynamics, as in [11], it would impose even higher restrictions. Here, the dynamic time constants are much larger. When studying also mid-term dynamics, the net load changes must be even slower than when only considering transient and sub-transient dynamics.

In power systems that are more or less always in motion, and cannot be said to work around a certain point of operation, like for instance electric traction systems [63], it is not clear whether the above-listed assumptions would hold. It is not unusual with individual loads changing from 0 to 4 MegaWatt (MW) in around 8 seconds (and from full load to no load instantaneously) [64] for locally installed apparent powers ranging from 20 MVA up to above 100 MVA.

3.1.2 Assumptions regarding contingencies and other power system uncertainties

A power system can be exposed to many different kinds of contingencies and uncertainties. In the classical $N - 1$ criterion, the planned system operation is supposed to withstand an outage of any of a list of important system components such as transmission lines, generators, transformers, etc.

As argued in Section 1.1, and in Section 2.7.2, and some of the following subchapters of the latter, in future power systems, a larger share of the production will be made up of many small production units. Within this project, the individual outages of such are not considered as outages in the classical sense, but rather as a part of the stochastic model of the net-loads of these uncontrolled production units. This is done for rational and practical reasons, for small outages in relation to the total consumption, and it keeps the model size and thereby the computational burden limited. A similar argument can be made for outages of smaller uncontrolled consumption units. Moreover, in contrast to outages of lines, generators, or transformers, outages of uncontrolled loads do not affect the power system configuration or its controllability.

3.2 Generator, load, and grid models

In this project, for simplicity, it is assumed that the generators can be modeled according to the so-called one-axis model with attached AVRs. The vector of time derivatives $\dot{x}$ and the vector of functions $f(\cdot)$ introduced in Eq. (1) explicitly becomes

$$\dot{\delta}_i = \omega_i, \qquad \forall i \in \mathbf{G} \setminus s \quad (116)$$

$$\dot{\omega}_i = \frac{1}{M_i}\left(P_{m,i} - \frac{E'_{q,i}U_i}{X'_{d,i}}\sin\left(\delta_i - \theta_i\right) - D_i\omega_i\right), \qquad \forall i \in \mathbf{G} \setminus s \quad (117)$$

$$\dot{E'_{q,i}} = \frac{1}{T'_{d0,i}}\left(E'_{f,i} - \frac{X_{d,i}}{X'_{d,i}}E'_{q,i} + \frac{X_{d,i} - X'_{d,i}}{X'_{d,i}}U_i\cos\left(\delta_i - \theta_i\right)\right), \forall i \in \mathbf{G} \quad (118)$$

$$\dot{E'_{f,i}} = \frac{1}{T_{e,i}}\left(-E'_{f,i} + K_{A,i}\left(U_{\mathrm{ref},i} - U_i\right)\right), \qquad \forall i \in \mathbf{G_a} \quad (119)$$

where δ, the rotor angle of the generator, obeys

$$\delta = \omega_r t - \omega_0 t + \delta_0 = \omega t + \delta_0 \quad (120)$$

for which ω_r is the actual angular velocity of the generator, ω_0 is the reference angular velocity of the synchronous grid, δ_0 is the rotor angle at some start point in time t_0, and finally ω is thus the deviation in angular velocity between the generator and the grid. By definition,

$$\delta_s = 0 \quad (121)$$

$$\omega_s = 0. \quad (122)$$

Moreover, in Eq. (117), M represents the inertia coefficient of the generator, P_m represents the mechanical power of the generator, $E'_{q,i}$ represents the EMF behind the transient reactance of the generator, U represents bus voltage amplitudes, X'_d represents the direct axis transient reactance of the generator, θ represents bus voltage angles, and D represents the damping coefficient of the generator. Not yet introduced denotations in Eq. (118) are: T'_{d0} which represents the open-circuit transient time constant of the generator; the excitation EMF, E'_f; and the direct-axis synchronous reactance of the generator, X_d. In Eq. (119), the time constant of the exciter, T_e; the gain of the exciter, K_A; and the terminal voltage reference of the exciter U_{ref} are used.

The vector of zeroes and functions $g(\cdot)$ introduced in Eq. (2) explicitly becomes

$$0 = -E'_{f,i} + E^{\lim}_{f,i}, \qquad \forall i \in \mathbf{G_b} \quad (123)$$

$$0 = P_{D,i} - P_{G,i} + U_i \sum_{\forall j \in \mathbf{B}} U_j \left(G_{i,j} \cos\left(\theta_{i,j}\right) + B_{i,j} \sin\left(\theta_{i,j}\right)\right), \forall i \in \mathbf{B} \quad (124)$$

$$0 = Q_{D,i} - Q_{G,i} + U_i \sum_{\forall j \in \mathbf{B}} U_j \left(G_{i,j} \sin\left(\theta_{i,j}\right) - B_{i,j} \cos\left(\theta_{i,j}\right)\right), \forall i \in \mathbf{B} \quad (125)$$

where the sets in Eqs. (116) to (119) and (123) to (125) are defined by $\mathbf{G}$ which denotes the set of all generators in the system, s denotes the slack bus, $\mathbf{G_a}$ the set of generators under AVR control, and $\mathbf{G_b}$ the set of generators under OXL control. The abbreviation used, OXL, stands for OvereXcitation Limit. Note that underexcitation may also be an issue [65, 66], but it is not considered here. Finally, $\mathbf{B}$ denotes all the busses in the power system of study. For clarity,

$$\mathbf{G} \setminus \mathbf{G_b} = \mathbf{G_a} \quad (126)$$

$$\mathbf{G_a} \cap \mathbf{G_b} = \emptyset \quad (127)$$

$$s \in \mathbf{G_a} \vee \mathbf{G_b} \quad (128)$$

$$\mathbf{G} \subseteq \mathbf{B}. \quad (129)$$

In Eq. (123), $E^{\lim}_{f,i}$ represents the limit of the exciter in the AVR. Following the traditional notation, $\theta_{i,j}$ in Eqs. (124) and (125) denotes the angular difference between θ_i and θ_j, P_D and Q_D represents active and reactive power loads, and G and B represents the real and imaginary parts of the admittance matrix. It is worth noting that the generated active power P_G in Eq. (124) and reactive power Q_G in Eq. (125) obey

$$P_{G,i} = \frac{E'_{q,i} U_i}{X'_{d,i}} \sin\left(\delta_i - \theta_i\right), \qquad \forall i \in \mathbf{G} \quad (130)$$

$$Q_{G,i} = -\frac{U_i}{X'_{d,i}} \left(U_i - E'_{q,i} \cos\left(\delta_i - \theta_i\right)\right), \forall i \in \mathbf{G} \quad (131)$$

for the generators.

3.3 Numerically determine the system variables for the present load

The load flow solution of the system at the present point of operation, $\lambda_0 = \zeta_0 = (\zeta_0, Q(\zeta_0)) = (P_{D,0}, Q_{D,0})$, is used in some practical tricks within the OPF of Section 3.4 solved for finding the surfaces. The parameter $|J|^{\max}$ in Eqs. (200) and (201) is estimated by the help of this solution. Its solutions may also be used as initial values, for some or all, of the variables in the surface-finding OPF of Section 3.4. Otherwise, its solution would not have been needed in the study of Section 4.1 besides as a means of confirming the model's correctness by comparisons to the literature.

Since the optimization method approach was used in this project to find the operation limit surfaces of Section 2.3, an optimization problem was formulated also for the load flow problem of the present operation point $\lambda_0 = (P_{D,0}, Q_{D,0})$.

That problem includes the load flow equations Eqs. (124) and (125), and their corresponding active and reactive power generation equations Eqs. (130) and (131) and the steady-state representations of Eqs. (118) and (119):

$$0 = E'_{f,i} - \frac{X_{d,i}}{X'_{d,i}} E'_{q,i} + \frac{X_{d,i} - X'_{d,i}}{X'_{d,i}} U_i \cos\left(\delta_i - \theta_i\right), \forall i \in \mathbf{G} \tag{132}$$

$$0 = K_{A,i}\left(U_{\mathrm{ref},i} - U_i\right) - E'_{f,i}, \qquad \forall i \in \mathbf{G} \tag{133}$$

and a dummy objective to minimize

$$z = 1. \tag{134}$$

The problem was solved as an NonLinear Programming (NLP) optimization problem in General Algebraic Modeling System (GAMS) [67–69] using LINDO [35, 36]. At steady state, from Eq. (116), it can be seen that ω will be zero, ensuring that the mechanical and electrical powers in Eq. (117) equal each other. Therefore, Eqs. (116) and (117) are omitted in steady state studies. Moreover, note that since SLLs have not been studied in Section 4.1, it has been assumed that

$$\mathbf{G_b} = \emptyset, \tag{135}$$

and therefore Eq. (123) has not been considered in the model.

In this model, in contrast to the one of Section 3.4, $P_{D,i}, Q_{D,i}, i \in \mathbf{B}$ are treated as parameters, as well as $P_{G,i}, i \in \mathbf{G} \setminus s$ are.

3.4 The OPF finding the surfaces

3.4.1 The optimization problem summarized

Summarizing without all the details given in the forthcoming subsections, the objective of the optimization problem is to minimize Eq. (137), that is, to find the smallest change in net-load from λ_0 for which the constraints are met. The constraints are the ones of load flow Eqs. (124) and (125), generation Eqs. (130) and (131), the steady-state representations of the generator and exciter EMFs Eqs. (132) and (133), the reactive load model assumption Eq. (139), the thermal limit constraints Eqs. (140) and (141), the SNB constraints Eqs. (200) to (203), and finally the constraint Eq. (204) ensuring that at least one operational limit has been reached.

The details about the Jacobian associated to an SNB point can be found in Section 3.4.6 and its paragraphs. Beforehand computed parameters are neglected from this summary in order to maintain the intended simplicity.

Naturally, $\zeta = P_{D,l}$ cannot be a parameter in this problem, as in the load flow problem of Section 3.3. It follows by technical reasons that $Q_{D,l}$ neither can be a parameter. The modeling of $Q_{D,l}$ is described in Section 3.4.3.

The main purpose of the study presented in Section 4.1 is to graphically illustrate the operational limit surfaces found. Since the surfaces can only be illustrated easily in $\mathbb{R}^3$, and the number of loads in the IEEE 9-bus test system [10, Appendix C.1] are three, the restriction from Section 3.3 of

$$u = P_{G,i}, i \in \mathbf{G} \setminus s \tag{136}$$

being parameters where kept. When determining the surfaces for actual usage however – as a part in the construction of the SOPF (Section 2.7.5.2) problem

constraints – u of Eq. (136) needs to be treated as variables. Following the *most important point* approach of Section 2.3.1, u will be modeled as stochastic variables depending on ζ.

3.4.2 The objective function

To start with, the objective function

$$z = \sum_{\forall l \in \mathbf{L}} \left(P_{D,0,l} - P_{D,l} \right) \tag{137}$$

which is to be minimized makes sure that the closest operational limit from the present (load) point of operation,

$$\lambda_0 = \left\{ \begin{array}{c} \text{for this study, } u, \\ \text{is kept constant for} \\ \text{illustrative purposes} \end{array} \right\} = \zeta_0 = P_{D,0,l} \tag{138}$$

is found first.

3.4.3 The reactive loads

In contrast to the load flow problem being solved in Section 3.3 the loads of the load buses, (P_D, Q_D) are no longer given parameters, but variables. The variable P_D plays an important role in the objective function Eq. (137). By the assumption

$$Q_{D,l} = P_{D,l} \frac{Q_{D,0,l}}{Q_{D,0,l}}, \forall l \in \mathbf{L} \tag{139}$$

where $\mathbf{L}$ denotes the set of load buses, the power factor of each load is maintained in the search for the closest operational limit from the present load point, $(P_{D,0,l}, Q_{D,0,l})$. Thus, $Q_{D,l}$ is a variable in the OPF locating the closest (with different objective: the *most important*) points of the operational limit surfaces. The value of the variable is however completely determined by the variable $P_{D,l}$.

3.4.4 Load flow equations, transient equilibrium equations

The active and reactive power load flow equations used are the same as Eqs. (124) and (125); the active and reactive generation equations used are the same as Eqs. (130) and (131); and the steady-state representations of the generator and exciter EMFs, Eqs. (118) and (119), that is Eqs. (132) and (133) are also included in the optimization problem.

3.4.5 Thermal Constraints

In the optimization problem where the closest operation limit to the present operation point is to be found, the conditions

$$\begin{aligned} 0 \geq & -G_{i,j} \left(U_i \right)^2 - \left(U_i U_j \right) \left(-G_{i,j} \cos\left(\theta_{i,j} \right) - B_{i,j} \sin\left(\theta_{i,j} \right) \right) - \\ & - P_{i,j}^{\lim} \left(1 + \epsilon \left(\alpha_{i,j} - 1 \right) \right), \left\{ \{i,j\} \in \mathbf{B} \;\middle|\; \alpha_{i,j}^{\text{regard}} = 1 \right\} \end{aligned} \tag{140}$$

$$\begin{aligned} 0 \leq & -G_{i,j} \left(U_i \right)^2 - \left(U_i U_j \right) \left(-G_{i,j} \cos\left(\theta_{i,j} \right) - B_{i,j} \sin\left(\theta_{i,j} \right) \right) - \\ & - P_{i,j}^{\lim} \left(\left(2 - \epsilon \right) \alpha_{i,j} - 1 \right), \left\{ \{i,j\} \in \mathbf{B} \;\middle|\; \alpha_{i,j}^{\text{regard}} = 1 \right\} \end{aligned} \tag{141}$$

ensure that the binary variable $\alpha_{i,j}$ is forced to 1 when the active power flow from bus i to bus j in line $\{i,j\}$ has reached its power transfer limit $P_{i,j}^{\lim}$. The parameter ϵ is a small positive number (in the case studies of this report 10^{-4}) chosen in order to simplify the identification of power flows at, or close enough to, the thermal transfer limit. The model is general in the sense that it considers power flow restrictions in both directions by considering all possible combinations $\{i,j\}$.

For an explanation of the user-defined parameter $\alpha_{i,j}^{\text{regard}}$ in Eqs. (140) and (141), the reader is referred to Sections 3.4.7 and 3.5.

3.4.6 The SNB

3.4.6.1 The partial derivatives for the Jacobian For the identification of SNB points, the modeling becomes more intricate. In particular, the definition of the system Jacobian and its corresponding eigenvectors within the frame of an optimization problem defined within an algebraic modeling system.

The contributions to the system Jacobian from Eq. (116)

$$\frac{\partial \dot{\delta_{g^{\text{ns}}}}}{\partial \omega_{g^{\text{ns}}}} = 1, \forall g^{\text{ns}} \in \mathbf{G} \setminus s \tag{142}$$

will purely be constants/parameters and such can be computed before the optimization starts. The only contribution to J from Eq. (116) is Eq. (142) which contributes to the f_x submatrix of J introduced in Eq. (7). The contributions to the system Jacobian of Eq. (117) do however include variables, and some of its partial derivatives, like

$$\frac{\partial \dot{\omega_{g^{\text{ns}}}}}{\partial \delta_{g^{\text{ns}}}} = \frac{-E'_{q,g^{\text{ns}}} U_{g^{\text{ns}}} \cos\left(\delta_{g^{\text{ns}}} - \theta_{g^{\text{ns}}}\right)}{M_{g^{\text{ns}}} X'_{d,g^{\text{ns}}}}, \forall g^{\text{ns}} \in \mathbf{G} \setminus s \tag{143}$$

also does. Like for Eq. (142),

$$\frac{\partial \dot{\omega_{g^{\text{ns}}}}}{\partial \omega_{g^{\text{ns}}}} = -\frac{D_{g^{\text{ns}}}}{M_{g^{\text{ns}}}}, \forall g^{\text{ns}} \in \mathbf{G} \setminus s \tag{144}$$

is purely a constant/parameter from the optimization model's point of view, whereas

$$\frac{\partial \dot{\omega_{g^{\text{ns}}}}}{\partial E'_{q,g^{\text{ns}}}} = -\frac{U_{g^{\text{ns}}} \sin\left(\delta_{g^{\text{ns}}} - \theta_{g^{\text{ns}}}\right)}{M_{g^{\text{ns}}} X'_{d,g^{\text{ns}}}}, \forall g^{\text{ns}} \in \mathbf{G} \setminus s \tag{145}$$

will be treated as variables in the optimization problem. The partial derivatives Eqs. (143) to (145) all contributes to f_x, whereas

$$\frac{\partial \dot{\omega_{g^{\text{ns}}}}}{\partial \theta_{g^{\text{ns}}}} = \frac{E'_{q,g^{\text{ns}}} U_{g^{\text{ns}}} \cos\left(\delta_{g^{\text{ns}}} - \theta_{g^{\text{ns}}}\right)}{M_{g^{\text{ns}}} X'_{d,g^{\text{ns}}}}, \forall g^{\text{ns}} \in \mathbf{G} \setminus s \tag{146}$$

$$\frac{\partial \dot{\omega_{g^{\text{ns}}}}}{\partial U_{g^{\text{ns}}}} = -\frac{E'_{q,g^{\text{ns}}} \sin\left(\delta_{g^{\text{ns}}} - \theta_{g^{\text{ns}}}\right)}{M_{g^{\text{ns}}} X'_{d,g^{\text{ns}}}}, \quad \forall g^{\text{ns}} \in \mathbf{G} \setminus s \tag{147}$$

contributes to the submatrix f_y of J introduced in Eq. (7). From Eq. (118) the partial derivative

$$\frac{\partial \dot{E'_{q,g^{\text{ns}}}}}{\partial \delta_{g^{\text{ns}}}} = -\frac{\left(X_{d,g^{\text{ns}}} - X'_{d,g^{\text{ns}}}\right) U_{g^{\text{ns}}} \sin\left(\delta_{g^{\text{ns}}} - \theta_{g^{\text{ns}}}\right)}{T'_{d0,g^{\text{ns}}} X'_{d,g^{\text{ns}}}}, \forall g^{\text{ns}} \in \mathbf{G} \setminus s \tag{148}$$

and the parameterswill be treated as variable, whereas

$$\frac{\partial \dot{E'_{q,g}}}{\partial E'_{q,g}} = -\frac{X_{d,g}}{T'_{d0,g}X'_{d,g}}, \forall g \in \mathbf{G} \tag{149}$$

$$\frac{\partial \dot{E'_{q,g}}}{\partial E'_{f,g}} = \frac{1}{T'_{d0,g}}, \qquad \forall g \in \mathbf{G} \tag{150}$$

are constants/paramters. The partial derivatives of Eqs. (148) to (150) belongs to f_x, whereas

$$\frac{\partial \dot{E'_{q,g}}}{\partial \theta_g} = \frac{\left(X_{d,g^{\text{ns}}} - X'_{d,g^{\text{ns}}}\right) U_g \sin\left(\delta_g - \theta_g\right)}{T'_{d0,g}X'_{d,g}}, \forall g \in \mathbf{G} \tag{151}$$

$$\frac{\partial \dot{E'_{q,g}}}{\partial U_g} = \frac{\left(X_{d,g^{\text{ns}}} - X'_{d,g^{\text{ns}}}\right) \cos\left(\delta_g - \theta_g\right)}{T'_{d0,g}X'_{d,g}}, \quad \forall g \in \mathbf{G} \tag{152}$$

are obtained to take part in f_y. As seen, Eqs. (151) and (152) will be treated as variable in the optimization program. The last contribution to f_x and f_y comes from Eq. (119): for f_x only the parameters

$$\frac{\partial \dot{E'_{f,g}}}{\partial E'_{f,g}} = -\frac{1}{T_{e,g}}, \forall g \in \mathbf{G} \tag{153}$$

and for f_y the parameters

$$\frac{\partial \dot{E'_{f,g}}}{\partial U'_g} = -\frac{K_{A,g}}{T_{e,g}}, \forall g \in \mathbf{G}. \tag{154}$$

From Eqs. (124) and (130), the contributions to the submatrix g_x of J, introduced in Eq. (7), are the variables

$$\frac{\partial P_g}{\partial \delta_g} = -\frac{E'_{q,g}U_g \cos\left(\delta_g - \theta_g\right)}{X'_{d,g}}, \forall g \in \mathbf{G} \setminus s \tag{155}$$

$$\frac{\partial P_g}{\partial E'_{q,g}} = -\frac{U_g \sin\left(\delta_g - \theta_g\right)}{X'_{d,g}}, \qquad \forall g \in \mathbf{G} \tag{156}$$

and the contributions to the submatrix g_y of J introduced in Eq. (7) are the variables

$$\begin{aligned}\frac{\partial P_g}{\partial \theta_g} = &\frac{E'_{q,g}U_g \cos\left(\delta_g - \theta_g\right)}{X'_{d,g}} + \\ &+ U_g \sum_{\forall j \in \mathbf{B} \setminus g} \left(U_j \left(-G_{g,j} \sin\left(\theta_{g,j}\right) + B_{g,j} \cos\left(\theta_{g,j}\right)\right)\right), \forall g \in \mathbf{G}\end{aligned} \tag{157}$$

$$\frac{\partial P_i}{\partial \theta_i} = U_i \sum_{\forall j \in \mathbf{B} \setminus i} \left(U_j \left(-G_{i,j} \sin\left(\theta_{i,j}\right) + B_{i,j} \cos\left(\theta_{i,j}\right)\right)\right), \forall i \in \mathbf{B} \setminus \mathbf{G} \tag{158}$$

$$\frac{\partial P_i}{\partial \theta_j} = U_i U_j \left(G_{i,j} \sin\left(\theta_{i,j}\right) - B_{i,j} \cos\left(\theta_{i,j}\right)\right), \forall i \neq j \in \mathbf{B} \tag{159}$$

$$\frac{\partial P_g}{\partial U_g} = -\frac{E'_{q,g}\sin(\delta_g - \theta_g)}{X'_{d,g}} + 2U_g G_{g,g} + \\ + \sum_{\forall j \in \mathbf{B}\setminus g} U_j \left(G_{g,j}\cos(\theta_{g,j}) + B_{g,j}\sin(\theta_{g,j})\right), \forall g \in \mathbf{G} \tag{160}$$

$$\frac{\partial P_i}{\partial U_i} = 2U_i G_{i,i} + \sum_{\forall j \in \mathbf{B}\setminus i} U_j \left(G_{i,j}\cos(\theta_{i,j}) + B_{i,j}\sin(\theta_{i,j})\right), \forall i \in \mathbf{B}\setminus\mathbf{G} \tag{161}$$

$$\frac{\partial P_i}{\partial U_j} = U_i \left(G_{i,j}\cos(\theta_{i,j}) + B_{i,j}\sin(\theta_{i,j})\right), \forall i \neq j \in \mathbf{B}. \tag{162}$$

Similarly (as from Eqs. (124) and (130)) from Eqs. (125) and (131),

$$\frac{\partial Q_g}{\partial \delta_g} = \frac{E'_{q,g}U_g\sin(\delta_g - \theta_g)}{X'_{d,g}}, \forall g \in \mathbf{G}\setminus s \tag{163}$$

$$\frac{\partial Q_g}{\partial E'_{q,g}} = -\frac{U_g\cos(\delta_g - \theta_g)}{X'_{d,g}}, \quad \forall g \in \mathbf{G} \tag{164}$$

comes, which are used as variables in the operation limit finding optimization problem. Eqs. (163) and (164) are contributing to the submatrix g_x of J, whereas

$$\frac{\partial Q_g}{\partial \theta_g} = -\frac{E'_{q,g}U_g\sin(\delta_g - \theta_g)}{X'_{d,g}} + \\ + U_g \sum_{\forall j \in \mathbf{B}\setminus g} \left(U_j \left(G_{g,j}\cos(\theta_{g,j}) + B_{g,j}\sin(\theta_{g,j})\right)\right), \forall g \in \mathbf{G} \tag{165}$$

$$\frac{\partial Q_i}{\partial \theta_i} = U_i \sum_{\forall j \in \mathbf{B}\setminus i} \left(U_j \left(G_{i,j}\cos(\theta_{i,j}) + B_{i,j}\sin(\theta_{i,j})\right)\right), \forall i \in \mathbf{B}\setminus\mathbf{G} \tag{166}$$

$$\frac{\partial Q_i}{\partial \theta_j} = U_i U_j \left(-G_{i,j}\cos(\theta_{i,j}) - B_{i,j}\sin(\theta_{i,j})\right), \forall i \neq j \in \mathbf{B} \tag{167}$$

$$\frac{\partial Q_g}{\partial U_g} = \frac{2U_g - E'_{q,g}\cos(\delta_g - \theta_g)}{X'_{d,g}} - 2U_g B_{g,g} + \\ + \sum_{\forall j \in \mathbf{B}\setminus g} U_j \left(G_{g,j}\sin(\theta_{g,j}) - B_{g,j}\cos(\theta_{g,j})\right), \forall g \in \mathbf{G} \tag{168}$$

$$\frac{\partial Q_i}{\partial U_i} = -2U_i B_{i,i} + \sum_{\forall j \in \mathbf{B}\setminus i} U_j \left(G_{i,j}\sin(\theta_{i,j}) - B_{i,j}\cos(\theta_{i,j})\right), \forall i \in \mathbf{B}\setminus\mathbf{G} \tag{169}$$

$$\frac{\partial Q_i}{\partial U_j} = U_i \left(G_{i,j}\sin(\theta_{i,j}) - B_{i,j}\cos(\theta_{i,j})\right), \forall i \neq j \in \mathbf{B} \tag{170}$$

are all variable, and contributing to g_y.

3.4.6.2 Putting the Jacobian Together The benefits of using general algebraic modeling systems are maybe obvious:

- straight-forward modeling,
- easy access and adaptation to a large variety of off-the-shelf solvers,

- thanks to the algebraic nature of the model the computer can take care of and automatically compute the optimization model's Jacobians, Hessians, and other solver-internal tools needed,
- etc.

One major complication for the program designer is however that definitions of sets and subsets must be clearly and stringently defined. In this particular case, it involves the inclusion of the system Jacobian and its corresponding eigenvectors into the optimization model.

The dimensions of the system Jacobian, J, and its submatrices f_x, f_y, g_x, and g_y will in the general (as general as having a single slack bus) case be:

J**:** $\left(2 \cdot \left(2 \cdot g^b - 1 + b^b\right)\right) \times \left(2 \cdot \left(2 \cdot g^b - 1 + b^b\right)\right)$,

f_x**:** $\left(2 \cdot \left(g^b - 1\right) + 2 \cdot g^b\right) \times \left(2 \cdot \left(g^b - 1\right) + 2 \cdot g^b\right)$,

f_y**:** $\left(2 \cdot \left(g^b - 1\right) + 2 \cdot g^b\right) \times 2 \cdot b^b$,

g_x**:** $2 \cdot b^b \times \left(2 \cdot \left(g^b - 1\right) + 2 \cdot g^b\right)$, and

g_y**:** $2 \cdot b^b \times 2 \cdot b^b$,

in which g^b denotes the number of generator buses in the system, $g^b - 1$ the number of generator buses that are not slack buses in the system, and b^b the number of buses in the system. For the particular case of the IEEE 9-bus test system [10, Appendix C.1] used in the numerical example of Section 4.1 these figures are 28×28, 10×10, 10×18, 18×10, and 18×18, respectively.

Since these dimensions cannot be defined as sets containing the sets $\mathbf{G}$, $\mathbf{G} \backslash s$, $\mathbf{B}$, and $\mathbf{B} \backslash \mathbf{G}$ in a straightforward fashion, some manipulations of the constraints, containing projections from the above mentioned, bus-number based sets onto other, larger, sets will have to be introduced. This will be noted and present in the following.

For simplicity: let $\mathbf{s}$ denote the number of slack generators; $\mathbf{g}^{\mathrm{ns}}$ denote the number of non-slack generators, $|\mathbf{G} \setminus s|$; and let $g_i^{\mathrm{ns}} \in \{1, 2, ..., g^{\mathrm{ns}}\}$ denote the ith element in the set $\mathbf{G} \setminus s$. Once again, using the example of the IEEE 9-bus system of [10, Appendix C.1]: $\mathbf{s} = s = 1$; $i \in \{1, 2\}$; $|\mathbf{G} \setminus s| \in \{2, 3\}$; $g_i^{\mathrm{ns}} \in \{1, 2\}$; $\mathbf{B} \in \{1, 2, ..., 9\}$; $\mathbf{B} \setminus \mathbf{G} \in \{4, 5, ..., 9\}$; but for $J_{i,j}$, the dimensions are $\{i, j\} \in \{(1, 2, ..., 18) \times (1, 2, ..., 18)\}$. Thus, it is clearly not straight-forward to define the sets describing the Jacobian (and its eigenvectors) as sets containing the other sets, since they are numbered differently. The other sets are numbered in relation to either their order in their respective subsets, or to their respective node numbers.

One way of managing the issue of incompatible set dimensions introduced above, using the above introduced notation, for the f_x part of J, is to define

$$J_{i,\mathbf{g}^{\mathrm{ns}}+i} = \frac{\partial \dot{\delta_{g_i^{\mathrm{ns}}}}}{\partial \omega_{g_i^{\mathrm{ns}}}}, \quad \forall i \in \{1, 2, ..., \mathbf{g}^{\mathrm{ns}}\} \tag{171}$$

$$J_{\mathbf{g}^{\mathrm{ns}}+i,i} = \frac{\partial \dot{\omega_{g_i^{\mathrm{ns}}}}}{\partial \delta_{g_i^{\mathrm{ns}}}}, \quad \forall i \in \{1, 2, ..., \mathbf{g}^{\mathrm{ns}}\} \tag{172}$$

$$J_{\mathbf{g}^{\mathrm{ns}}+i,\mathbf{g}^{\mathrm{ns}}+i} = \frac{\partial \dot{\omega_{g_i^{\mathrm{ns}}}}}{\partial \omega_{g_i^{\mathrm{ns}}}}, \quad \forall i \in \{1, 2, ..., \mathbf{g}^{\mathrm{ns}}\} \tag{173}$$

$$J_{\mathbf{g}^{\mathrm{ns}}+i,2\mathbf{g}^{\mathrm{ns}}+g_i^{\mathrm{ns}}} = \frac{\partial \dot{\omega_{g_i^{\mathrm{ns}}}}}{\partial E'_{q,g_i^{\mathrm{ns}}}}, \forall i \in \{1,2,...,\mathbf{g}^{\mathrm{ns}}\} \tag{174}$$

$$J_{2\mathbf{g}^{\mathrm{ns}}+g_i^{\mathrm{ns}},i} = \frac{\partial \dot{E'_{q,g^{\mathrm{ns}}}}}{\partial \delta_{g_i^{\mathrm{ns}}}}, \forall i \in \{1,2,...,\mathbf{g}^{\mathrm{ns}}\} \tag{175}$$

$$J_{2\mathbf{g}^{\mathrm{ns}}+g,2\mathbf{g}^{\mathrm{ns}}+g} = \frac{\partial \dot{E'_{q,g}}}{\partial E'_{q,g}}, \ \ \forall g \in \mathbf{G} \tag{176}$$

$$J_{2\mathbf{g}^{\mathrm{ns}}+g,2\mathbf{g}^{\mathrm{ns}}+\mathbf{g}+g} = \frac{\partial \dot{E'_{q,g}}}{\partial E'_{f,g}}, \ \ \forall g \in \mathbf{G} \tag{177}$$

$$J_{2\mathbf{g}^{\mathrm{ns}}+\mathbf{g}+g,2\mathbf{g}^{\mathrm{ns}}+\mathbf{g}+g} = \frac{\partial \dot{E'_{f,g}}}{\partial E'_{f,g}}, \ \ \forall g \in \mathbf{G} \tag{178}$$

by using Eqs. (142) to (145), (148) to (150) and (153). Moreover, and similarly, the parts of J that correspond to the submatrix f_y can be defined by using Eqs. (146), (147), (151), (152) and (154):

$$J_{\mathbf{g}^{\mathrm{ns}}+i,2\mathbf{g}^{\mathrm{ns}}+2\mathbf{g}+g_i^{\mathrm{ns}}} = \frac{\partial \dot{\omega_{g_i^{\mathrm{ns}}}}}{\partial \theta_{g_i^{\mathrm{ns}}}}, \forall i \in \{1,2,...,\mathbf{g}^{\mathrm{ns}}\} \tag{179}$$

$$J_{\mathbf{g}^{\mathrm{ns}}+i,2\mathbf{g}^{\mathrm{ns}}+2\mathbf{g}+\mathbf{b}+g_i^{\mathrm{ns}}} = \frac{\partial \dot{\omega_{g_i^{\mathrm{ns}}}}}{\partial U_{g_i^{\mathrm{ns}}}}, \forall i \in \{1,2,...,\mathbf{g}^{\mathrm{ns}}\} \tag{180}$$

$$J_{2\mathbf{g}^{\mathrm{ns}}+g,2\mathbf{g}^{\mathrm{ns}}+2\mathbf{g}+g} = \frac{\partial \dot{E'_{q,g}}}{\partial \theta_g}, \forall g \in \mathbf{G} \tag{181}$$

$$J_{2\mathbf{g}^{\mathrm{ns}}+g,2\mathbf{g}^{\mathrm{ns}}+2\mathbf{g}+\mathbf{b}+g} = \frac{\partial \dot{E'_{q,g}}}{\partial U_g}, \forall g \in \mathbf{G} \tag{182}$$

$$J_{2\mathbf{g}^{\mathrm{ns}}+\mathbf{g}+g,2\mathbf{g}^{\mathrm{ns}}+2\mathbf{g}+\mathbf{b}+g} = \frac{\partial \dot{E'_{f,g}}}{\partial U'_g} \ \forall g \in \mathbf{G} \tag{183}$$

in which $\mathbf{b}$ denotes the number of busses in the system. The parts of J that correspond to the submatrix g_x are defined by using Eqs. (155), (156), (163) and (164):

$$J_{2\mathbf{g}^{\mathrm{ns}}+2\mathbf{g}+g_i^{\mathrm{ns}},i} = \frac{\partial P_{g_i^{\mathrm{ns}}}}{\partial \delta_{g_i^{\mathrm{ns}}}} \forall i \in \{1,2,...,\mathbf{g}^{\mathrm{ns}}\} \tag{184}$$

$$J_{2\mathbf{g}^{\mathrm{ns}}+2\mathbf{g}+g,2\mathbf{g}^{\mathrm{ns}}+g} = \frac{\partial P_g}{\partial E'_{q,g}} \forall g \in \mathbf{G} \tag{185}$$

$$J_{2\mathbf{g}^{\mathrm{ns}}+2\mathbf{g}+\mathbf{b}+g_i^{\mathrm{ns}},i} = \frac{\partial Q_{g_i^{\mathrm{ns}}}}{\partial \delta_{g_i^{\mathrm{ns}}}} \forall i \in \{1,2,...,\mathbf{g}^{\mathrm{ns}}\} \tag{186}$$

$$J_{2\mathbf{g}^{\mathrm{ns}}+2\mathbf{g}+\mathbf{b}+g,2\mathbf{g}^{\mathrm{ns}}+g} = \frac{\partial Q_g}{\partial E'_{q,g}} \forall g \in \mathbf{G}, \tag{187}$$

and, finally, the parts of J that correspond to the submatrix g_y are defined by using Eqs. (157) to (162) and (165) to (170):

$$J_{2\mathbf{g}^{\mathrm{ns}}+2\mathbf{g}+g,2\mathbf{g}^{\mathrm{ns}}+2\mathbf{g}+g} = \frac{\partial P_g}{\partial \theta_g}, \forall g \in \mathbf{G} \tag{188}$$

$$J_{2\mathbf{g}^{\mathrm{ns}}+2\mathbf{g}+i,2\mathbf{g}^{\mathrm{ns}}+2\mathbf{g}+i} = \frac{\partial P_i}{\partial \theta_i}, \forall i \notin \mathbf{G} \tag{189}$$

$$J_{2\mathbf{g}^{\mathrm{ns}}+2\mathbf{g}+i,2\mathbf{g}^{\mathrm{ns}}+2\mathbf{g}+j} = \frac{\partial P_i}{\partial \theta_j}, \forall \{i \neq j\} \in \mathbf{B} \tag{190}$$

$$J_{2\mathbf{g}^{\mathrm{ns}}+2\mathbf{g}+g,2\mathbf{g}^{\mathrm{ns}}+2\mathbf{g}+\mathbf{b}+g} = \frac{\partial P_g}{\partial U_g}, \forall g \in \mathbf{G} \tag{191}$$

$$J_{2\mathbf{g}^{\mathrm{ns}}+2\mathbf{g}+i,2\mathbf{g}^{\mathrm{ns}}+2\mathbf{g}+\mathbf{b}+i} = \frac{\partial P_i}{\partial U_i}, \forall i \notin \mathbf{G} \tag{192}$$

$$J_{2\mathbf{g}^{\mathrm{ns}}+2\mathbf{g}+i,2\mathbf{g}^{\mathrm{ns}}+2\mathbf{g}+\mathbf{b}+j} = \frac{\partial P_i}{\partial U_j}, \forall \{i \neq j\} \in \mathbf{B} \tag{193}$$

$$J_{2\mathbf{g}^{\mathrm{ns}}+2\mathbf{g}+\mathbf{b}+g,2\mathbf{g}^{\mathrm{ns}}+2\mathbf{g}+g} = \frac{\partial Q_g}{\partial \theta_g}, \forall g \in \mathbf{G} \tag{194}$$

$$J_{2\mathbf{g}^{\mathrm{ns}}+2\mathbf{g}+\mathbf{b}+i,2\mathbf{g}^{\mathrm{ns}}+2\mathbf{g}+i} = \frac{\partial Q_i}{\partial \theta_i}, \forall i \notin \mathbf{G} \tag{195}$$

$$J_{2\mathbf{g}^{\mathrm{ns}}+2\mathbf{g}+\mathbf{b}+i,2\mathbf{g}^{\mathrm{ns}}+2\mathbf{g}+j} = \frac{\partial Q_i}{\partial \theta_j}, \forall \{i \neq j\} \in \mathbf{B} \tag{196}$$

$$J_{2\mathbf{g}^{\mathrm{ns}}+2\mathbf{g}+\mathbf{b}+g,2\mathbf{g}^{\mathrm{ns}}+2\mathbf{g}+\mathbf{b}+g} = \frac{\partial Q_g}{\partial U_g}, \forall g \in \mathbf{G} \tag{197}$$

$$J_{2\mathbf{g}^{\mathrm{ns}}+2\mathbf{g}+\mathbf{b}+i,2\mathbf{g}^{\mathrm{ns}}+2\mathbf{g}+\mathbf{b}+i} = \frac{\partial Q_i}{\partial U_i}, \forall i \notin \mathbf{G} \tag{198}$$

$$J_{2\mathbf{g}^{\mathrm{ns}}+2\mathbf{g}+\mathbf{b}+i,2\mathbf{g}^{\mathrm{ns}}+2\mathbf{g}+\mathbf{b}+j} = \frac{\partial Q_i}{\partial U_j}, \forall \{i \neq j\} \in \mathbf{B}. \tag{199}$$

Now, J can be determined according to the above.

3.4.6.3 The actual SNB-detecting constraints In order to detect the first reach of an SNB point in the optimization program, the constraints

$$\sum_{i=1}^{2\mathbf{g}^{\mathrm{ns}}+2\mathbf{g}+2\mathbf{b}} u_i J_{i,j} \geq |J|^{\max} (\beta - 1), \forall j \in \{1, 2, ..., 2\mathbf{g}^{\mathrm{ns}} + 2\mathbf{g} + 2\mathbf{b}\} \tag{200}$$

$$\sum_{i=1}^{2\mathbf{g}^{\mathrm{ns}}+2\mathbf{g}+2\mathbf{b}} u_i J_{i,j} \leq |J|^{\max} (1 - \beta), \forall j \in \{1, 2, ..., 2\mathbf{g}^{\mathrm{ns}} + 2\mathbf{g} + 2\mathbf{b}\} \tag{201}$$

$$\sum_{i=1}^{2\mathbf{g}^{\mathrm{ns}}+2\mathbf{g}+2\mathbf{b}} (u_i)^2 \geq \epsilon + (1 - \epsilon) \beta \tag{202}$$

$$\sum_{i=1}^{2\mathbf{g}^{\mathrm{ns}}+2\mathbf{g}+2\mathbf{b}} (u_i)^2 \leq 1 \tag{203}$$

are used, in which u_i represents a left-hand eigenvector of J, β is a binary variable indicating that an SNB point has been reached, $|J|^{\max}$ is a constant parameter empirically set to 3 times the Frobenius norm of the Jacobian in the present point of operation (that is, $\lambda_0 = \zeta_0 = P_{D,0,l}$ from the solution of Section 3.3), where Eq. (202) prevents the (trivial and irrelevant) zero-eigenvector solution, Eq. (203) sets an upper bound on the 2-norm of the eigenvectors, and where Eqs. (202) and (203) together forces the 2-norm of the eigenvector to be 1 in the SNB-point. Note that right-hand eigenvectors could have been used as well.

3.4.7 Ensuring at least one surface is reached

One constraint making sure at least one (additional) operation limit has been reached is also needed:

$$1 \leq \sum_{\forall i,j \in \mathbf{B}} \alpha_{i,j} \cdot \alpha_{i,j}^{\text{account}} + \beta \cdot \beta^{\text{account}}, \tag{204}$$

where $\alpha_{i,j}^{\text{account}}$ is a user-defined parameter. The parameter is set to 1 if the transfer limit of power flowing from node i to node j should be *accounted* for in Eq. (204), and 0 if not. Being accounted for in Eq. (204), means implicitly, that this surface has not yet been found and identified. Moreover, in Eq. (204), the user-defined parameter β^{account} is in a similar fashion set to 1 if reaching the SNB should be accounted for as finding a new yet unfound surface. Finally, in Eq. (204), the binary variable β from Eqs. (200) to (202) indicates whether or not the point-of-operation of the power system in the optimization solving procedure is at an SNB limit.

Since the model does not consider SLLs, and since any deeper analysis of which kind of SNB point has been reached, the SNB surface can only be reached once in the surface identification process presented Section 3.5.

The parameter $\alpha_{i,j}^{\text{regard}}$, until now only used in Eqs. (140) and (141), includes the thermal limit constraints of active power transfer from bus i to bus j, in the optimization problem if set to 1, and excludes it is set to 0. Moreover, the parameter $\alpha_{i,j}^{\text{regard}}$ of Eqs. (140) and (141) is related to $\alpha_{i,j}^{\text{account}}$ in this study as

$$\alpha_{i,j}^{\text{regard}} = \alpha_{i,j}^{\text{account}} \tag{205}$$

but in other types of studies the relation expressed by Eq. (205) may not be needed.

A similar approach of a *regard*-parameter also for SNB is not possible, since SNBs are of the SL type of Sections 1.1 and 2.2.1 which borders cannot be violated without immediate putting the system stability at stake.

3.5 Finding the surfaces in order of importance

The process of the method of finding the surfaces in their respective orders of load-space distance (or, with some modifications; of importance) will be presented in the numbered list below naming the states by the numbers.

1. Initially, no surface has yet been found. The parameters $\alpha_{i,j}^{\text{account}}$ and β^{account} are set to 1. Then the first run of the optimization problem finding the closest operational limit takes place. There are four possible outcomes:

   (a) The SNB surface is reached. Then β^{account} is set to 0. Thereafter, the process goes to *Step 2*.

   (b) A thermal transfer limit between the nodes i and j is reached. Then $\alpha_{i,j}^{\text{account}}$ is set to 0. Thereafter, the process goes to *Step 3*.

   (c) To a lower probability, the intersection of a thermal transfer limit and an SNB surface might be the closest point meeting the OPF constraint Eq. (204). Then, the parameters $\alpha_{i,j}^{\text{account}}$ and β^{account} are

set to 0. This is a CP [6, 70, 71]. CPs are not of the same relevance for this type of study where, according to Section 1.3, each surface should be treated individually. Thus, two separate surfaces should be approximated in accordance with Section 2.3.3, with one main exception: Since the point of evaluation, λ_c, is at an SNB, for the thermal limit surface approximation; similar considerations as for CPs needs to be taken – particularly that $F_z = J$ is singular and thus not invertible. Thereafter, the process goes to *Step 4*.

(d) There are no surfaces to be found: at all, within the upper bound on numbers of surfaces m to maximally be identified, or within a possible upper bound of distances in load space away from λ_0 to search for operational limit surfaces. This outcome is not likely, unless m is mistakenly set to 0, the system is very stable, or the possible upper bound of the distance is too conservatively set. Thereafter, the process goes to *Step 5*.

2. An SNB has occurred. There are two options, of which one is associated with a lower probability:

   (a) A thermal limit is reached. Then $\alpha_{i,j}^{\text{account}}$ is set to 0. If this point also lies on an SNB surface, it should be treated as described in subpoint *c)* of *Point 1* and *Point 3*. Thereafter, the process goes to *Step 4*.

   (b) There are no further surfaces to be found: at all, within the upper bound on numbers of surfaces m to maximally be identified, or within a possible upper bound of distances in load space away from λ_0 to search for operational limit surfaces. Thereafter, the process goes to *Step 5*.

3. A thermal limit is reached. As in *Point 1* there are four possible outcomes:

   (a) The SNB surface is reached. Then β^{account} is set to 0. Thereafter, the process goes to *Step 4*.

   (b) A thermal transfer limit between the nodes i and j is reached. Then $\alpha_{i,j}^{\text{account}}$ is set to 0. Thereafter, the process goes back to *Step 3* again.

   (c) To a lower probability, the intersection of a thermal transfer limit and an SNB surface might be the closest point meeting the OPF constraint Eq. (204). Then, the parameters $\alpha_{i,j}^{\text{account}}$ and β^{account} are set to 0. This is a CP [6, 70–72]. CPs are not of the same relevance for this type of study, where, according to Section 1.3, each surface should be treated individually. Thus, two separate surfaces should be approximated in accordance with Section 2.3.3, with one main exception: Since the point of evaluation, λ_c, is at an SNB, for the thermal limit surface approximation; similar considerations as for CPs needs to be taken – particularly that $F_z = J$ is singular and thus not invertible. Thereafter, the process goes to *Step 4*.

   (d) There are no further surfaces to be found: at all, within the upper bound on numbers of surfaces m to maximally be identified, or within a possible upper bound of distances in load space away from λ_0 to search for operational limit surfaces. Thereafter, the process goes to *Step 5*.

4. At least one thermal limit has been identified, as well as the SNB surface. As for *Step 2* there are two options:

   (a) A thermal limit is reached. Then $\alpha_{i,j}^{\text{account}}$ is set to 0. If this point also lies on an SNB surface, it should be treated as described in sub-point *c)* of *Point 1* and *Point 3*. Thereafter, the process goes to *Step 4*.

   (b) There are no further surfaces to be found: at all, within the upper bound on numbers of surfaces m to maximally be identified, or within a possible upper bound of distances in load space away from λ_0 to search for operational limit surfaces. Thereafter, the process goes to *Step 5*.

5. The process is over. It is now time to start approximating the surfaces found. This is described in Section 2.3.3.

One additional approach that was tried out, but only resulted in longer computation times; was to, besides setting the *account*-parameters to 0 after a surface has been found, update the lower bound of z in Eq. (137) in order to reduce the feasible search space for the solver. Probably it did just make it harder for the solver since it resulted in an even more pronounced non-convexity of the feasible search space than it already was since before.

3.6 Ending discussion

The models presented in the above can however be further improved from the computational point of view. As the model is presented now, the entire Jacobian matrix is computed despite its comparative sparsity. From the viewpoint of an algebraic modeling language like GAMS [67], the set definitions and projections back, from, and onto different sets are nontrivial and due to time constraints of the project, that kind of improvement is not considered within the scope of this report for the actual study.

The need for making use of the sparsity can however be justified both from theory and empirics:

Theory: In [12, p. 330] it is clearly stated that "The use of very efficient sparsity techniques is essential, in order to preserve the computational advantages of optimization over the simpler continuation methods.".

Empirics: Finding the globally closest SNB point in a small fictitious two-node purely static system with one slack bus and one load bus keeping P and Q equal, took with the explicit Jacobian 0.842 seconds, and using sparsity 0.078 seconds. In the explicit Jacobian model, the optimization problem had 47 equations and 48 variables, whereas the model using sparsity had 15 equations and 16 variables.

Optimization methods and continuation methods, briefly treated in the *Theory:* point above are described in more detail in Sections 2.3.2.2 and 2.3.2.3.

4 Study Results

The results of the GAMS model have been verified with appropriate modifications using the IEEE 9-bus system model in Matpower [73].

4.1 Results out of Numerical Studies

The second order approximations of the surfaces presented in this section are all pre-contingency surfaces. Due to space and time limitations, no post-contingency surfaces have been presented here. The procedure is however similar and comparatively straightforward.

For the sake of simplicity, within this report, the case of HBs are not studied. Initial modeling approaches have however proven successful.

4.1.1 IEEE 9-bus test system description, and base-case load flow results

The test system chosen in the numerical case study was the IEEE 9-bus test system [10, Appendix C.1] visualized in Fig. 4. It was chosen in order to comply with [6] and its related work, and because of two other reasons:

1. In a small, technically relevant, but still not trivial system, results are easier to visualize. A small dimension of the load space facilitates debugging and the identification of challenges not expected beforehand. Debugging and challenge identifications are suitable at early stages of long-term research lines. Three load nodes are just right for what the human mind easily can visualize.

2. Last, but not least, the problem sizes are somewhat limited at the stages of model development when the models are not yet optimized from numerical, memory consumption, and algorithmic points-of-view.

The reader should be alert to that a variety of node numberings and system data exist for the IEEE 9-bus test system. Node numbering and system data have been chosen here to comply with the case studies done in [6]. Data regarding the test system is presented in Tables 1 to 5 in Section 4.1.1. Some details from the basic load flow solution at $P_{D,0}$ can be found in Tables 6 to 8 and 19

The data of Tables 1 to 3 are taken from [10, Appendix C.1] except the load bus numbers which are in accordance with [6, Appendix A.2]. The exciter and AVR parameters in Table 4 have the following origins: the exciter limits $E_{f,i}^{\lim}$ (confer for example Eq. (123)) and the reference voltages $U_{\mathrm{ref},i}$ (confer for example Eq. (119)) are taken from [6], whereas the time constant of the exciter, T_e, and the gain of the exciter, K_A, are taken from [10, Appendix C.1]. The thermal power transfer limits $P_{i,j}^{\lim}$ (confer equations Eqs. (140) and (141)) of Table 5 are taken from [6].

The parameter M in Eq. (117) is determined as

$$M = 2 \cdot H, \tag{206}$$

using H of Table 3. Moreover, the voltage is only controlled in the PU (PU) busses according to Table 2 when not considering the dynamic part of the system, that is when merely studying the system as

$$0 = g\left(y\right), \tag{207}$$

whereas, when modeling the system as

$$0 = F\left(z\right), \tag{208}$$

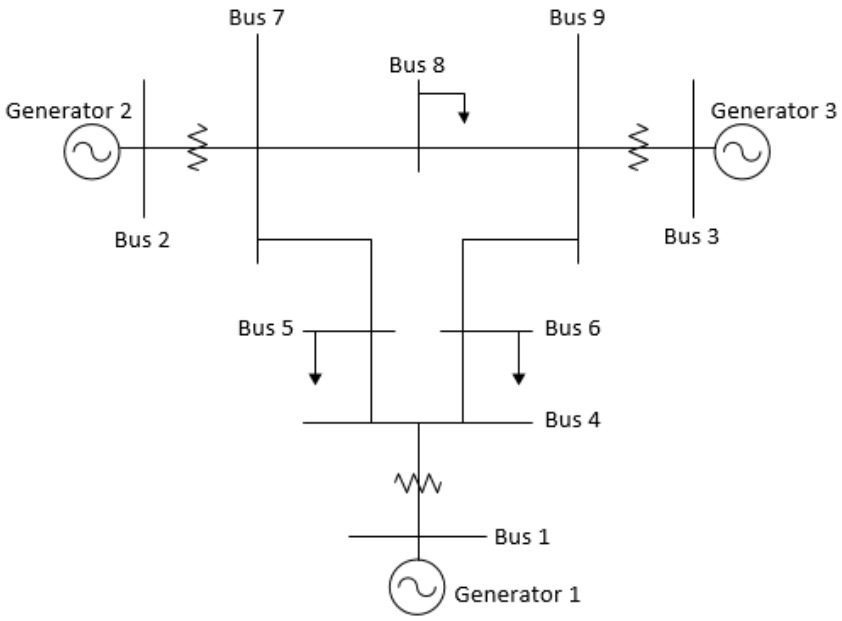

Figure 4: The IEEE 9-bus test system

the resulting voltages when finding the initial steady-state solution, λ_0, is different. The voltages in the initial steady state solution are listed in Table 7, the resulting generation in Table 6, and the active power flows between the busses in the system in Table 8. When AVRs are considered in the stability studies voltage in the slack bus and in the PU busses are instead indirectly controlled by Eqs. (132) and (133).

4.1.2 Obtained operational limit surfaces

In all pictures, the color red denotes the thermal limit on line 4-5, magenta denotes the thermal limit on line 4-6, blue denotes the thermal limit on line 7-8, green denotes the thermal limit on line 5-4, cyan denotes the thermal limit

Table 1: Line data; resistances, reactances, and capacitances. Units: p.u.

Line between busses			R	X	B
4	and	5	0.0100	0.0850	0.176
4	and	6	0.0170	0.0920	0.158
5	and	7	0.0320	0.1610	0.306
6	and	9	0.0390	0.1700	0.358
7	and	8	0.0085	0.0720	0.149
8	and	9	0.0119	0.1008	0.209

Table 2: Bus data. Units: p.u.

Bus	Type	P	Q	U	δ
1	slack	-	-	1.04	0.00
2	PU	1.63	-	1.025	-
3	PU	0.85	-	1.025	-
4	PQ	0.00	0.00	-	-
5	PQ	1.25	0.50	-	-
6	PQ	0.90	0.30	-	-
7	PQ	0.00	0.00	-	-
8	PQ	1.00	0.35	-	-

Table 3: Generator data. Units: p.u.

Generator g	Bus b	$X_{b,g}$	X_d	X'_d	T'_{d0}	H	D
1	4	0.0576	0.1460	0.0608	8.96	23.64	0.02540
2	7	0.0625	0.8958	0.1198	6.00	06.40	0.00660
3	9	0.0586	1.3125	0.1813	5.89	03.01	0.00260

Table 4: Exciter and AVR data. Units: p.u.

Generator g	K_A	T_e	$E_{f,i}^{\lim}$	$U_{\mathrm{ref},i}$
1	20	0.314	2.0	1.1
2	20	0.314	2.2	1.05
3	20	0.314	1.7	1.05

Table 5: Power transfer limits. Units: p.u., base power 100 MVA

Line	Between busses	Limit
1	1 & 4	5.0
2	4 & 5	2.5
3	5 & 7	2.5
4	4 & 6	2.5
5	6 & 9	2.5
6	7 & 8	2.5
7	2 & 7	2.5
8	8 & 9	2.5
9	3 & 9	2.5

Table 6: Resulting generation in the initial steady-state solution at $P_{D,0}$. Units: p.u.

Generator g	P_G	Q_G
1	0.7201	0.4703
2	1.6300	-0.0239
3	0.8500	-0.1170

Table 7: Resulting voltage levels at the initial steady-state solution at $P_{D,0}$. Units: p.u.

Bus b	U
1	1.0443
2	0.9881
3	0.9995
4	1.0192
5	0.9794
6	0.9989
7	0.9950
8	0.9867
9	1.0076

Table 8: Resulting power transfers at the initial steady-state solution at $P_{D,0}$. Units: p.u.

Line	From bus i	To bus j	$P_{i,j}$
1	1	4	3.7961
7	2	7	1.6300
9	3	9	0.8500
1	4	1	-0.7201
2	4	5	0.4117
4	4	6	0.3084
2	5	4	-0.4083
3	5	7	-0.8417
4	6	4	-0.3064
5	6	9	-0.5935
7	7	2	-1.6300
3	7	5	0.8660
6	7	8	0.7640
6	8	7	-0.7590
8	8	9	-0.2410
9	9	3	-0.8500
5	9	6	0.6079
8	9	8	0.2421

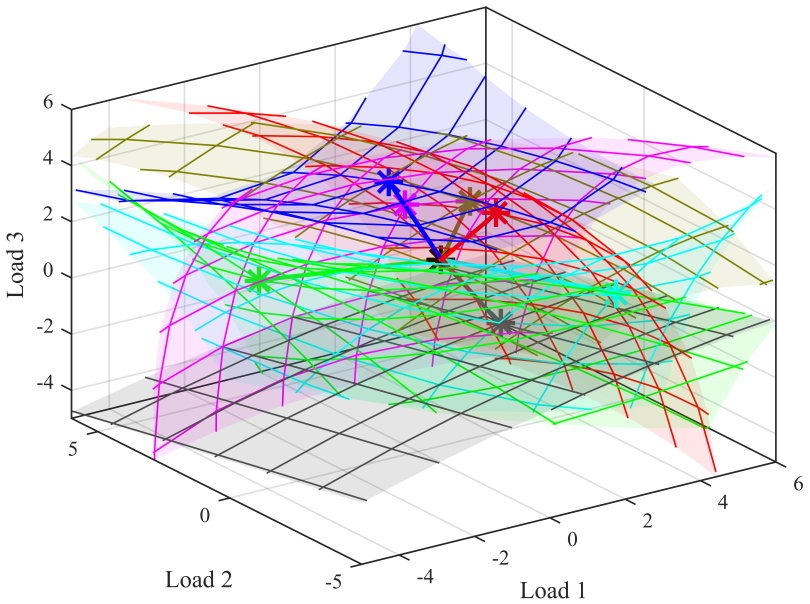

Figure 5: General picture of the 7 first identified and approximated operational limits of the IEEE 9-bus test system

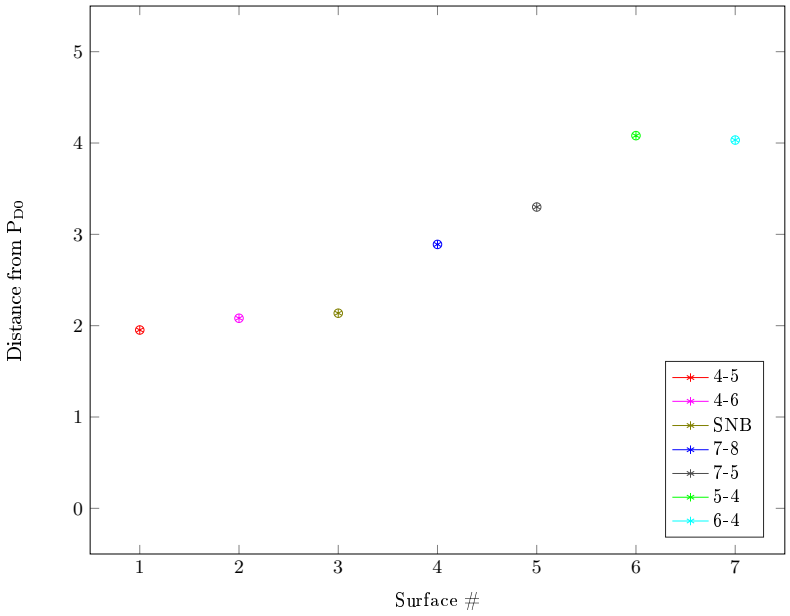

Figure 6: The shortest distances from $P_{D,0}$ to each of the surfaces

on line 6-4, gray denotes the thermal limit on line 7-5, and finally dark yellow denotes the SNB. Moreover, asterisks "*" denote (optimal) load flow solutions. The colored asterisks denote the optimal points, λ_c, obtained by solving the problems of Section 3.4. The black asterisk denotes λ_0, the solution of the present load point.

Each surface is approximated to the second order in load space following the theories presented in Section 2.3.3. The approximations are evaluated around the corresponding closest-point solution points λ_c. The three axes in load space represent the three loads in the IEEE 9-bus test system of Fig. 4, that is; busses 5 (Load 1), 6 (Load 2), and 8 (Load 3). The thick lines connecting black and colored asterisks illustrates the direction and distance of net load change from the present load point, λ_0, to the closest operational limit, λ_c. All the surfaces found are approximated and visualized in Fig. 5.

The shortest distances from the present load point, $\lambda_0 = P_{D0}$ to each of the operational limits are plotted in Fig. 6. The distances are in Fig. 6 plotted in their order of appearance following the method presented in Section 3.5. The respective distances are visualized in Fig. 7 by spheres in the 3-dimensional load space of the IEEE 9-bus test system. All (net-)loads in the plots are given in per-unit (p.u.) on a 100-MVA base.

In the forthcoming subsections, the results of each surface will be treated individually in separate sections. Results will however be interlinked in the embedded analysis, when applicable.

4.1.2.1 Thermal limit of Line 4-5 This is the operation limit closest to the present stable operating point, $P_{D,0}$, or λ_0. The shortest Euclidean distance from $P_{D,0}$ to this limit is 1.9526 p.u., where the particular net loads P_D are presented in Table 9 together with P_G and Q_G. Since the load power factor is

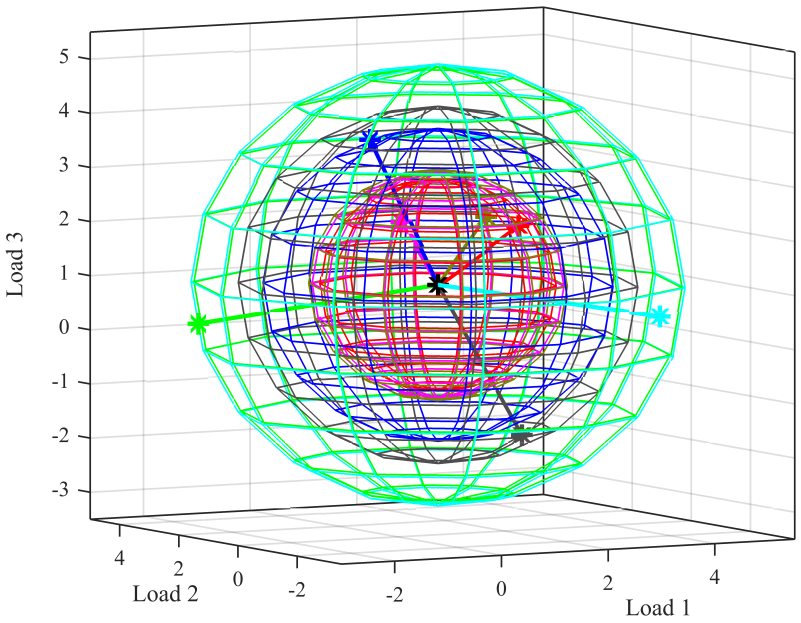

Figure 7: The shortest distances from $P_{D,0}$ to each of the surfaces illustrated in 3-dimensional load space by spheres centered at $P_{D,0}$

kept constant, Q_D is not listed, but can easily be computed from P_D, $P_{D,0}$, and $Q_{D,0}$.

For completion, the bus voltages U at the point of solution are presented in Table 10, and the transferred active powers are presented in Table 11.

In Figs. 13 to 15 the red surface is shown from viewpoints that make it easily identifiable. In Fig. 8 the red sphere illustrates that the optimization method used identified line 4-5 correctly to be the closest surface to encounter.

4.1.2.2 Thermal limit of Line 4-6 This is the operation limit second closest to the present stable operating point, $P_{D,0}$, or λ_0. The shortest Euclidean distance from $P_{D,0}$ to this limit is 2.0815 p.u., where the particular net loads P_D are presented in Table 12 together with P_G and Q_G. Since the load power

Table 9: Resulting loads and generation at the closest point from $P_{D,0}$ to the surface of the busses 4 to 5 (line 2) thermal power transfer limit. Units: p.u.

Load l	P_D	Generator g	P_G	Q_G
5	2.9179	1	3.7961	2.6272
6	1.1903	2	1.6300	0.9400
8	1.9730	3	0.8500	0.5863

Table 10: Resulting voltage levels at the closest point from $P_{D,0}$ to the surface of the busses 4 to 5 (line 2) thermal power transfer limit. Units: p.u.

Bus b	U
1	1.0262
2	0.9452
3	0.9542
4	0.9042
5	0.7716
6	0.8747
7	0.8896
8	0.8585
9	0.9197

Table 11: Resulting power transfers at the closest point from $P_{D,0}$ to the surface of the busses 4 to 5 (line 2) thermal power transfer limit. Units: p.u.

Line	From bus i	To bus j	$P_{i,j}$
1	1	4	3.7961
7	2	7	1.6300
9	3	9	0.8500
1	4	1	- 3.7961
2	4	5	2.4998
4	4	6	1.2963
2	5	4	-2.3975
3	5	7	-0.5204
4	6	4	-1.2609
5	6	9	0.0707
7	7	2	-1.6300
3	7	5	0.5453
6	7	8	1.0847
6	8	7	-1.0710
8	8	9	-0.9020
9	9	3	-0.8500
5	9	6	-0.0673
8	9	8	0.9173

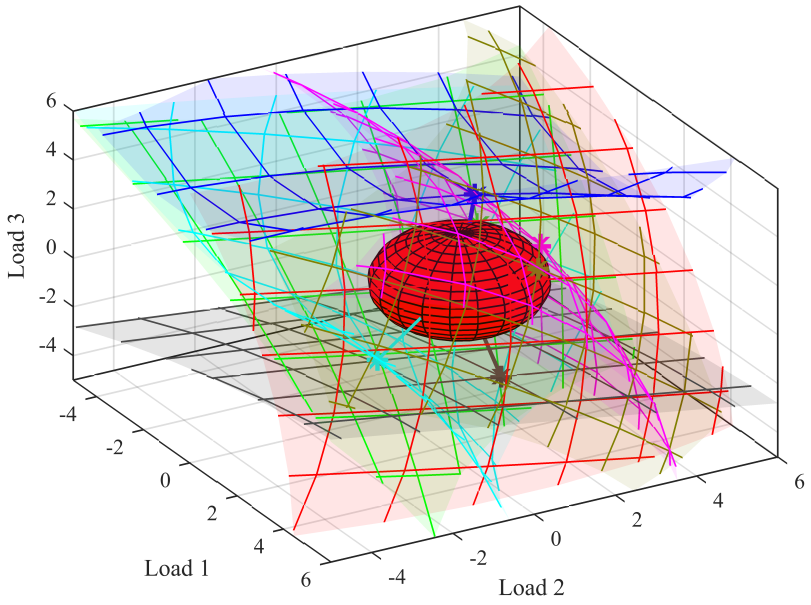

Figure 8: Using a sphere to illustrate that no other closest points are closer to $\lambda_0 = P_{D,0}$ than the one of thermal limit 4-5. Focus is set on the two subsequent closest points representing thermal limit 4-6 and the single node bifurcation (SNB)

Table 12: Resulting loads and generation at the closest point from $P_{D,0}$ to the surface of the busses 4 to 6 (line 4) thermal power transfer limit. Units: p.u.

Load l	P_D	Generator g	P_G	Q_G
5	1.5675	1	4.0231	2.7684
6	2.7122	2	1.6300	0.8340
8	1.9735	3	0.8500	0.7629

Table 13: Resulting voltage levels at the closest point from $P_{D,0}$ to the surface of the busses 4 to 6 (line 4) thermal power transfer limit. Units: p.u.

Bus b	U
1	1.0248
2	0.9501
3	0.9421
4	0.8981
5	0.8492
6	0.7709
7	0.9016
8	0.8547
9	0.8962

factor is kept constant, Q_D is not listed, but can easily be computed from P_D, $P_{D,0}$, and $Q_{D,0}$.

For completion, the bus voltages U at the point of solution are presented in Table 13, and the transferred active powers are presented in Table 14.

The front picture of thermal limit 4-6 surface is illustrated in Fig. 9, whereas the backside picture of the same surface can be found in Fig. 10. This surface turned out to be easy to illustrate without extreme twisting of the viewing axes in load space.

4.1.2.3 The SNB This is the operation limit third closest to the present stable operating point, $P_{D,0}$, or λ_0. The shortest Euclidean distance from $P_{D,0}$ to this limit is 2.1365 p.u., where the particular net loads P_D are presented in Table 15 together with P_G and Q_G. Since the load power factor is kept constant, Q_D is not listed, but can easily be computed from P_D, $P_{D,0}$, and $Q_{D,0}$.

For completion, the bus voltages U at the point of solution are presented in Table 16, and the transferred active powers are presented in Table 17. It is noteworthy that the thermal limit on Line 2, from bus 4 to bus 5 has been violated here.

It should be noted that in the pre-contingency cases studied in [6, Chapter 7], no SNB where found as part of that stability surface. That can be explained by two main differences between the study made there and the one of this report:

Table 14: Resulting power transfers at the closest point from $P_{D,0}$ to the surface of the busses 4 to 6 (line 4) thermal power transfer limit. Units: p.u.

Line	From bus i	To bus j	$P_{i,j}$
1	1	4	4.0231
7	2	7	1.6300
9	3	9	0.8500
1	4	1	-4.0231
2	4	5	1.5234
4	4	6	2.4998
2	5	4	-1.4920
3	5	7	-0.0756
4	6	4	-2.3408
5	6	9	-0.3714
7	7	2	-1.6300
3	7	5	0.0788
6	7	8	1.5512
6	8	7	-1.5233
8	8	9	-0.4502
9	9	3	-0.8500
5	9	6	0.3952
8	9	8	0.4548

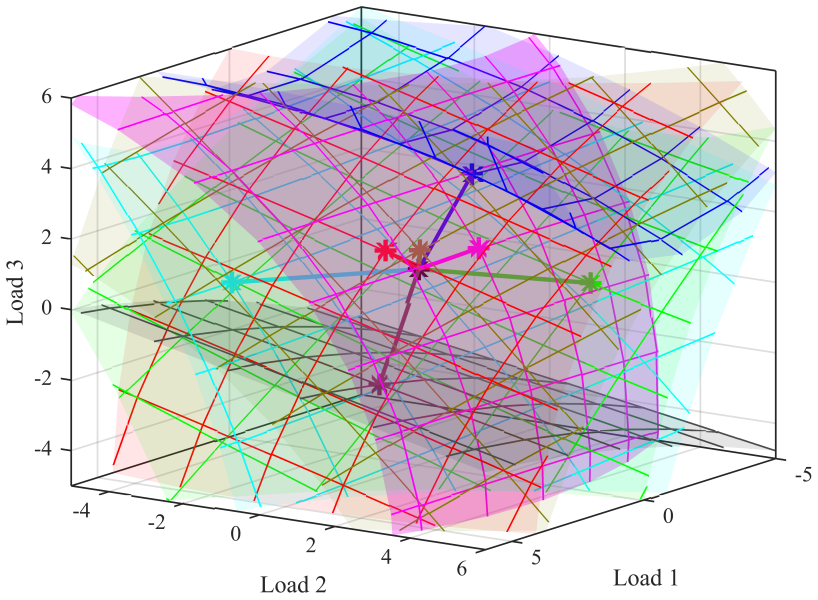

Figure 9: The surface of the thermal limit 4-6 from the front

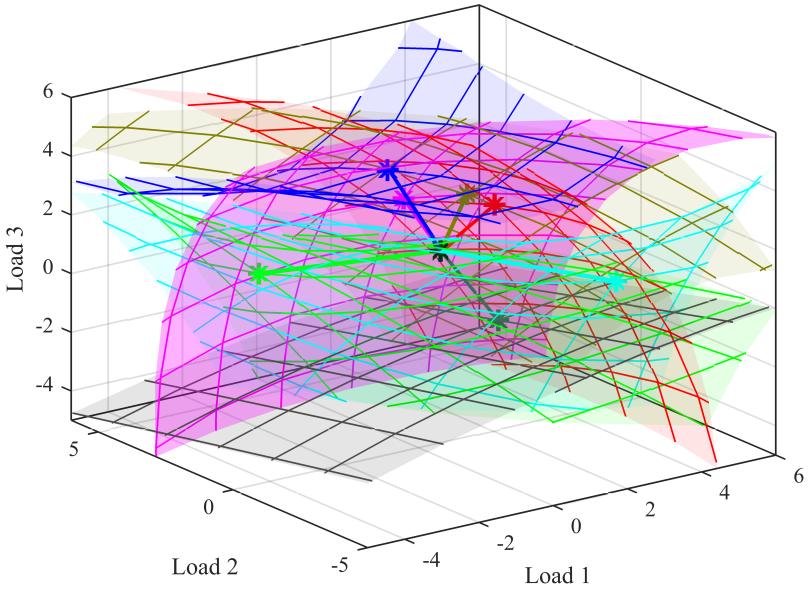

Figure 10: The surface of the thermal limit 4-6 from behind

Table 15: Resulting loads and generation at the closest point from $P_{D,0}$ to the surface of the SNB. Units: p.u.

Load l	P_D	Generator g	P_G	Q_G
5	2.7505	1	4.7095	4.6571
6	1.9785	2	1.6300	1.5109
8	2.0724	3	0.8500	1.1334

Table 16: Resulting voltage levels at the closest point from $P_{D,0}$ to the surface of the SNB. Units: p.u.

Bus b	U
1	1.0105
2	0.9176
3	0.9154
4	0.7919
5	0.6413
6	0.7058
7	0.8222
8	0.7779
9	0.8446

Table 17: Resulting power transfers at the closest point from $P_{D,0}$ to the SNB surface. Units: p.u.

Line	From bus i	To bus j	$P_{i,j}$
1	1	4	4.7095
7	2	7	1.6300
9	3	9	0.8500
1	4	1	-4.7095
2	4	5	2.5850
4	4	6	2.1245
2	5	4	-2.4375
3	5	7	-0.3129
4	6	4	-1.9894
5	6	9	0.0110
7	7	2	-1.6300
3	7	5	0.3538
6	7	8	1.2762
6	8	7	-1.2533
8	8	9	-0.8191
9	9	3	-0.8500
5	9	6	0.0150
8	9	8	0.8350

1. In that study, only the first operation limit encountered was considered and made part of the aggregated stability surface. In this report, many different surfaces are considered individually, also if one is encountered beyond the other when that is physically relevant and feasible.

2. This study is limited to considering a smaller number of SL-types compared to the study in [6, Chapter 7]. Besides thermal limits, in the study of [6, Chapter 7] one SLL was identified, as well as two HB surfaces belonging to different control modes of the AVRs.

   a) In the initial limited study of this report, the switching of control modes of AVRs are disregarded.

   b) In the initial limited study of this report, HBs are disregarded.

   so since these surfaces were ignored in the numerical study of this report, the SNB could be found in the pre-contingency case.

Bearing in mind that ϵ in Eq. (202) is set to equal 10^{-4}, the resulting eigenvalues identified as belonging to the SNB might be of interest to analyze. The eigenvalue of J with the smallest attainable absolute value (modulus) closest to $\lambda_0 = P_{D,0}$ was with the local LINDO solver $-1.0014 \cdot 10^{-4}$. From a practical point of view, this must be considered close-enough. Lower values of ϵ could be used, but its numerical implications need to be evaluated. A bit peculiar from the numerical point of view, was that with the models and methods used in this study, smaller values than $-1.0014 \cdot 10^{-4}$ of the eigenvalues were not possible to

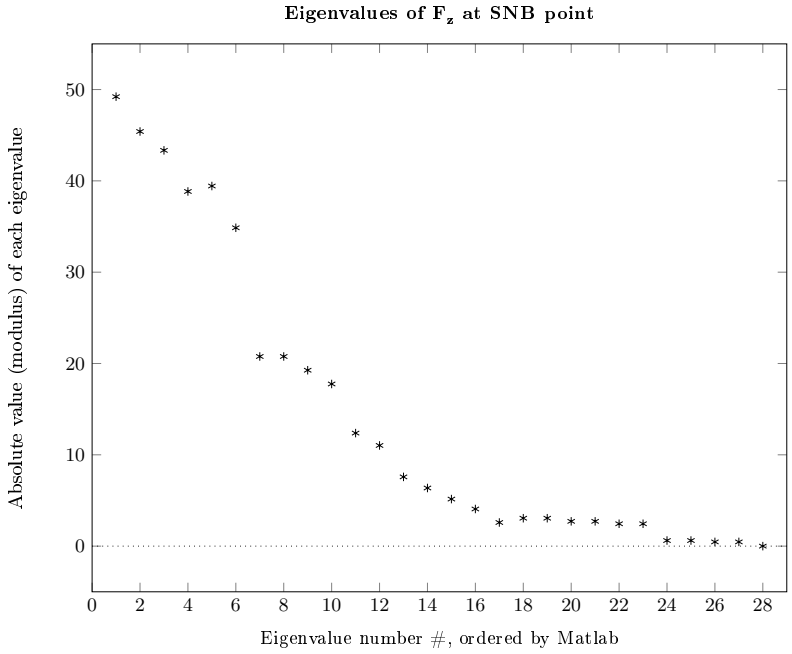

Figure 11: The absolute values (moduli) of the eigenvalues of $J = F_z$ at the identified SNB point closest to $P_{D,0}$

obtain. Using the global LINDO solver, the value obtained was $1.0016 \cdot 10^{-4}$, for a significantly longer computation time. Due to time constraints, not many alternative formulations of the SNB-identification constraints besides the one presented in Section 3.4.6 have been evaluated.

In Fig. 11, the moduli of the eigenvalues of $J = F_z$ are depicted. Their order of appearance is related to the MATrix LABoratory (MATLAB) command `eig`. It is clear that the 28th eigenvalue is the one related to the SNB. In Fig. 12, the same eigenvalues of $J = F_z$ are plotted in the complex plane, $\mathbb{C}$. The SNB-related eigenvalue is easily identified, as it is located in the origin. Since HB were not sought for in this study, no analysis of the eigenvalues of A has been made.

In Fig. 13 one can see that the SNB point is slightly beyond the thermal limit of line 4-5. That is confirmed in the numerical results of Table 17 by the red figures. Moreover, one can see that the SNB surface and the surface of the thermal limit of line 4-5 intersect each other. In cases when the SNB surface is fully on the inner side of a thermal limit, that thermal limit can and will never be reached. The intersection of the SNB and line 4-5 thermal limit surfaces is further illustrated in Fig. 14. In the view of Fig. 13 it is clear that the thermal limit's surface is inside the SNB's surface for higher values of $P_{D,5}$ and $P_{D,6}$, whereas for lower values of $P_{D,5}$ and $P_{D,6}$ (and higher values of $P_{D,9}$) the SNB's surface is inside the thermal limit's surface.

An alternative way of illustrating that the closest SNB point is further away from $P_{D,0}$ than the closest 4-5 point, is in Fig. 15. In that figure, a sphere with the same radius as the distance to the closest SNB point has been inserted.

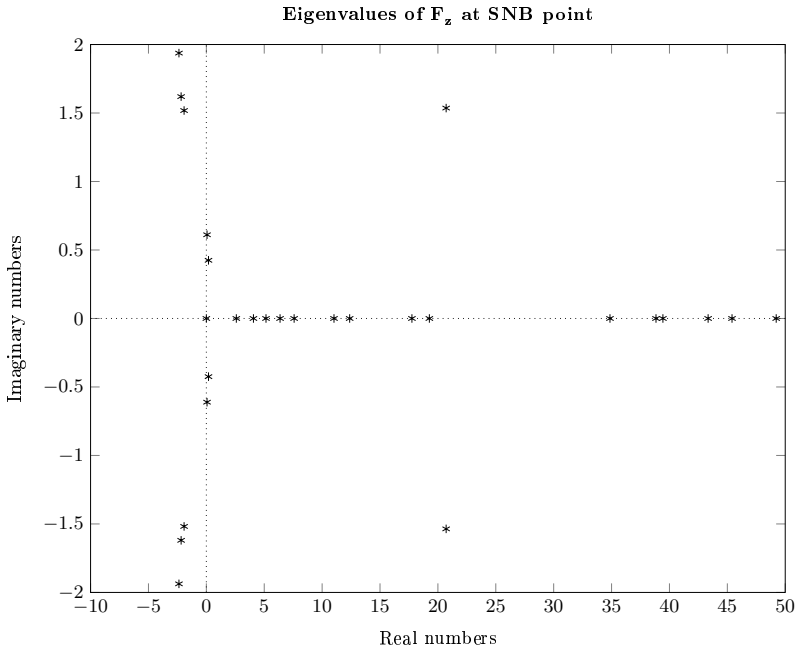

Figure 12: The complex-valued eigenvalues of $J = F_z$ at the identified SNB point closest to $P_{D,0}$

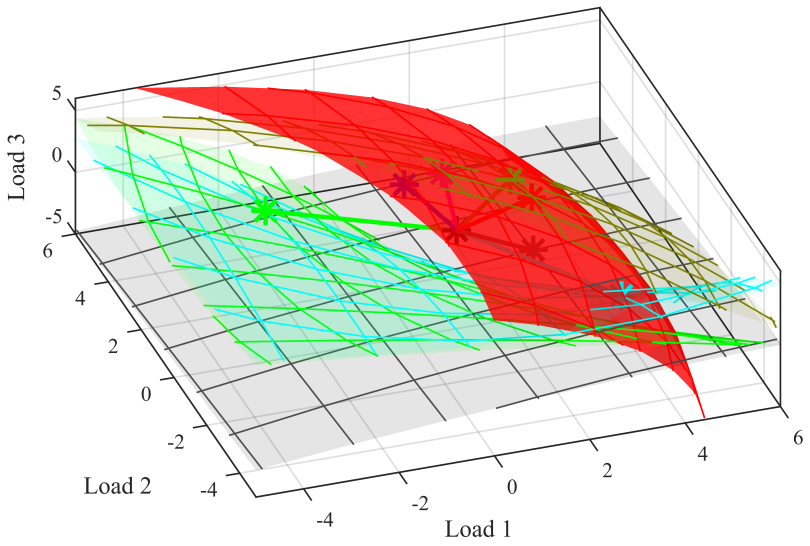

Figure 13: Illustrating that the closest SNB point is slightly beyond the closest thermal limit of line 4-5, and that their corresponding surfaces intersect

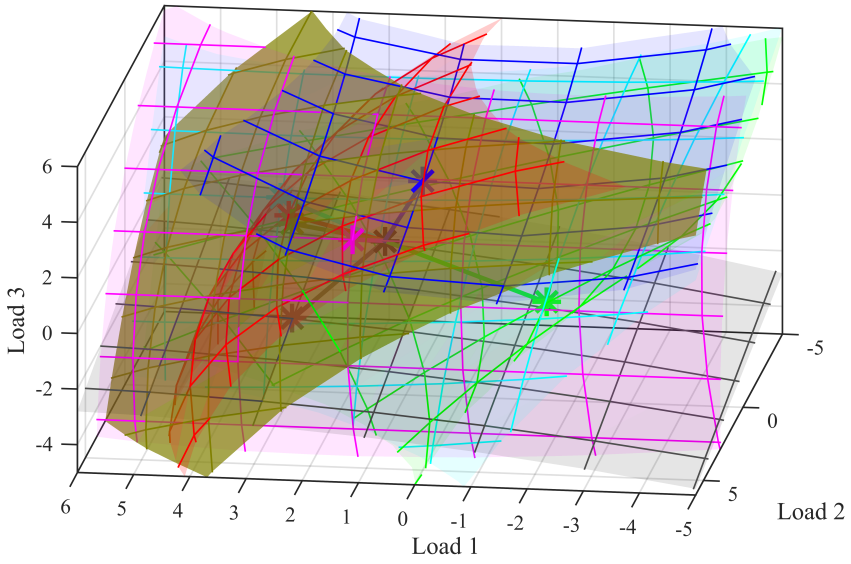

Figure 14: Illustrating the SNB surface intersecting the surface of the thermal limit of line 4-5

That sphere surpasses the 4-5 surface exactly in the area where the closest 4-5 point is located. It should be noted that parts of the 4-5 asterisk poke out of the sphere on the Load 1-side of Fig. 15.

In a similar way, it is illustrated in Fig. 16 that the closest SNB point is further away from $P_{D,0}$ than the closest 4-6 point. Also in this case the difference is small, actually so small

$$2.1365 - 2.0815 = 0.0550 \tag{209}$$

that only the outer parts of the 4-6 asterisk are visible.

4.1.2.4 Thermal limit of Line 7-8 This is the operation limit fourth closest to the present stable operating point, $P_{D,0}$, or λ_0. The shortest Euclidean distance from $P_{D,0}$ to this limit is 2.8897 p.u., where the particular net loads P_D are presented in Table 18 together with P_G and Q_G. Since the load power factor is kept constant, Q_D is not listed, but can easily be computed from P_D, $P_{D,0}$, and $Q_{D,0}$.

For completion, the bus voltages U at the point of solution are presented in Table 19, and the transferred active powers are presented in Table 20.

The surface of the thermal limit 7-8 is illustrated in Fig. 17, where it is located high up in the third dimension of load space, that is for high positive values of $P_{D,8}$. The surface approximation is above most of the other surface approximations in most of load space, except for low loads in bus 5 (that is, Load 1) where the thermal limit 4-5 surface approximation lies above the thermal limit 7-8 surface. For high values of load in bus 6 (that is Load 2) and low values of load in bus 5 (that is Load 1), the thermal limit 5-4 surface approximation exceeds the thermal limit 7-8 surface approximation, and for low or negative

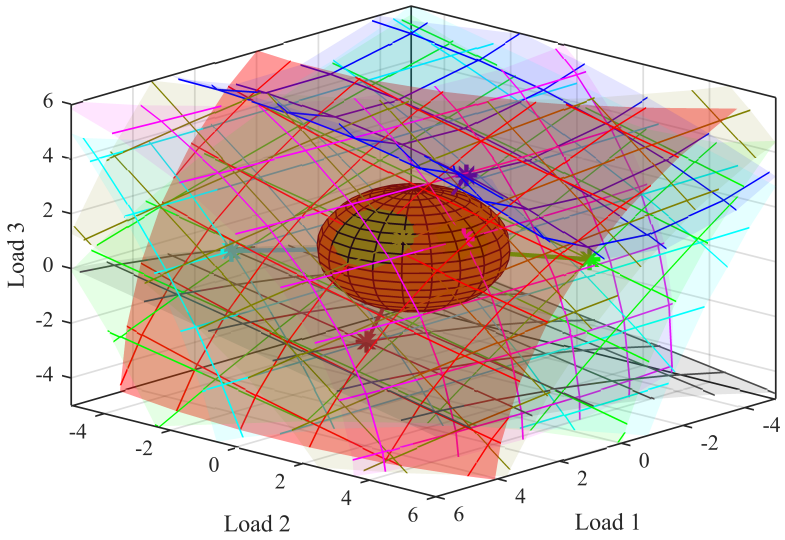

Figure 15: Illustrating that the closest SNB point is slightly further away from $P_{D,0}$ than the closest point of the thermal limit of line 4-5

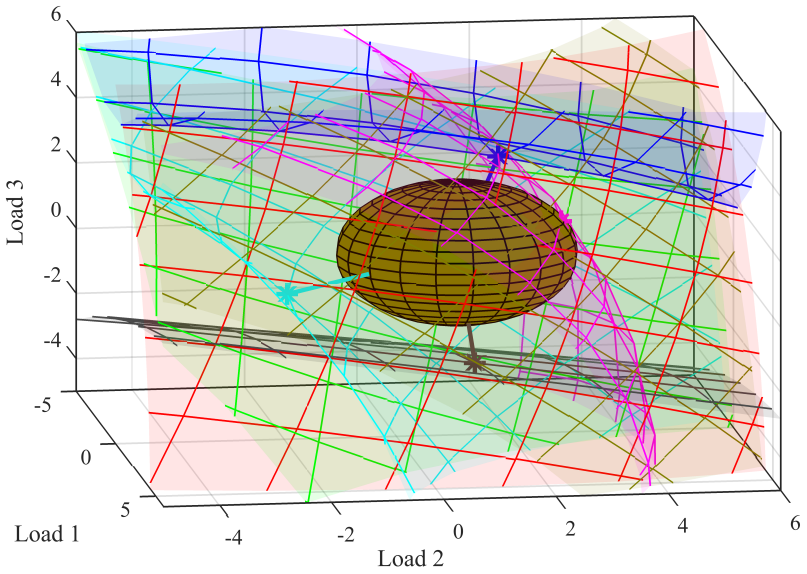

Figure 16: Illustrating that the closest SNB point is slightly further away from $P_{D,0}$ than the closest point of the thermal limit of line 4-6

Table 18: Resulting loads and generation at the closest point from $P_{D,0}$ to the surface of the busses 7 to 8 (line 6) thermal power transfer limit. Units: p.u.

Load l	P_D	Generator g	P_G	Q_G
5	0.4441	1	3.8777	3.1487
6	1.7467	2	1.6300	2.3173
8	3.6427	3	0.8500	1.8121

Table 19: Resulting voltage levels at the closest point from $P_{D,0}$ to the surface of the busses 7 to 8 (line 6) thermal power transfer limit. Units: p.u.

Bus b	U
1	1.0225
2	0.8751
3	0.8615
4	0.8729
5	0.8055
6	0.7305
7	0.7190
8	0.5495
9	0.7405

Table 20: Resulting power transfers at the closest point from $P_{D,0}$ to the surface of the busses 7 to 8 (line 6) thermal power transfer limit. Units: p.u.

Line	From bus i	To bus j	$P_{i,j}$
1	1	4	3.8777
7	2	7	1.6300
9	3	9	0.8500
1	4	1	-3.8777
2	4	5	1.3922
4	4	6	2.4855
2	5	4	-1.3615
3	5	7	0.9173
4	6	4	-2.3118
5	6	9	0.5652
7	7	2	-1.6300
3	7	5	-0.8698
6	7	8	2.4998
6	8	7	-2.3382
8	8	9	-1.3046
9	9	3	-0.8500
5	9	6	-0.5408
8	9	8	1.3908

values combined of loads in buses 5 and 6 (Load 1 and 2), the thermal limit 7-8 surface approximation lies above the thermal limit 7-8 surface approximation in the dimension of load in bus 8. Finally, the SNB surface approximation seems related to the thermal limit 7-8 surface approximations like a compromise between the thermal limit 4-5 surface approximation and the thermal limit 7-8 surface approximation.

The surface of the thermal limit 7-8 is illustrated in Fig. 18 to droop in the bus 8 load direction for large loads in bus 6 and no net load in bus 5. Moreover, the graph shows that the curvature in bus 5 load direction is also increasing for large loads in bus 6.

4.1.2.5 Thermal limit of Line 7-5 This is the operation limit fifth closest to the present stable operating point, $P_{D,0}$, or λ_0. The shortest Euclidean distance from $P_{D,0}$ to this limit is 3.2991 p.u., where the particular net loads P_D are presented in Table 21 together with P_G and Q_G. Since the load power factor is kept constant, Q_D is not listed, but can easily be computed from P_D, $P_{D,0}$, and $Q_{D,0}$.

For completion, the bus voltages U at the point of solution are presented in Table 22, and the transferred active powers are presented in Table 23.

The most plane-like surface encountered within this study is the thermal limit 7-5 surface, depicted in Fig. 19. Comparatively large amounts of net power generation (that is, negative net loads) in bus 8 in the IEEE 9-bus test system is needed for this thermal limit to be reached according to the second

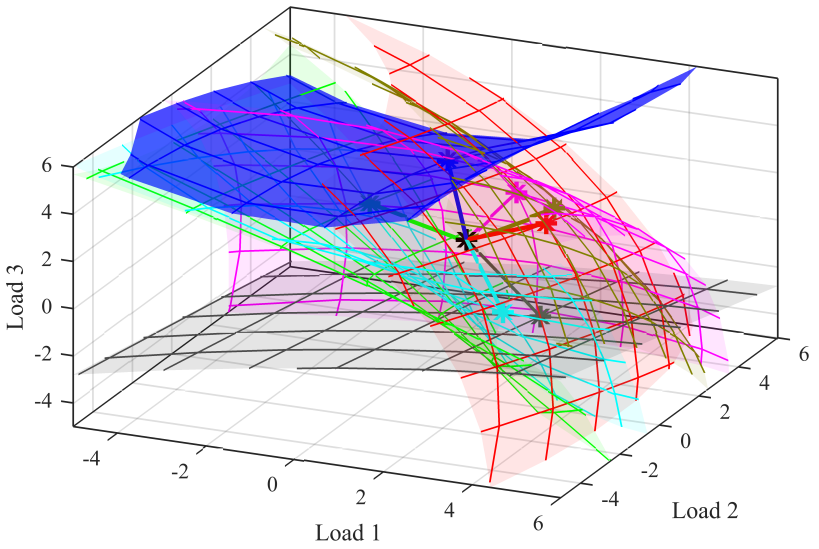

Figure 17: Illustrating that the thermal limit 7-8 surface is located high up in the $P_{D,8}$ dimension in load space above the other surface approximations with some exceptions.

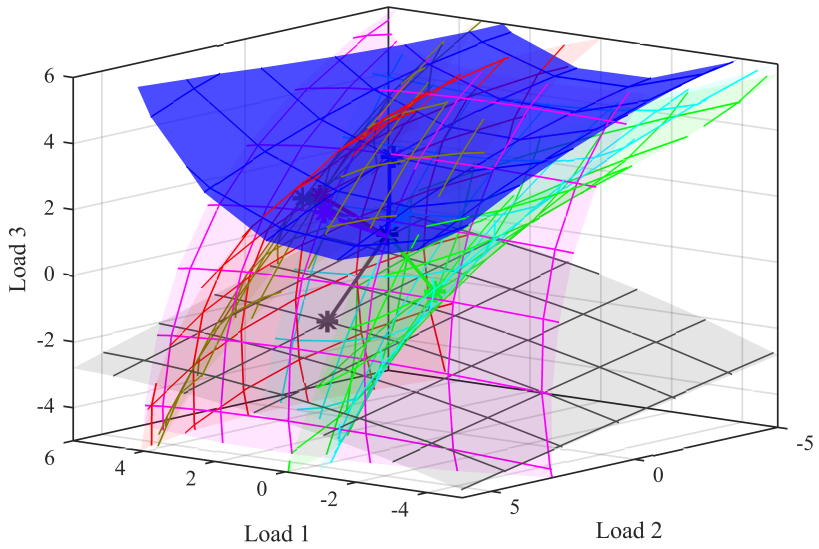

Figure 18: Illustrating that the the thermal limit 7-8 surface approximation is quite flat, but drooping downward in $P_{D,8}$ direction

Table 21: Resulting loads and generation at the closest point from $P_{D,0}$ to the surface of the busses 7 to 5 (line 3) thermal power transfer limit. Units: p.u.

Load l	P_D	Generator g	P_G	Q_G
5	2.8733	1	0.0000	2.0698
6	0.9934	2	1.6300	0.4939
8	-1.8706	3	0.8500	0.1345

Table 22: Resulting voltage levels at the closest point from $P_{D,0}$ to the surface of the busses 7 to 5 (line 3) thermal power transfer limit. Units: p.u.

Bus b	U
1	1.0337
2	0.9655
3	0.9838
4	0.9184
5	0.7694
6	0.8906
7	0.9395
8	0.9966
9	0.9771

Table 23: Resulting power transfers at the closest point from $P_{D,0}$ to the surface of the busses 7 to 5 (line 3) thermal power transfer limit. Units: p.u.

Line	From bus i	To bus j	$P_{i,j}$
1	1	4	0.0000
7	2	7	1.6300
9	3	9	0.8500
1	4	1	0.0000
2	4	5	0.6790
4	4	6	-0.6790
2	5	4	-0.6453
3	5	7	-2.2280
4	6	4	-0.6921
5	6	9	-1.6855
7	7	2	-1.6300
3	7	5	2.4997
6	7	8	-0.8697
6	8	7	0.8807
8	8	9	0.9899
9	9	3	-0.8500
5	9	6	1.8280
8	9	8	-0.9780

order approximation curve.

With the help of the sphere associated to the distance to the closest thermal limit 7-5 point, one can graphically confirm that only two more identified surfaces, remain to be investigated. This is shown in Fig. 20. These two remaining surfaces are the ones associated to the thermal limit 5-4 and the thermal limit 6-4.

4.1.2.6 Thermal limit of Line 5-4 This is the operation limit sixth closest (and the one second furthest away within the scope of this study) to the present stable operating point, $P_{D,0}$, or λ_0. The shortest Euclidean distance from $P_{D,0}$ to this limit is 4.0342 p.u., where the particular net loads P_D are presented in Table 24 together with P_G and Q_G. Since the load power factor is kept constant, Q_D is not listed, but can easily be computed from P_D, $P_{D,0}$, and $Q_{D,0}$.

For completion, the bus voltages U at the point of solution are presented in Table 25, and the transferred active powers are presented in Table 26.

Since the point associated to the line 5-4 thermal constraint with the shortest distance to $P_{D,0}$ was located quite far away from $\lambda_0 = P_{D,0}$ (negative net loads in busses 5 and 6) in load space, many of the other surface approximations were removed from Fig. 21 in order to visualize the point of shortest distance.

By the help of a sphere centered at $P_{D,0}$ with the radius of the shortest distance from $P_{D,0}$ to the thermal limit of the line 5-4, Fig. 22 shows similarities in distances of surfaces line 5-4 and the line 6-4.

With Fig. 23, the intention is to visualize the approximated line 5-4 surface.

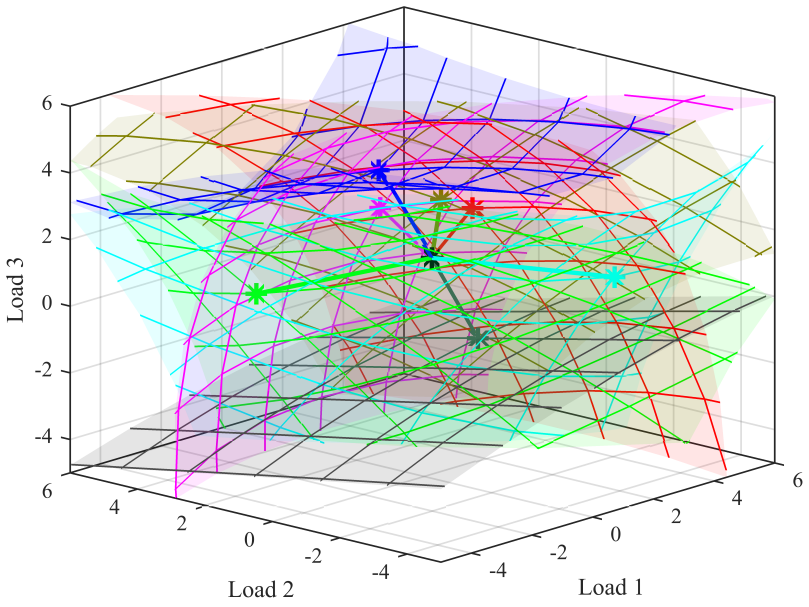

Figure 19: Illustrating that the thermal limit 7-5 surface is located slightly tilted deep down in the $P_{D,8}$ dimension in load space below the other surfaces with some exceptions.

Table 24: Resulting loads and generation at the closest point from $P_{D,0}$ to the surface of the busses 5 to 4 (line 2) thermal power transfer limit. Units: p.u.

Load l	P_D	Generator g	P_G	Q_G
5	-1.9642	1	0.0000	3.9879
6	3.2111	2	1.6300	0.7299
8	0.2331	3	0.8500	1.5125

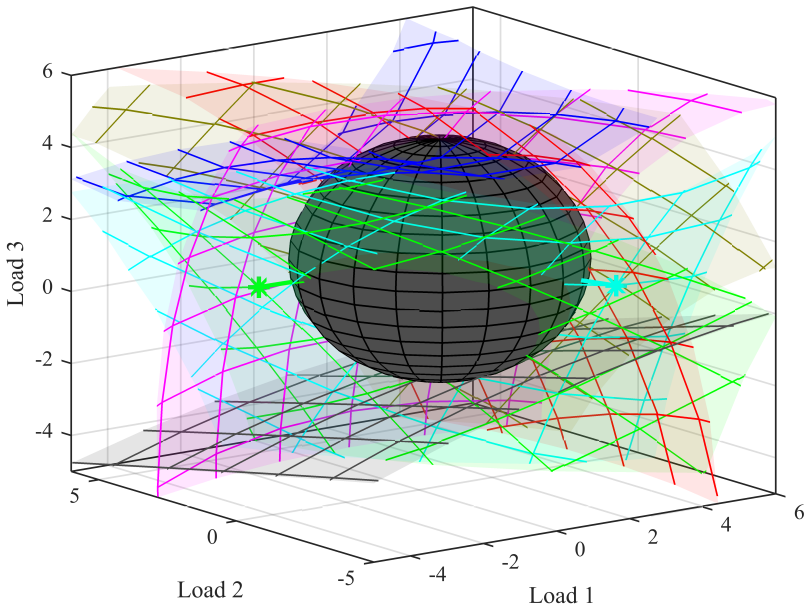

Figure 20: Graphically confirming with the help of the sphere that the closest thermal limit 7-5 point is further out than all but two of the other found and identified closest limit points

Table 25: Resulting voltage levels at the closest point from $P_{D,0}$ to the surface of the busses 5 to 4 (line 2) thermal power transfer limit. Units: p.u.

Bus b	U
1	1.0204
2	0.9549
3	0.8863
4	0.7953
5	0.8854
6	0.4040
7	0.9134
8	0.8579
9	0.7882

Table 26: Resulting power transfers at the closest point from $P_{D,0}$ to the surface of the busses 5 to 4 (line 2) thermal power transfer limit. Units: p.u.

Line	From bus i	To bus j	$P_{i,j}$
1	1	4	0.0000
7	2	7	1.6300
9	3	9	0.8500
1	4	1	0.0000
2	4	5	-2.4074
4	4	6	2.4074
2	5	4	2.4998
3	5	7	-0.5355
4	6	4	-1.9368
5	6	9	-1.2742
7	7	2	-1.6300
3	7	5	0.5473
6	7	8	1.0827
6	8	7	-1.0668
8	8	9	0.8337
9	9	3	-0.8500
5	9	6	1.6678
8	9	8	-0.8178

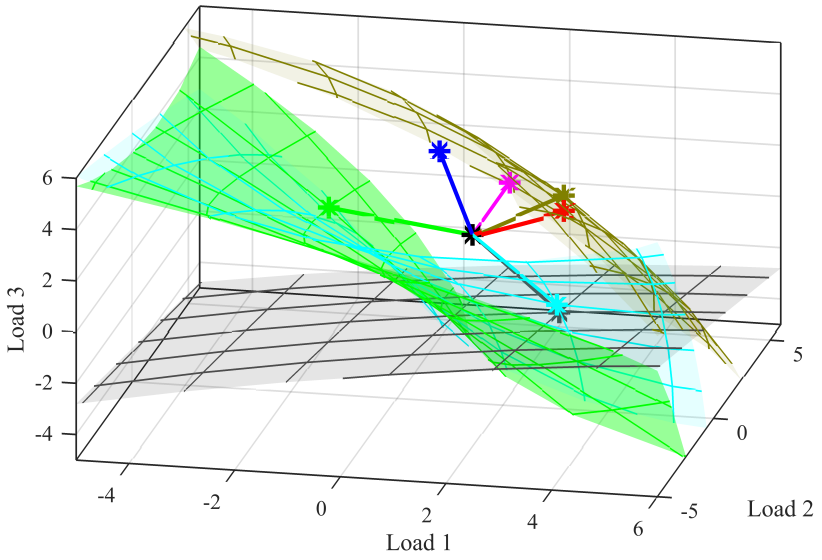

Figure 21: Visualizing the closest point on the surfaces of the thermal limit of line 5-4 by removing some other surfaces from the plot

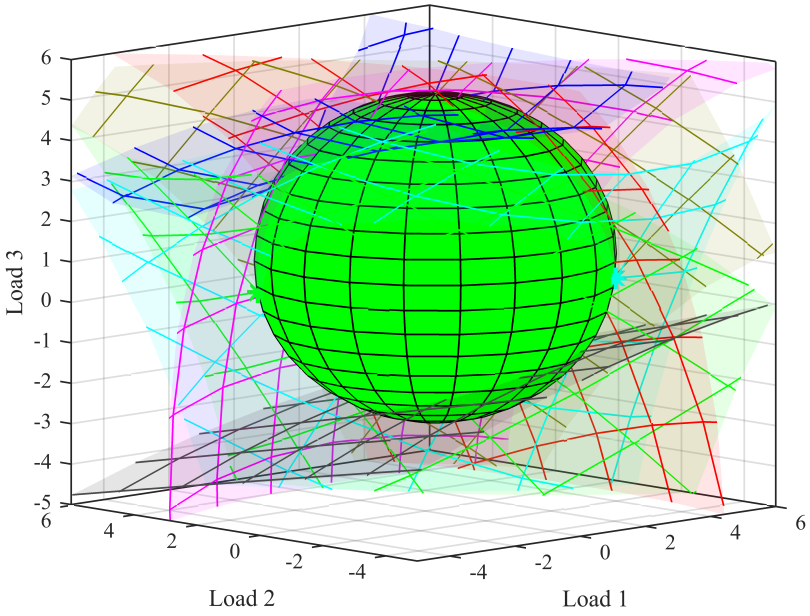

Figure 22: Visualizing the similar distances of the closest points on the surfaces of the thermal limit of the line 5-4 and the line 6-4 with the help of a sphere

The approximated surface is shaped as an arc, almost a quarter of a circle for net loads of -5 p.u. in bus 8, in the Load 1-Load 2-plane defined by busses 5 and 6, raising in the bus 8 dimension for further decreased net loads in busses 5 and 6. The surface of the 6-4 thermal limit looks quite similar but is slightly shifted in the bus 5-bus 6 plane as further discussed in Section 4.1.2.7.

4.1.2.7 Thermal limit of Line 6-4 This is the operation limit seventh closest (and the one furthest away within the scope of this study) to the present stable operating point, $P_{D,0}$, or λ_0. The shortest Euclidean distance from $P_{D,0}$ to this limit is 4.0808 p.u., where the particular net loads P_D are presented in Table 27 together with P_G and Q_G. Since the load power factor is kept constant, Q_D is not listed, but can easily be computed from P_D, $P_{D,0}$, and $Q_{D,0}$.

For completion, the bus voltages U at the point of solution are presented in Table 28, and the transferred active powers are presented in Table 29.

Firstly, a peculiarity worth pointing out, clearly viewed in Fig. 24 it is the similarities between the surfaces representing the thermal limit of power flowing from bus 6 to 4 and the one for bus 5 to 4.

Another view illustrating the similarity between and complementarity of the surfaces of the thermal limit of line 6-4 and the one of line 5-4 but from another viewpoint is Fig. 25. In Fig. 25 it is visible that the line 6-4 surface is closer to $P_{D,0}$ when net loads in bus 5 are positive and net loads in bus 6 drops towards negative values. Conversely, Fig. 25 shows that the line 5-4 surface is closer to $P_{D,0}$ when net loads in bus 6 are positive, and net loads in bus 5 drops towards

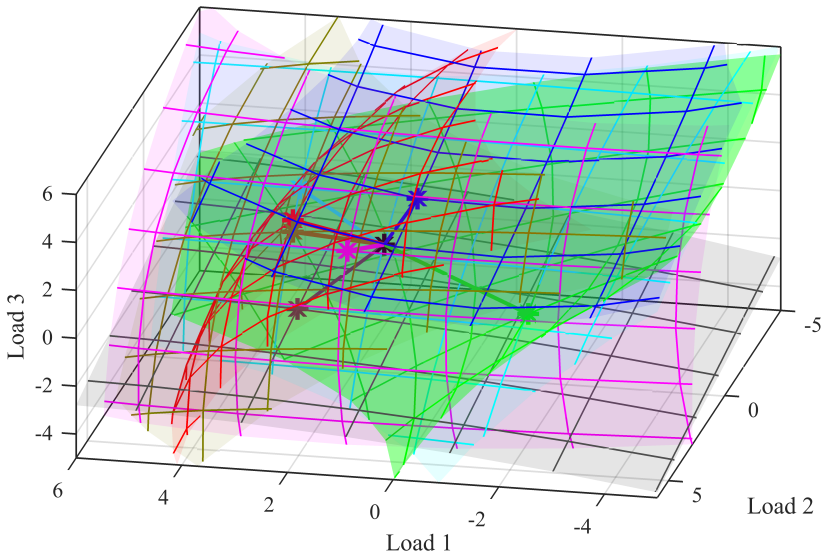

Figure 23: Visualizing the surface of the thermal limit of the line 5-4

Table 27: Resulting loads and generation at the closest point from $P_{D,0}$ to the surface of the busses 6 to 4 (line 4) thermal power transfer limit. Units: p.u.

Load l	P_D	Generator g	P_G	Q_G
5	3.5580	1	0.0000	3.8263
6	-2.4437	2	1.6300	1.6376
8	0.6181	3	0.8500	0.5182

Table 28: Resulting voltage levels at the closest point from $P_{D,0}$ to the surface of the busses 6 to 4 (line 4) thermal power transfer limit. Units: p.u.

Bus b	U
1	1.0216
2	0.9112
3	0.9588
4	0.8058
5	0.4676
6	0.9231
7	0.8066
8	0.8478
9	0.9286

Table 29: Resulting power transfers at the closest point from $P_{D,0}$ to the surface of the busses 6 to 4 (line 4) thermal power transfer limit. Units: p.u.

Line	From bus i	To bus j	$P_{i,j}$
1	1	4	0.0000
7	2	7	1.6300
9	3	9	0.8500
1	4	1	0.0000
2	4	5	2.3531
4	4	6	-2.3531
2	5	4	-2.0915
3	5	7	-1.4665
4	6	4	2.4998
5	6	9	-0.0561
7	7	2	-1.6300
3	7	5	1.7877
6	7	8	-0.1577
6	8	7	0.1606
8	8	9	-0.7787
9	9	3	-0.8500
5	9	6	0.0561
8	9	8	0.7938

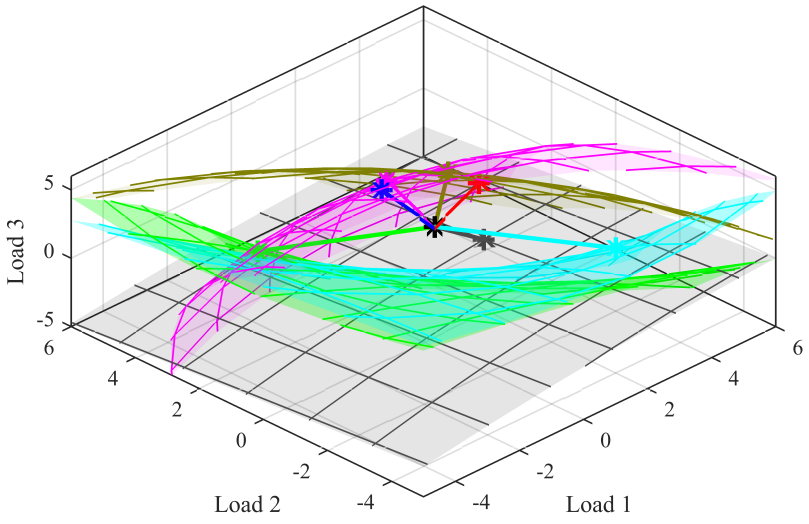

Figure 24: Visualizing the similarities between the surfaces of the thermal limit of line 6-4 and the one of line 5-4

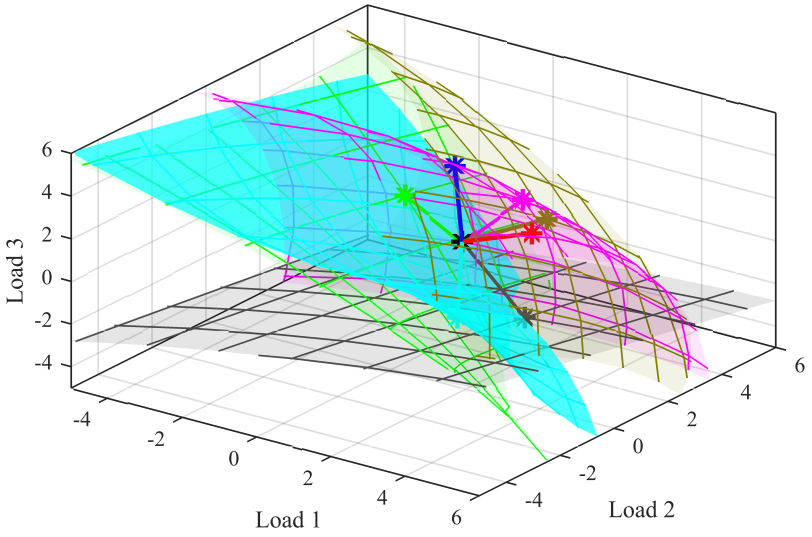

Figure 25: Visualizing the symmetric similarities between and the complementarity of the surfaces of the thermal limit of line 6-4 and the one of line 5-4

negative values.

Recalling the topography of the IEEE 9-bus test system in Fig. 4, the symmetry between the lines 2 (busses 4 and 5) and 4 (busses 4 and 6) with respect to the slack bus (bus 1) and the similarly (but not identically) controlled PU busses, the results are reasonable. Moreover, recalling from for example Table 2 that generator 2 has a higher level of generation than generator 3, one can explain why surface 5-4 is slightly closer to $P_{D,0}$ in load space than surface 6-4. The net load in bus 5 needs to be less negative to reach the limit than the net load in bus 6 has to be. This is because the generator in node 2 is "helping" the load in bus 5 more than the generator in bus 3 is helping the load in bus 6.

In Fig. 26, the transparency levels of the surface approximation of line 6-4 has been increased in order to make the asterisk indicating the closest load point of the thermal limit of line 6-4 easily visible.

4.1.3 On the usability of second order approximations

In [6, Chapter 7.4], it was demonstrated that the second order approximations and the distance function, as defined in that publication, resulted in small errors compared to reality for the pre-contingency case study. That study differs however from the one of this report in two relevant aspects:

- Only the first encountered operational limit was considered.
- The search for surfaces and limits was only done in the positive eighth of the three-dimensional net-load space. That means that negative net-loads were not considered. Such would represent large amounts of uncontrollable power production, or possible storage systems discharging on the consumer side.

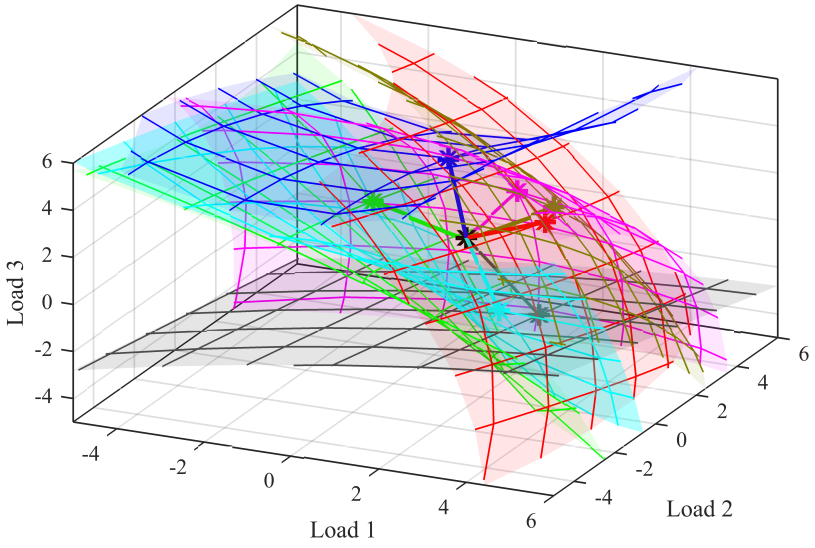

Figure 26: Visualizing the closest load point of the thermal limit of line 6-4 with respect to $P_{D,0}$

Some indications have been found in this early study that suggest that the second order approximations made of the operational limit surfaces might not always be accurate enough in the context of the aims (presented in Section 1.2) of this project. Often they seem to be accurate however. Figs. 27 and 28, illustrate examples on when the approximation seems reliable because of consistency, and when it does not, respectively:

- Fig. 27 shows that the point of shortest distance to surface 6-4 is very close to the surface of 4-5. This can be confirmed by the power transferred from bus 4 to 5 (2.35 p.u.) listed in Table 29 in Section 4.1.2.7.
- For Fig. 28 there are two symmetrical counterexamples, where the approximation does not seem reliable:
  - Fig. 28, on the other hand shows that the closest point from the present load, $P_{D,0}$, to the line thermal limit 5-4 is very closely located to the surface approximation of the line thermal limit 6-4 . Referring to Table 26 the power transferred from bus 6 to bus 4 is however -1.94 p.u. Thus, one can conclude that close to $P_D^{5\text{-}4}$, the power transfer limit from bus 6 to bus 4 has not been reached.
  - Similarly, still in Fig. 28, for the point of shortest distance to surface 6-4 is also very close to the surface approximation of 5-4. This can be concluded to not be the case at all, when finding out from Table 29 in Section 4.1.2.7 that the power transferred from bus 5 to bus 4 is -2.09 p.u.

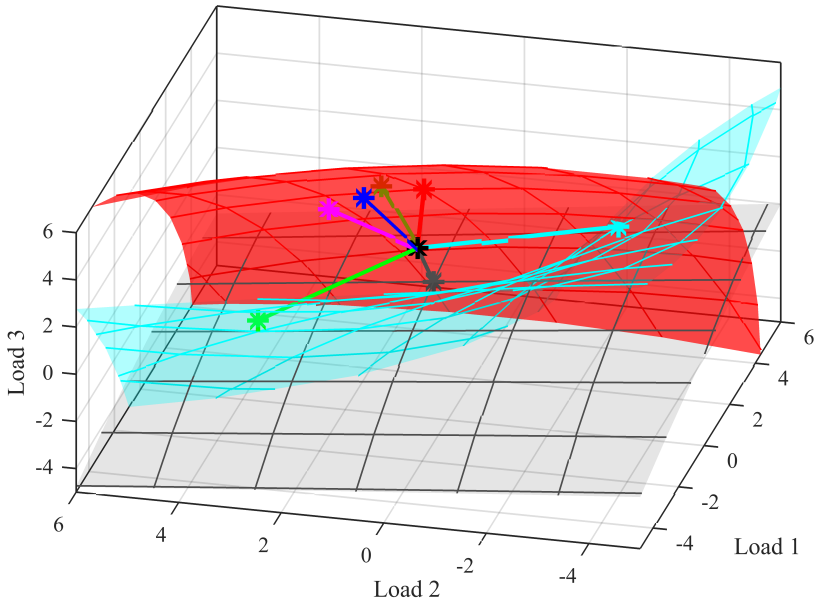

Figure 27: Illustrating that when transfer 6-4 is at its limit, the approximations suggest that transfer 4-5 is as well

By very logical and obvious reasons, the surface representations of both line thermal limit 4-5, and line thermal limit 5-4 cannot be close to each other in load space. Since line thermal limit 4-5, and line thermal limit 5-4 represent the same connection, but opposite directions of power flows, both of them cannot reached or violated for the same load situation. An occurrence of this problem is clearly visible in Fig. 13.

Analogously, one can for the pair of surface approximations representing line thermal limit 6-4 and line thermal limit 4-6 note that in Fig. 24 they intersect each other which is not making sense technically. Thus, one can conclude that the surface approximations are not valid all over the illustrated load space. One clear such case in Fig. 24 is for bus 6 (Load 2) net loads of about 3 p.u. and bus 5 (Load 1) net loads of about -1 p.u. That point of intersection is, as can be seen in the figure, comparatively far away from $P_D^{6\text{-}4}$ and "medium-far" from $P_D^{4\text{-}6}$.

This phenomenon is not deeper analyzed in this report. One can at least conclude that the distance in load space between $P_D^{6\text{-}4}$ and $P_D^{4\text{-}5}$ is 3.9308 p.u., whereas the distance between $P_D^{6\text{-}4}$ and $P_D^{5\text{-}4}$ is 7.9133 p.u. The latter being more than twice as large as the former distance. Is it a well-known fact that Taylor-approximations are typically more valid, the closer to the point of approximation you are.

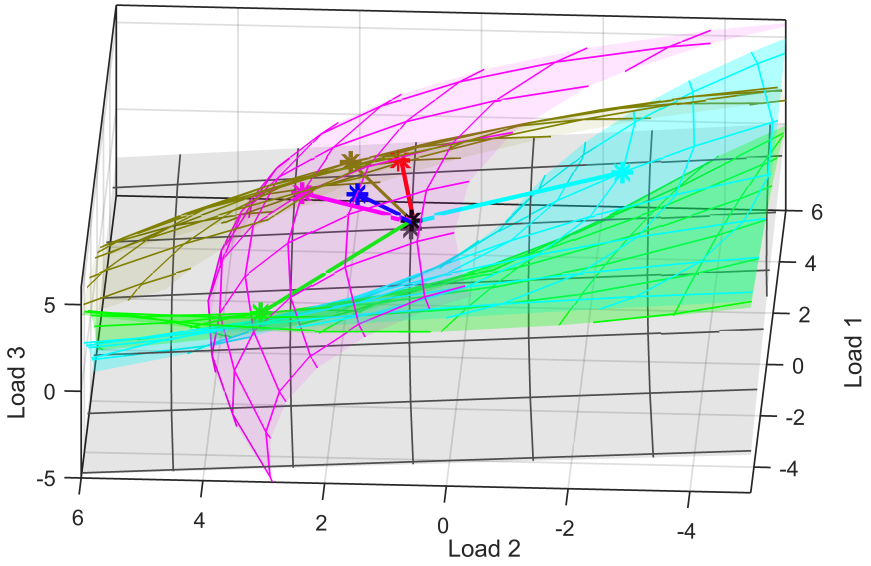

Figure 28: Illustrating that when transfer 5-4 is at its limit, the approximations suggest that transfer 6-4 is as well

4.2 Structured Outline of Future Work

Naturally, the immediate continuation of the work within this project (if the time would have been unlimited) is comparatively clear, whereas the further on in the future, the research line also starts to be obstructed by uncertainties that might come up as the research work proceeds. The parts of the future work that are comparatively clear and straight-forward are listed in the following:

1. Obtain relevant stochastic models of the uncontrollable net loads of the test system
2. Identify a small, but reasonable number of important contingencies
3. Determine the post-contingency surface approximations of the in *Point 2* identified contingencies, and the pre-contingency surface approximation with respect to the stochastic models obtained in *Point 1*
4. Obtain realistic probabilities for the selection of explicitly modeled contingencies
5. Approximate the distance functions
6. Obtain relevant and representative regulating bid prices for the test system in question

The steps following thereafter are less clear, and thus presented differently.

From here on, there are three possible steps to take – all of them with both pros and cons:

Starting with *Step 1*. Apply these regulating bid prices, distance functions, and contingency probabilities to the proposed *Step 1* model of Section 4.2.2. In order to be able to do that, however, for the SL surfaces, if there is more than one, considerations needs to be taken to the pairwise exclusion method presented in e.g. [9], in order to not account for certain SL-subspaces more than once.

And thereafter *Step 2*. In this approach Section 4.2.3, the SL surfaces are not longer treated as an aggregated surface with chance constraints merely, and the possibility of total blackout is also considered and cost-weighted. However, for this model to be applied, and estimation of all the possible costs related to rapid emergency control actions related to SL-occurrences needs to be obtained. Similarly, costs for OL violation, in particular their violation over time and in depth of surface penetrations needs to be estimated. Then there are some design parameters that must be empirically defined by the user of the model.

And the remaining *Step 3* being proposed. In this approach, Section 4.2.4 no more information compared to *Step 2* is needed. However, some experience of the solutions of the previous steps might be beneficial for heuristically choosing a relevant sampling grid of u. It is not stated explicitly how the sampled expected cost functions should be handled. Without seeing the resulting one possible way forward could be piecewise hyperplane approximations with e.g. the usage of Specially Ordered Set of type 2 (SOS2) variables [69, 74, 75] in GAMS. There might be many other options.

Until the first three steps of Sections 4.2.2 to 4.2.4 have been approached and evaluated, it is too early to go any further and speculate how these modeling approaches would perform. At the level of "Step 3" being implemented and evaluated, one is anyhow pretty close to the initially stated aim of this project, as stated in Section 1.2.

In parallel with the above described work, model improvements and expansion with regards to consideration can take place with respect to the issues targeted in Chapters 5 and 6.

4.2.1 Identifying the targeted goal

Recall the SOPF approach presented in Section 2.7.5.2

$$\min_{u} C(u) \tag{210}$$

$$\text{s.t.} \sum_{\forall i} p_i P\left(\min_{j \in J_i} d_{i,j}(u, \zeta) < 0\right) \leq \alpha \tag{211}$$

in which the overall risk of violating any of the operational limits were forced to be below the small nonnegative number α. The reader should note that the risk-defining parameter α used in the SOPF models in this report has nothing to do with the parameters and binary variables named α in Section 3.4.

Ideally, following the aims for this project, Section 1.2, the intention would

be to have a SOPF of the kind:

$$\min_{u} \; C(u) + \sum_{\forall i} p_i \cdot \left(\mathbb{E}_{d_{i,j}(u,\zeta),\forall j \in \mathbf{SL}} \left[\sum_{\forall k} c_k^{\mathrm{SL}} \cdot u_{i,j,k}^{\mathrm{SL}} \right] + \right. \\ \left. + \sum_{\forall j \in \mathbf{OL}} c_j^{\mathrm{OL}} \cdot \mathbb{E}_{d_{i,j}(u,\zeta)} \left[d_{i,j}^{-}(u,\zeta) \right] \right) \tag{212}$$

such that

$$d_{i,j}\left(u, u_{i,j,k}^{\mathrm{SL}}, \zeta\right) \geq 0, j \in \mathbf{SL}, \forall k \tag{213}$$

and such that

$$d_{i,j}^{-}(u,\zeta) = \begin{cases} -d_{i,j}(u,\zeta) & , d_{i,j}(u,\zeta) < 0 \\ 0 & , d_{i,j}(u,\zeta) \geq 0 \end{cases} , \forall j \in \mathbf{OL} \tag{214}$$

in which c_k^{SL} denotes the costs for the load shedding or production curtailment that has to take place in order to meet Eq. (213). Moreover, note that u_k^{SL} generally contains both a subset of all the u that exists in the model Eqs. (210) and (211), but also includes possible disconnections and switching operations. Finally, c_j^{OL} denotes the costs related to OL violations, and since the distance function is defined negative when a surface is violated, the constraint Eq. (214) is needed. For simplifying and already complex problem, the costs c_k^{SL} and c_j^{OL} are set to be constants in the above. Indeed, c_k^{SL} could in reality be likely to vary with u_k^{SL}, and c_j^{OL} could similarly be likely to increase for increased levels of $d_{i,j}^{-}(u,\zeta)$. The sets **OL** and **SL**, respectively, denote the surface approximations of OL-type and of SL-type, respectively.

Since an SL cannot be violated more than instantaneously, rapid automatic control actions u^{SL} need to take place, immediately bringing the system out of the instability. There is no time to wait for 15 minutes of executing regulating bids. Possibly some extremely rapidly ramped production units could be considered as part of u^{SL}. Some customers are paid by the TSO for being prepared for disconnections. Therefore, the costs of disconnection, c_k^{SL} can be significantly differently valued.

Since an OL, as discussed before, can be violated, the resulting operating costs depend on how deep and for how long duration of time each surface is being penetrated. Since these kinds of models (confer Section 2.7.5.3) work in the present, and are continuously updated, the historical depth-duration combinatorial affects the actual values of c_j^{OL} in each time-instant. The penetration depth is directly taken care of in the third term in the objective Eq. (212).

Clearly, the ideal problem formulation of Eqs. (212) to (214), cannot be implemented straight-away in line with the project approach of Section 1.3. The distribution functions can probably be used as they are in the ideally proposed SOPF above, but the expectation values are not implementable straight-away.

Also note that even in the ideal model, Eq. (213) needs to be modified for distribution functions $d_{i,j}$ which do not have compact support, and maybe also for distribution functions with long tails. Then, still, one needs to accept Eq. (213) to be violated for some probability β. It is however reasonable to assume that probability $\beta \ll \alpha$ considering the inclusion of the emergency control actions u_k^{SL} into the model. In real life, the distribution functions $f_\Lambda(\lambda)$

of the net-loads must have compact support, bounded from below for each bus by the aggregated maximal consumption, and conversely, bounded from above for each bus by the aggregated maximal production. For practical reasons however, there might be cases when normal distributions might be used, and such do not have compact support.

A clear benefit with the ideal approach, compared to the one used in [6, 9] and the work related to them, is that pairwise exclusion due to overlapping instability spaces does not need to be considered.

4.2.2 Step 1

A first, tiny step from Eqs. (210) and (211), towards the idealized goal of Eqs. (212) to (214), can be

$$\min_u \; C(u) \tag{215}$$

$$\text{s.t.} \sum_{\forall i} p_i P\left(\min_{j \in \mathbf{SL}} d_{i,j}(u,\zeta) < 0\right) \leq \alpha^{\mathrm{SL}} \tag{216}$$

$$\sum_{\forall i} p_i P\left(d_{i,j}(u,\zeta) < 0\right) \qquad \leq \alpha_j^{\mathrm{OL}},\ j \in \mathbf{OL} \tag{217}$$

which, besides working in load-space has some similarities with [51], in which each OL is treated individually. Here, the accepted risk for violating the OL surfaces, α_j^{OL} can be set much higher than α_j^{SL}.

A possible benefit with this approach compared to the one used in [6,9] and the work related to them is that pairwise exclusion due to overlapping instability spaces does not need to be considered for the thermal operational limits. Each thermal limit can be assumed to be overridden with some probability. That can be technically justified by the fact that one thermal limit (OL) being overridden will not explicitly affect the other thermal limits (OL) unless it would result in a contingency that in turn would result in a post-contingency system with more overload.

In this approach, however, power system stability (SL) is still being maintained to a certain level of probability. This probability, α^{SL} in Eq. (217), is defined as the probability of violating one aggregated stability surface that for practical reasons is modeled as a patchwork of many surfaces rather than many different surfaces actually representing different instabilities.

4.2.3 Step 2

The second step towards the idealized model of Eqs. (212) to (214) introduces certain operational costs depending on how deeply the OL surface is penetrated. In this second step, also the SLs will be treated as individuals.

The proposed objective function is

$$\begin{aligned}\min_u \; C(u) + \sum_{\forall i} p_i \cdot \Bigg(& \sum_{\forall j \in \mathbf{SL}, \forall s \in \{1,2,\ldots,S\}} \left(p_{i,j,s-1}^{\mathrm{SL}} - p_{i,j,s}^{\mathrm{SL}}\right) c_s^{\mathrm{SL}} \cdot u_{i,j,s}^{\mathrm{SL}} + \\ & + \sum_{\forall j \in \mathbf{OL}, \forall t \in \{0,1,\ldots,T\}} c_{i,j,t}^{\mathrm{OL}} \cdot p_{i,j,t}^{\mathrm{OL}} \Bigg)\end{aligned} \tag{218}$$

such that

$$P\left(d_{i,j}\left(u,\zeta\right)\leq -l_{j,t-1}\right)-P\left(d_{i,j}\left(u,\zeta\right)\leq -l_{j,t}\right)=p_{i,j,t}^{\mathrm{OL}} \quad \begin{array}{l}\forall t\in\{1,2,...,T-1,T\}\\ \forall j\in\mathbf{OL}\\ \forall i\end{array} \tag{219}$$

and such that

$$P\left(d_{i,j}\left(u,u_{s}^{\mathrm{SL}},\zeta\right)\leq 0\right)=p_{i,j,s}^{\mathrm{SL}} \quad \begin{array}{l}\forall s\in\{1,2,...,S-2,S-1\}\\ \forall j\in\mathbf{SL}\\ \forall i\end{array} \tag{220}$$

for which $p_{i,j,t}^{\mathrm{OL}}$ are variables, and $c_{i,j,t}^{\mathrm{OL}}$ are parameters. For SLs, the cost-minimizing actions u^{SL} are hard to determine beforehand. Therefore they are modeled as variables. The probabilities $p_{i,j,0}^{\mathrm{SL}}$ are variables as well, resulting in a slightly more nonlinear contribution to the objective function. These probabilities are given predefined interrelations

$$p_{i,j,s-1}^{\mathrm{SL}}=k_{i,j,s}\cdot p_{i,j,s}^{\mathrm{SL}} \quad \begin{array}{l}\forall s\in\{1,2,...,S-2,S-1\}\\ \forall j\in\mathbf{SL}\\ \forall i\end{array} \tag{221}$$

for which the parameters/constant $k_{i,j,s}>1$ are predefined interrelation factors. The control actions u_{0}^{SL} for $s=0$ are none, whereas the control actions u_{s}^{SL} for $s=S$ are all possible control actions maximized. Thus, $p_{i,j,S}^{\mathrm{SL}}=0$, since there is nothing left of the power system when everything has been disconnected. Thus, the complete black-out possibility is explicitly considered in this model.

The the approach decided for in this project, Section 1.3, was to continue with working with PDFs, rather than outcomes of stochastic variables. One identified possible way forward, still working with probability constraints determined by polynomial approximations using the Edgeworth series expansion method is to discretize the problem. For OLs, the discretization can be done into a finite number T of thermal limit penetration depths. The different penetration depths of Eq. (219) are spanning from long-time thermal violation $t=T$ to short-term violation $t=0$. That is done for each contingency i and each thermal limit j, where the beginning of the first discretized slice is represented by the short-term limit

$$l_{j,0}=0,\forall j\in\mathbf{SL} \tag{222}$$

and where the outer end of the last discretized slice representing the long-term thermal violation of the line/unit j,

$$l_{j,T}=\infty,\forall j\in\mathbf{SL}, \tag{223}$$

and thus

$$P\left(d_{i,j}\left(u,\zeta\right)\leq -l_{j,T}\right)=0,\forall i,\forall\in\mathbf{SL}. \tag{224}$$

Moreover, $p^{\mathrm{OL}}_{i,j,t}$ are variables representing the probabilities for each layer of thermal violation, for which the associated costs $c_{i,j,t}$ used in the objective function Eq. (218) are pre-defined costs for each contingency (including the non-contingent state) i, each thermal limit j and each level of short-term thermal overload t. The historical loading of lines (and other equipment) can be taken into account in (at least) three alternative ways.

1. By redefining the numerical values of the costs $c_{i,j,t}$ in order to reflect the induced risks of the system by further load on level t of item j.

2. More physically; by redefining the T levels of overload such that e.g. the long-term limit is much lower for an already heated line.

3. Yet another possible step to take could be to let the contingency probabilities p_i be updated depending on historical heating of equipment.

For the SLs, the problem is discretized in a slightly different fashion. Here, it begins in one end of the discretization, for $s = 0$, with the probability $p^{\mathrm{SL}}_{i,j,0}$ of instability given no automatic emergency control actions (introduced in Section 4.2.1). Then the automatic emergency control actions u^{SL}_1 needed for having the power system at risk level of a probability $p^{\mathrm{SL}}_{i,j,1} = \frac{p^{\mathrm{SL}}_{i,j,0}}{k_{i,j,1}}$ can be determined. In the objective, the costs related to the automatic emergency control actions are weighted against the incremental change in probabilities, $p^{\mathrm{SL}}_{i,j,s-1} - p^{\mathrm{SL}}_{i,j,s}$. This then continues for $s = 2$ until $s = S - 1$. On the other boundary of the SL discretization, $s = S$, the probability $p^{\mathrm{SL}}_{i,j,S-1}$ is in the objective Eq. (218) is weighted against the total black-out costs.

4.2.4 Step 3

The third step is based upon parametrization. For each given control decision of u, and each uncontrollable net-load stochastic parameter ζ, the minimal-cost control actions of the second term in the ideal objective Eq. (212) under the constraint Eq. (213) can comparatively easily be obtained. Since the stochastic distribution of ζ is known, the expected cost with respect to ζ for each given u can be computed off-line beforehand. Thereafter, the number of given u:s need to be sampled in a way that considers the compromise between problem size and accuracy. The expected cost function related to SLs are now sampled with respect to u. These samples can be put together in a variety of ways, for example piecewise linearly between the sampling points.

In a similar way, for OLs, the third term of Eq. (212) can be computed for a cleverly chosen set of samples of control variables u. In this approach, like for the above discussed SLs, quite complicated cost functions c^{OL}_j can be considered without introducing any extra complexities in the resulting SOPF. After sampling in u, the expected cost with respect to ζ, under the condition of Eq. (213) can be computed off-line beforehand. Thereafter, the solutions of each sample u needs to be interpolated in an appropriate way.

The resulting SOPF

$$\min_u \; C(u) + \sum_{\forall i} p_i \cdot \left(\sum_{\forall j \in \mathbf{SL}} c^{\mathbb{E},\mathrm{SL}}_{i,j}(u) + \sum_{\forall j \in \mathbf{OL}} c^{\mathbb{E},\mathrm{OL}}_{i,j}(u) \right) \tag{225}$$

have no explicit constraints. But for accuracy, the sampling in u might be dense and the problem size could be a challenge, especially for larger power systems with many players participating in the tertiary control.

4.3 On margins

In [6, Chapter 6.6] it is stated that safety margins are not only useful and implementable when working with traditional OPF or SCOPF. Also with the surface approach margins can be considered. It is proposed that margins to stability limits can be considered when computing the second-order approximations in the following ways for the different smooth parts:

SNB For SNB points, stability limits are defined as the point at which the system Jacobian J has a zero eigenvalue, or equivalently, at which either the dynamic Jacobian A or the static Jacobian g_y has a zero eigenvalue [11]. Let μ be this eigenvalue for A. The boundary corresponding to $\mu = -\epsilon < 0$ can be considered instead of the stability boundary with $\mu = 0$. Note that if we use the eigenvalue μ^J of the system Jacobian J or the eigenvalue μ^{g_y} for the static Jacobian g_y, then the margin must be applied on the absolute value instead, such that $|\mu| = \epsilon$ constitutes the border.

HB For HBs, as for SNB, the boundary corresponding to $\Re(\mu) = -\epsilon < 0$ can be considered instead of the stability boundary $\Re(\mu) = 0$, where μ is the eigenvalue that becomes purely imaginary at the HB point.

OL OL For an OL characterized by Eq. (33), the right-hand side of it would be changed from $P_{i,j}^{\lim}$ to $P_{i,j}^{\lim} + \epsilon$, $\epsilon > 0$.

When computing the second-order approximations, the characterizations of each smooth part are proposed to be changed according to the margins defined above.

It is however not clear how well a surface approximation around such a point as described in the above would follow the original surface but with a constant offset to the feasible side of the surface strictly defined by μ in load space.

There might exist an attractive alternative to the proposed margin approach where the margin is defined in the load space instead; for instance, let λ_c be the most important point determined to approximate the surface around. Then a margin can be defined for a certain amount of load along the inward pointing vector in load space from λ_c to λ_0. At that point the approximation of the surface can be done. A comparison between these approaches and how well they represent the ideal constant offset of the actual surface would be a technically and academically relevant topic for future studies.

The approach proposed in this report and the one of [6, Chapter 6.6] are likely to behave similarly for operational limits representing active power flow limitations on lines, but for most other operational limits they would behave differently.

5 Discussion

5.1 Obstacles working with stochasticities

5.1.1 General and common practical obstacles

Limitations with stochastic approaches are discussed in for instance [14]. There it is highlighted that sufficiently accurate values may not be available for probabilities of disturbances. That can be by the simple reason that some equipment fails so seldom that it is hard to accurately estimate the associated probabilities. To complicate things further, the probability of a contingency may, according to [14], also depend on the circumstances (e.g. adverse weather conditions or terrorist threat).

5.1.2 Challenges with possible multimodal distributions

As briefly mentioned in Section 2.3.1, the there proposed, and in [9] used approach, is clearly attractive as long as the distribution functions of the net loads are unimodal. In the unimodal cases, the *most important point* on a surface to be detected is clearly the one point on that surface with the highest probability density.

For a multimodal distribution it is less clear. Imagine a bimodal distribution, with two equally probable peaks located on the surface of the operational limit to be detected. With the approach presented in Section 2.3.1 and in [9], the resulting *most important point* would be one of these two points, here denoted λ^{c^1} and λ^{c^2}, respectively. If these points are comparatively far away from each other in load space, a surface approximation made around λ^{c^1} might result in inaccuracy in the neighborhood of λ^{c^2}, and vice versa.

Within the scope of having simply one unique *most important point*, the procedure of finding it might need to be redefined in a more complicated manner. One possible approach is to aim at finding the expectation value of λ, provided that $\lambda \in \Sigma$. There might be other, computationally more efficient approaches as well.

It is left for future research and investigations whether and when, in practice, one can assume the distributions of ζ (and thus indirectly probably also of u) to be unimodal. Moreover, the actual impact on the solutions by using the approach presented in Section 2.3.1 for multimodal distributions needs to be investigated and compared with more accurate approaches. Many aspects will affect such an impact; how pronounced the modes are, how curved the surface is, how important the surface is for the resulting SOPF solution; to name a few.

5.1.3 Impact of stochastically modeling u for the most important point

As mentioned in Section 2.3.1, the control variables u are modeled as normal variables with covariances defined by linearizing u around the solution of a SCOPF approximation of the SOPF problem to be solved. Thus, u becomes a function of the stochastic uncontrollable net loads ζ.

From a practical engineering point-of-view it is more important to have a reasonable estimate of u, than not having one at all. And it is not straight-forward

to the author of this report how to quickly find an approximative solution of the SOPF to be solved, other than approximating it with a SCOPF.

The normal assumption in this procedure does not need to have any sever impact. Stochastic distributions can be approximated as series expansions of normal distributions, wherefore a good-enough accuracy could be obtained by just not cutting the series expansion at the first coefficient.

5.2 SOPF problem size

A possible critique against treating operational limit surfaces individually as proposed in different ways in Section 4.2 could be that the problem size of the SOPF problem would increase. Compared to the approach, that this project is based upon [5–9, 70–72] however, the sizes of the problems are likely to be in the same orders of magnitude. That is since the unified aggregated surface there seems to be treated as a compound of second order approximations of all the closest surfaces found in positive net-load space.

In the approach proposed in this report, also surfaces beyond the first OLs being encountered are considered, and the models are generalized to consider also the possibilities of negative net-loads. This would still probably not result in a tremendous increase of surface approximations being considered in this approach. If the SOPF size turns out to be a problem from the computational time point-of-view, the number of surfaces could be limited. Such a limitation is considered in the method presented in Section 3.5. The issue of limiting the load space in which operational limit surfaces are searched for considering stochasticities is discussed in Section 5.4

5.3 Improvement for surface detection

5.3.1 Load flow constraints nonlinearities

In the models used in this study, the load flow constraints in the optimization problem Eqs. (124) and (125) finding the operational limit surfaces are of the form

$$P_i = \Re\left(U_i \cdot I_i^*\right) = \Re\left(U_i \sum_j Y_{i,j}^* U_j^*\right) \tag{226}$$

$$Q_i = \Im\left(U_i \cdot I_i^*\right) = \Im\left(U_i \sum_j Y_{i,j}^* U_j^*\right) \tag{227}$$

for complex valued voltages U, admittances Y, and currents I. The constraints Eqs. (226) and (227) are quadratic in voltage absolute values for $j = i$, and bilinear in voltage absolute values multiplied with sin or cos functions of the voltage angles for $j \neq i$.

For some solvers, and some problem types it might be more computationally efficient to use the formulation

$$\Re\left(I_i\right) = \Re\left(\sum_j Y_{i,j}^* U_j^*\right) \tag{228}$$

$$\Im\left(I_i\right) = \Im\left(\sum_j Y_{i,j}^* U_j^*\right) \tag{229}$$

$$P_i = \Re\left(U_i \cdot I_i^*\right) \tag{230}$$

$$Q_i = \Im\left(U_i \cdot I_i^*\right) \tag{231}$$

in which by the separation being done the left-hand sides of Eqs. (228) and (229) contains the absolute values of the complex valued currents I, multiplied by sin or cos functions of the corresponding current angles. The right-hand sides of Eqs. (228) and (229), analogously contains the absolute values of the complex valued voltages U, multiplied by sin or cos functions of the corresponding voltage angles. Clearly, Eqs. (228) to (229) are "less nonlinear" than Eqs. (226) and (227). Finally, the right-hand sides of Eqs. (230) and (231) are bilinear in voltage and current absolute values, but only once for each i (and not for every $j \neq i$), multiplied by sin or cos functions of the corresponding voltage and current angles.

In future studies, alternative, potentially computationally simpler load flow formulations could be evaluated in the optimization model of Section 3.4, in order to reduce computational times. One example of such is Eqs. (228) to (231) introduced above.

5.3.2 Computation-efficient surface identification modeling

There are also many alternative ways of identifying SLs on. It would make sense to empirically be evaluated which formulation that is the computationally most efficient approach.

5.3.2.1 SNB detection For the particular case of SNB, there are a variety of alternatives. One possible drawback with the present approach is that no particular eigenvector is followed all through the search space of the algorithm. That might cause undesired discontinuities in the process.

The left hand sides of Eqs. (200) and (201) are quite nonlinear, so it might be undesired having a binary variable in the right-hand side of them as is the case in the present proposed approach. One alternative formulation could be

$$\sum_{i=1}^{2\mathbf{g}^{\mathrm{ns}}+2\mathbf{g}+2\mathbf{b}} \left(u_i^{\mathrm{r}} + iu_i^{\mathrm{i}}\right) J_{i,j} = \left(\sigma + i\omega\right)\left(u_j^{\mathrm{r}} + iu_j^{\mathrm{i}}\right), \quad \begin{matrix}\forall j \in \{1,2,... \\ ...,2\mathbf{g}^{\mathrm{ns}}+2\mathbf{g}+2\mathbf{b}\}\end{matrix} \tag{232}$$

$$\sigma^2 \leq |J|^{\max}\left(1-\beta\right) + \epsilon\beta \tag{233}$$

$$\sigma^2 \geq 0 \tag{234}$$

$$\omega^2 \leq |J|^{\max}\left(1-\beta\right) + \epsilon\beta \tag{235}$$

$$\omega^2 \geq 0 \tag{236}$$

$$\sum_{i=1}^{2\mathbf{g}^{\mathrm{ns}}+2\mathbf{g}+2\mathbf{b}} \left(u_i^{\mathrm{r}}\right)^2 + \left(u_i^{\mathrm{i}}\right)^2 = 1 \tag{237}$$

$$\sum_{i=1}^{2\mathbf{g}^{\mathrm{ns}}+2\mathbf{g}+2\mathbf{b}} \left(u_i^{\mathrm{r}}\right)^2 \geq \epsilon \tag{238}$$

$$\sum_{i=1}^{2\mathbf{g}^{\mathrm{ns}}+2\mathbf{g}+2\mathbf{b}} \left(u_i^{\mathrm{i}}\right)^2 \geq \epsilon\,(1-\beta) \tag{239}$$

$$\sum_{i=1}^{2\mathbf{g}^{\mathrm{ns}}+2\mathbf{g}+2\mathbf{b}} \left(u_i^{\mathrm{r}}-u_i^{\mathrm{i}}\right)^2 \geq \epsilon \tag{240}$$

$$\sum_{i=1}^{2\mathbf{g}^{\mathrm{ns}}+2\mathbf{g}+2\mathbf{b}} \left(u_i^{\mathrm{r}}+u_i^{\mathrm{i}}\right)^2 \geq \epsilon \tag{241}$$

for which superscripts "r" and "i" denote the real and imaginary parts of the eigenvector, respectively. Moreover, σ denotes the real part of the eigenvalue, and ω the imaginary part of it. The eigenvector is normalized by Eq. (237), and the trivial solution is avoided by Eqs. (238) and (239). For completeness, Eq. (240) outrule the resulting "imaginary eigenvector" for an SNB-point from being a blue-copy of the actual real eigenvector, whereas Eq. (241) outrules the possibility of a copy of the real eigenvector but with opposite signs. With this approach it is more likely that the algorithm "follows" the eigenvector that will cause an SNB a bit longer than in the approach used in this report. Moreover, this approach can with only tiny modifications be used for identifications of HBs; by introducing another binary variable, γ, by considering A instead of J, and by adapting the dimensions of the vectors and matrices accordingly. Since solvers work with real numbers, Eq. (232) needs to be separated into a real and an imaginary part for practical usage.

Another approach, somewhat simpler than the one presented above is to only consider real valued eigenvectors and eigenvalues, respectively. That results in a slightly smaller optimization problem, but there might be risks associated to an eigenvector changing to become complex valued through the iteration procedure. Such would probably result in an undesired discontinuity for the solver. This is however not yet investigated.

One possible alternative way forward is making use of the Schur decomposition for which the Jacobian matrix J can be decomposed into

$$J = QBQ^{-1} \tag{242}$$

in which Q is a unitary matrix, and and in which B is upper triangular with the eigenvalues of both J and B in the diagonal. In that approach, each eigenvalue would be "followed" by the algorithm, all the way to finding the SNB or another operational limit. A possible drawback with this approach is that the problem size is likely to increase even if taking advantage of matrix sparsity. In the framework of GAMS, which like most optimization programs, work with real values, a separation would have to be done into real parts and imaginary part of Eq. (242).

It is an open question, even if it seems unlikely, whether usage of determinants of the Jacobian matrix for finding eigenvalues could be an attractive approach. Speaking against the determinant approach is that a very complicated polynomial would be needed in the optimization problem formulation. Like with the Schur decomposition, using determinants would correctly implemented result in finding all the possible eigenvalues.

5.3.2.2 Sparsity As already mentioned in Section 3.6, there is a great potential in exploiting the sparsity of the Jacobian matrix. In [12, p. 330] it is

clearly stated that "The use of very efficient sparsity techniques is essential, in order to preserve the computational advantages of optimization over the simpler continuation methods.". Thus, in order to keep the proposed optimization method approach of this report competitive in all aspects, sparsity needs to be concerned in future model development.

A small case study was done, investigating the potential in formulating the optimisation program such that it took advantage of the sparsity. For the objective of finding the globally (using the LINDO global solver) closest SNB point in a small fictitious 2 node purely static system with one slack bus and one load, bus keeping P and Q equal, the computational performance was evaluated. With the explicit Jacobian, solving the program took 0.842 seconds, while for the model using sparsity of the Jacobian it took only 0.078 seconds to solve – a reduction in computation time with 91 %. Additionally, the number of iterations reduced from 229 down to 67 – a reduction by 70 %. In the explicit Jacobian model, the optimization problem had 47 equations and 48 variables, whereas the model using sparsity had 15 equations and 16 variables – a reduction by 68 % and 67 %, respectively. The time savings of exploiting sparsity in problems like the one presented in Section 3.4 cannot be expected to be exactly as drastic, since such a problem considers so many other issues. Just for the sake of clarity: the two modeling approaches resulted in exactly identical solutions, as would be expected from such a solver.

5.3.2.3 HB detection with optimization methods From the literature, as explained in Section 2.2.1.3, it has been concluded that HBs are detected when the A-matrix of Eq. (8) has complex-valued pairs of eigenvalues $0 \pm i\omega$. For A to be computed, as shown in Eq. (8), the matrix-inverse of g_y needs to be computed.

Since the optimization problem of Section 3.4, and also future, improved versions of it, are likely to search for and encounter SNB points, this might be an obstacle for including the detection of HBs in that optimization problem. If the SNB is in the dynamic part of the power system model, A, this indeed not a problem. The SNB can however also be a simple transfer limit, for which g_y is singular. This makes it unattractive, but nevertheless probably not impossible to detect HBs by explicitly computing A in the optimization program. If an SNB is reached, one could formulate the problem such that the A matrix is not computed when β of Eqs. (200) to (202) equals 1. It might be possible also to consider generalized matrix inverses or pseudoinverses, but it is out of the scope of this report.

More attractive for the point-of-view of the continuation of this project, is however to find out if there are any general relations by eigenvalues of A of the type $0 \pm i\omega$, to the eigenvalues of J. It is not yet clear to the author of this report whether; such a general relation has been identified in the literature, if such a relation actually can be found, or if it is possible to at least empirically find relations that hold (at least locally) for the particular application in question. If it would be possible detecting HBs directly from J and/or its eigenvalues, it would be very attractive for the optimization method approach initiated in this project. It would reduce the memory usage and the number of variables working with "only" J, and not both J and A simultaneously. Moreover, inversions of the sub-matrix g_y would not be needed, neither the increased complexity in

managing the cases when g_y actually is singular.

5.3.3 Reactive modeling of uncontrollable loads

By simplistic reasons, and in alignment with [6], the assumption, Eq. (139) of Section 3.4.3, was that the reactive loads follow the active load changes linearly, keeping the power factor $\cos(\phi)$ constant. This is an assumption that might need to be let go off when practically justified.

For some (net-)load models, a generalized modeling approach might be necessary, in order to reflect reality. For some load types, it is likely to assume reactive and active consumption to be decoupled. For example for solar cells, railway power system feeding converters, and possibly for Voltage Source Converter (VSC)-HVDC link connections, it is attractive to control the reactive power net-consumption with regards to, for instance, voltage quality. In the cases when the reactive parts of the net-load become independent of the active parts, the reactive power consumption might be needed to be considered as a dimension in the net-load space λ of the SOPF.

For future tertiary control, it might even be attractive to include regulating bids and trade also in reactive power.

5.3.4 Parallelization

If, in a future implementation of more completed models from this project would take place, and the creation of the operational limit surface approximations would be time critical, it would possibly be very efficient to parallelize the surface identification process of Sections 3.4 and 3.5 for the pre-contingency scenario and each of the post-contingency scenarios of relevance [6, Chapter 7.5.1]. Such computations would reduce the computation time significantly, the more Central Processing Units (CPUs) there are available, and the more contingencies there are of considered relevance.

5.4 Generalizing the threshold in load space in which to search for operational limits considering stochasticities

Regarding having a threshold in distance in load space for the number of surfaces to identify in Section 3.5, a stochastic equivalent is not straightforward to determine:

One possible and "good-enough" approach could however be, using the approach of *the most important point* introduced in Section 2.3.1. By definition, that point is the point on the the particular surface approximation with the highest probability to be reached within the following 15 minute time period. In such an approach, one can decide a lowest level of probability of the most important point determined, for which the search for more surfaces should continue.

If the TSO wants to consider the entire probability of ending up on, or beyond a certain surface approximation, there seem however to be no easy way out. Then all of the surface needs to be found or approximated first, before that probability can be computed. The probability of ending up on, or beyond a surface approximation depends both on the probability distributions as well as

on the surface's geometry. Therefore, it would in general not be any guarantee for surfaces found in the order of declining probabilities of *the most important points*, to also have a declining order of probabilities of being encountered or surpassed. This is a topic worth, if not further investigations, at least be kept in mind as a risk factor.

5.5 SLL surfaces

5.5.1 SLL surface regionality in load space

An issue introduced in Section 2.3.3.1, was the challenges of SLL-surface treatment within the scope and the aims of this project, confer Section 1.2. It was stated that many aspects in this regard are still not cleared out, making it an issue for future studies. As explained in for example [6, Chapter 5.3.5], due to the nature of an SLL of representing switching (control) actions resulting in instabilities, an SLL surface is only defined for a limited region in load space. Therefore, unlike for example SNB surfaces, SLL surfaces cannot be found in any but very specific directions of (net-)load changes.

Typically, the SLL surface is at its endpoints tangential (except in very rare cases [6, Chapter 5.3.5] and [5, 8]) in load space to SNB surfaces, whereas it intersects with other surface types transversally [6, Chapter 5.3.5]. Examples of the latter kind of SLL-surface intersections are: one SLL surface intersecting another SLL surface, SLL surfaces intersecting with HB surfaces, etc.

Since the surface approximations are not explicitly used in the SOPF models proposed in this report, but rather the distance functions, there is a potential in finding attractive ways to overcome this obstacle.

5.5.2 Identifying SLLs

One issue noted under the *remark* in the end of Section 2.2.1.2 was possible obstacles and challenges in identifying SLL surfaces. Since the system has skipped passing through the SNB, other means of detecting the SLL might be needed, especially for large negative $\tan\phi$ of the loads. Moreover, many net-loads of the future with consumer-side storage, regenerating electrical vehicles, distributed generation, etc., is likely to need to consider also $\phi < 0$. This might be an important part of future work in relation to the other SLL-issues already discussed.

5.6 Further exploiting results from bifurcation theory

Lots of information is given by analyzing the SNB point in scrutiny; following [1] the sign and the sizes of Eqs. (21) and (22) will give information about how the system bifurcates locally. This could probably be utilized in future work, in order to estimate the costs of an SNB to occur, depending on what causes it and under which conditions. Also the eigenvectors may give valuable information.

The left hand eigenvectors are related to the constraints, whereas the right hand eigenvectors are related to the variables. It is likely, but left out of the scope of this report to investigate it, that this information could be made useful in a risk-based SOPF considering secure power system operation. It might be trickier with the left hand eigenvectors since they are related to the constraints,

which do not explicitly appear in the load-space SOPF. The right hand eigenvectors, however, could without too much complications be projected to load space from state space.

It is reasonable to assume that a thorough analysis of the eigenvectors and other system properties at the SNB point(s), it will be possible to determine what causes the bifurcation and where in the system the consequences would be the most severe. Information like this can be expected to say something about the expected consequences of a bifurcation to occur under these particular circumstances, and which control actions that are physically and economically the most feasible. Altogether, a deeper knowledge about this is likely to result in a deeper understanding of the risk levels the power system is exposed to at a given point of operation.

5.7 Instability severities and/or classifications

A HB is said to give rise to an (increasing [11]) oscillatory behaviour of the power system and not an immediate voltage collapse. Thus, one can identify a possibility that HBs are less severe than SNBs. It needs to further investigated whether one can say that a HB is less severe, or at least needs a longer time to become severe than an SNB. That would have implications of the emergency control actions available in e.g. Eqs. (218), (220) and (221), as well their corresponding costs.

Another question that arises is whether SNBs in the dynamic part are less sever than, or equally severe as, SNBs in the grid. When listing different bifurcations in [11], "collapses" and "blackouts" are mentioned specifically regarding g_y singularity, but not with respect to SNBs originating from the dynamic part of the system model.

A thorough description of other bifurcations occurring in power systems can be found [26,27]. Consideration of such may be an issue for future work, confer Chapter 5.

6 Conclusions

In this section, the major findings are listed in a summarized form alternated with recommendations related to the findings.

1. **Finding** A general algebraic optimization model approach for finding the set of closest (or most important) operational limits with respect to the present point of operation has been developed. It can be extended to consider the forecasts for the coming 15 minutes. The benefits with a general algebraic model are that it can be used with different solver algorithms. Provided a relevant solver is being used, the developed model will for solving only a handful of optimization problems find the operational limits sought for. Some challenges regarding efficient model development remain however.

   Recommendation Deeper studies are needed in developing even more computationally efficient models considering the balance between for instance small but complicated mathematical programs or larger but simpler ones. Is it for example more efficient to consider only the

entire system Jacobian, J, and find bifurcations within that one, or is it preferable working also, or only, with the the smaller sub-matrices?

2. **Finding** When looking for switching-related instabilities using a general algebraic optimization model, a number of challenges arises:
   (a) The sets for state variables as well as the sets for the active constraints of the power system change in size and in content. This needs to be managed considering both efficient memory usage as well as complexity.
   (b) In an algebraic modeling language, such as GAMS [68,69], like in real mathematic formulations, set sizes and corresponding subsets with sizes need to be clearly declared before sending the problem to the solver. Thus, set sizes cannot change depending on where in solution space the solver "stands" for different iterations.
   (c) In reality, all PU-curves do not always have the property of obeying $\frac{\partial U}{\partial P} < 0$ on the upper side of the bifurcation point. Therefore, it is not enough to study the partial derivatives of voltage with respect to active power load in order to identify an instability.
   (d) In the case of switching modes-of-operation, complementarity often well describes the switching of active and inactive variables and constraints. There are however many different approaches available, and is not yet clear which approach is preferable from a computational efficiency point-of-view.

   Examples of switching-related instabilities are: SLL, contingency-induced instabilities, or simply a switching taking place that eventually leads to a bifurcation.

   Recommendation To address these challenges, some possible ways forward have been identified:
   (a) The most attractive way forward for larger systems is probably to create a sparse description of the active constraints and the system Jacobian. This needs however some deeper investigations and is strongly intertwined and interrelated with (c) below.
   (b) The sets and the corresponding subsets need to be declared and defined such that the above point is ensured. The sets will need to be "oversized" generally, and then the active parts of them should be appropriately defined within the model.
   (c) One possible approach here is the study of higher order derivatives. How often first-order partial derivatives are not enough also needs to be further investigated in study cases.
   (d) For simpler power system models, without generator or load dynamics, special application-tailored approaches [65,66] have been proposed. Simpler models like the ones just introduces can be used for two main reasons: (1) computational advantages, and (2) lack of dynamic power system data for many systems. The applicability and accuracy of those approaches for dynamic load and generator models needs to be investigated. Modeling approaches such as the ones proposed in [65, 66] need to be compared with more "classical" optimization approaches managing

complementarity. Examples of a few possible and relevant such modeling approaches are: binary variables used for switching modes of operation, the more "new" modeling approaches with complementarity constraints that are beneficial to many modern solvers, or the Specially Ordered Set of type 1 (SOS1) [68, 69] variables. These could, at least for smaller systems be compared for benchmarking, with the naive "base case", where complementarity is modeled $a \cdot b = 0, a \leq 0, b \leq 0$ when a and b are complementary.

3. **Finding** One challenge using Edgeworth series expansions is that they seem to be very practical for approximating the CDFs, but less so for expectation values, variances, and other stochastic measures. Moreover, it is indicated in the literature [76], that CDFs containing step functions, needs special treatment. One example of a function, which CDF would contain a step function is Eq. (214).

   Recommendation Some approaches going around this obstacle has been proposed in Section 4.2. The approaches proposed in Section 4.2 need to be evaluated in practice. Many other possible approaches similar to the ones proposed may exist, and totally other approaches may be found by deeper studies in stochastic approximation theory.

4. **Finding** From the second order surface approximations obtained for the IEEE 9-bus test system, there were cases and locations in load space identified, for which the surface approximations were clearly inaccurate. These inaccuracies are presented in further detail in Section 4.1.3. The practical implications of this, and possible ways of getting more accurate surface representations, are yet to be determined.

   Recommendation First of all, it needs to be determined whether the identified cases of invalid parts of the approximated surfaces are representative for practical study cases. It needs, for example, to be determined how large the net-load changes in a 15 minute time-period can be. Moreover, even if parts of the surface approximations are invalid, the impact of this on the optimal re-dispatch solution needs to be evaluated. In the end, the resulting SOPF solutions are what matters for this project, not accuracy for its own purpose on every detail. To be able to do such an evaluation however, a more accurate surface representation needs to be developed. More accurate surface representations may be obtained by for example: higher order polynomials, patches of hyper planes (without introducing too many integer variables), or approximating each surface around more than one point.

5. **Finding** For a TSO, it is more attractive to have a conservative surface representation with lower accuracy, than a more accurate one which is not conservative. By *conservative*, it is in this report meant that the surface is represented by points either on the feasible side of it or right on it, but never on the infeasible side of it. Thus, small average-errors in *any* direction are worse than large average-errors in *the right*

direction. Surface conservatism can be increased by introducing margins. It has been found that margins can be introduced in at least two different ways, confer Section 4.3. Moreover, it is not unlikely, that conservative hyper-surface representations could be obtained also by other means. The questions is though at which computational cost. In practice, the TSO also wants to use comparatively fresh data in its 15-minute power balance planning, confer Section 2.7.5.3.

Recommendation Clearly, this point is partly interconnected with the above point treating different ways of representing the operational limit surfaces. As proposed in Section 4.3, there should exist at least two approaches of using margins for creating second-order approximations of the surfaces that are more conservative than the non-margin approach. In order to evaluate these two approaches, a comparison is needed for some representative numerical studies where many points on the actual surfaces are computed. It has not been investigated, but it is likely to expect approximation methods to exist which are able to curve-fit surfaces conservatively. Whether such surfaces can be found fast enough for a practical application needs to be studied further. Further studies are also needed on whether that surface representation would fit well in a chance-constrained SOPF with respect to computational burden.

6. **Finding** During the work, it was realized that the present-day approach for finding the *most important point* around which the operation limit surfaces are approximated is mainly applicable for unimodal stochastic distributions. It is however not clear how common clearly pronounced multimodal distributions are for uncontrollable net loads in power systems.

   Recommendation It needs to be determined, first how predictions of uncontrollable net loads in power systems may look, and how commonly they are represented by multimodal distributions. Thereafter, alternative ways are needed for approximating the surfaces (see the previous *finding*), including simply finding as many *most important points* as there are modes in the distribution. Another, but slightly more complicated approach is defining the *most important point* as the expected outcome in load space within the planning period, given that the net load will be located on the surface of interest. If the number of modes tends to infinity, the distribution tends to a uniform one, and then the latter approach seems less attractive. Finally, the new ways of approximating the surfaces needs to be compared with the approach presented in [9] and Section 2.3.1 in order to validate if it is worth the effort to consider and treat multimodal distributions exclusively.

7. **Finding** It was noticed in [9] that the distance function approach used and proposed there, and presented in some more detail in Section 2.4.2, is not the actual Euclidean distance to the approximation of the surface. The impact of this inaccuracy is not clear, neither is it fully investigated how much more complicated it would be to compute and

use the actual Euclidean distance (or other distances that might be relevant for the application).

Recommendation The first step to clear this out would be to compare for some representative study cases the approximated distances to the surface approximation with the actual distance to the surface approximation, as well as with the actual distance to the actual surface. If that preliminary study indicates a large discrepancy, a further investigation in determining a more accurate distance measure will have to take place. Some preliminary investigations indicated that a possible closed-form representation can be found since the surface approximation and the Euclidean distance measure both second order polynomials.

8. **Finding** It is in practice hard to find both models and model parameters for actual systems to study. Therefore, (and probably also to obtain simpler models) it is common in the literature that only transfer limits are studied (that is the g_y part of J). For more general instability studies, generator and load dynamics needs to be considered. In order to model all parts of the automatic control (such as primary and secondary control) implications for post-contingency equilibria, more detailed models than the ones of this report are needed.

   Recommendation Data gathering is needed, as well as improved models of the systems being studied.

9. **Finding** During the work, a substantial obstacle has been a very varying terminology with regards to denotation and classification of instabilities, and of various methods used for finding and locating the operational limit surfaces. Some effort has been made to bring some order to this issue in the report, even if lots of things still need to be cleared out. Sometimes also notation complicates things more than necessary, especially for differential geometric descriptions. Within this report, the mathematical descriptions are lengthier than common in the field, using classic "calculus" notation, in order to de-dramatize things that seem incomprehensible, but in reality are not.

   Recommendation More studies are needed for finding coherent, comprehensible, and logical descriptions of many of the topics treated in this report. Different systems of classifications need to be translated between and mapped onto each other.

10. **Finding** Comparatively late in this project, the existence of SIBs was "found". When an SIB occurs [11], the entire system Jacobian J, is non-singular, while the "grid part" g_y is singular with a zero eigenvalue. The dynamic part of the Jacobian, on the other hand, has an eigenvalue passing through $\pm\infty$ at the same time as one eigenvalue of g_y passes through ± 0 such that the "cancel each other out". Whether or not this kind of bifurcation is important for the grids of concern for this project is still not clear, but they seem to be of importance for power system stability [26,27]. However, if SIBs are to be considered, one probably needs to create a model that identifies such a surface

by finding the singularity in g_y, while at the same time outruling the SNB possibility by ensuring that the $\det J \in \mathbb{R} \setminus [0-\epsilon, 0+\epsilon], \epsilon > 0$.

Recommendation More studies are needed in combination with numerical experimental and comparative studies. It might be a numerical challenge to detect SIBs without explicitly working numerically with numbers close to infinity, since that would make the problem extremely hard to solve.

11. **Finding** One issue that has been identified, but not addressed due to time constraints, in this project is the challenge of surface representation of SLLs. Since switching modes of operation can be "harmless" as well causing voltage instability, the SLL surface has sharp endpoints. The topic is treated in some more length in Section 2.3.3.5.

    Recommendation Further investigations (experimental as well as in literature) regarding SLL representation in actual load space are needed to bring clarity in this issue. When that basic understanding has been achieved, research with regards to how to manage the end points of these surfaces when representing them a future SOPF problem including them.

7 Acknowledgements

First of all, I would like to show gratitude to the sponsors in the Risk Analysis Program, operated by Energiforsk making it possible to work on the topic. I would also thank the reference group being involved in the project.

A big thank to Magnus Perninge and Camille Hamon for hints regarding literature and for fruitful discussions during the project. Thanks to Lennart Söder and Camille Hamon for helping me formulating the research project. Thanks to Math Bollen for letting me finish the project at Luleå University of Technology (LTU) and for valuable advice wrapping up the report. Thanks to John Laury for proofreading and valuable suggestions regarding the improvement of this report. Also thanks to Robert Eriksson for general discussions, but particularly regarding the dynamic modeling.

8 References

[1] C. A. Canizares, "Calculating optimal system parameters to maximize the distance to saddle-node bifurcations," *IEEE Transactions on Circuits and Systems I: Fundamental Theory and Applications*, vol. 45, pp. 225 – 237, Mar. 1998. ISSN: 1057-7122.

[2] L. Abrahamsson, "Risker i drift av elkraftsystem och konsekvenser av olika accepterade risknivåer," tech. rep., Energiforsk, 2017. RAPPORT 2017:412. ISBN 978-91-7673-412-4.

[3] M. H. Bollen and F. Hassan, *Integration of Distributed Generation in the Power System*. Wiley-IEEE Press, Aug. 2011. ISBN: 978-0-470-64337-2.

[4] M. H. J. Bollen, *The Smart Grid: Adapting the Power System to New Challenges*. Synthesis Lectures on Power Electronics, Morgan and Claypool Publishers, Sept. 2011. doi:10.2200/S00385ED1V01Y201109PEL003.

[5] M. Perninge and L. Söder, "Geometric properties of the loadability surface at snb-sll intersections and tangential intersection points," in *Intelligent System Application to Power Systems (ISAP), 2011 16th International Conference on*, pp. 1–5, Sept 2011.

[6] C. Hamon, "On frequency control schemes in power systems with large amounts of wind power," licentiate thesis, KTH School of Electrical Engineering, Dec. 2012.

[7] C. Hamon, M. Perninge, and L. Söder, "A computational framework for risk-based power systems operations under uncertainty. part i: Theory," *Electric Power Systems Research*, vol. 119, pp. 45–53, Feb. 2015.

[8] M. Perninge and L. Söder, "On the validity of local approximations of the power system loadability surface," *IEEE Transactions on Power Systems*, vol. 26, pp. 2143–2153, Nov 2011.

[9] M. Perninge, "Stochastic optimal power flow by multi-variate edgeworth expansions," *Electric Power Systems Research*, vol. 109, pp. 90–100, 2014.

[10] M. C. de Oliviera Ferreira da Trinidade, "Optimal location of facts to optimize power system security," Master's thesis, Instituto Superior Técnico (Lisboa), 2013.

[11] T. V. Cutsem and C. D. Vournas, "Voltage stability analysis in transient and mid-term time scales," *IEEE Transactions on Power Systems*, vol. 11, pp. 146–154, Feb 1996.

[12] T. V. Cutsem and C. Vournas, *Voltage Stability of Electric Power Systems*. Springer, 1998.

[13] Power System Dynamic Performance Committee and Power System Stability Subcommittee, "Voltage Stability Assesment: Cpmcepts, Practices and Tools," Tech. Rep. PES-TR9 (Formerly SP101PSS), IEEE Power and & Energy Society, Aug. 2002.

[14] F. Capitanescu, J. M. Ramos, P. Panciatici, D. Kirschen, A. M. Marcolini, L. Platbrood, and L. Wehenkel, "State-of-the-art, challenges, and future trends in security constrained optimal power flow," *Electric Power Systems Research*, vol. 81, pp. 1731–1741, Aug. 2011.

[15] C. Vournas, P. Sauer, and M. Pai, "Relationships between voltage and angle stability of power systems," *International Journal of Electrical Power & Energy Systems*, vol. 18, no. 8, pp. 493 – 500, 1996.

[16] M. E. Karystianos, N. G. Maratos, and C. D. Vournas, "Maximizing power-system loadability in the presence of multiple binding complementarity constraints," *IEEE Transactions on Circuits and Systems I: Regular Papers*, vol. 54, pp. 1775–1787, Aug 2007.

[17] V. Venkatasubramanian, H. Schattler, and J. Zaborsky, "Dynamics of large constrained nonlinear systems-a taxonomy theory [power system stability]," *Proceedings of the IEEE*, vol. 83, pp. 1530–1561, Nov 1995.

[18] R. J. Avalos, C. A. Canizares, F. Milano, and A. J. Conejo, "Equivalency of continuation and optimization methods to determine saddle-node and limit-induced bifurcations in power systems," *IEEE Transactions on Circuits and Systems I: Regular Papers*, vol. 56, pp. 210–223, Jan 2009.

[19] Y. Kataoka and Y. Shinoda, "Voltage stability limit of electric power systems with generator reactive power constraints considered," *IEEE Transactions on Power Systems*, vol. 20, pp. 951–962, May 2005.

[20] N. Yorino, H.-Q. Li, and H. Sasaki, "A predictor/corrector scheme for obtaining q-limit points for power flow studies," *IEEE Transactions on Power Systems*, vol. 20, pp. 130–137, Feb 2005.

[21] C. Vournas and M. Karystianos, "Transmission system tap changer settings to maximize loadability margin," in *14th PSCC*, (Seville, Spain), pp. Session 30, Paper 5, Page 1–7, June 2002.

[22] J. Guckenheimer and P. Holmes, *Nonlinear Oscillations, Dynamical Systems, and Bifurcations of Vector Fields*. Springer, 1983.

[23] "Schur complement." URL: `https://en.wikipedia.org/wiki/Schur_complement`, Apr. 2016.

[24] N. Mithulananthan and C. A. Canizares, "Hopf bifurcations and critical mode damping of power systems for different static load models," in *Power Engineering Society General Meeting, 2004. IEEE*, pp. 1877–1882 Vol.2, June 2004.

[25] C. A. Canizares, F. L. Alvarado, C. L. DeMarco, I. Dobson, and W. F. Long, "Point of collapse methods applied to ac/dc power systems," *IEEE Transactions on Power Systems*, vol. 7, pp. 673–683, May 1992.

[26] V. Venkatasubramanian, H. Schättler, and J. Zaborszky, "A taxonomy theory of the dynamics of large power systems with emphasis on its voltage stability," in *in Proc. NSF Int. Workshop on Bulk Power Syst. Voltage Phenomena-II*, pp. 9–52, 1991.

[27] V. Venkatasubramanian, X. Jiang, H. Schättler, and J. Zaborszky, "Current status of the taxonomy theory of large power systems dynamics — dae systems with hard limits," in *Proc. Bulk Power System Voltage Phenomena III — Voltage Stability and Security* (L. H. Fink, ed.), (Fairfax, VA), pp. 15–103, Aug. 1994.

[28] C. A. Canizares, "Calculating optimal system parameters to maximize the distance to saddle-node bifurcations." Online on IEEE Explore, Oct. 2016. URL `http://ieeexplore.ieee.org/document/662696/references?ctx=references` visited 2016-10-19.

[29] C. Cañizares, "Conditions for saddle-node bifurcations in ac/dc power systems," *International Journal of Electrical Power & Energy Systems*, vol. 17, no. 1, pp. 61 – 68, 1995.

[30] Y. V. Makarov, P. Du, S. Lu, T. B. Nguyen, X. Guo, J. W. Burns, J. F. Gronquist, M. a. Pai, and S. Member, "PMU-based wide-area security assessment: Concept, method, and implementation," *IEEE Transactions on Smart Grid*, vol. 3, no. 3, pp. 1325–1332, 2012.

[31] F. L. Alvarado and T. H. Jung, "Direct detection of voltage collapse conditions," in *Proc. Bulk Power System Voltage Phenomena- Voltage Stability and Security, EL-6183, EPRI*, Jan. 1989.

[32] C. A. Canizares and F. L. Alvarado, "Point of collapse and continuation methods for large ac/dc systems," *IEEE Transactions on Power Systems*, vol. 8, pp. 1–8, Feb 1993.

[33] C. A. C. n. A. C. Z. de Souza and V. H. Quintana, "Critical bus and point of collapse determination using tangent vectors," in *Proc. NAPS, M.I.T.*, pp. 329–333, Nov. 1996.

[34] I. Dobson, "Computing a closest bifurcation instability in multidimensional parameter space," *Journal of Nonlinear Science*, vol. 3, no. 1, pp. 307–327, 1993.

[35] GAMS Development Corporation, Washington, DC, USA, *GAMS — The Solver Manuals*, May 2015. URL: `http://www.gams.com/dd/docs/solvers/allsolvers.pdf`.

[36] GAMS, "Solver Descriptions," 2011. `http://www.gams.com/solvers/solvers.htm`.

[37] I. Dobson, L. Lu, and Y. Hu, "A direct method for computing a closest saddle node bifurcation in the load power parameter space of an electric power system," in *Circuits and Systems, 1991., IEEE International Sympoisum on*, pp. 3019–3022 vol.5, Jun 1991.

[38] I. MacGill, "Electricity market design for facilitating the integration of wind energy: Experience and prospects with the australian national electricity market," *Energy Policy*, vol. 38, no. 7, pp. 3180 – 3191, 2010. Large-scale wind power in electricity markets with Regular Papers.

[39] I. Wangensten, *Power System Economics: The Nordic Electricity Market – The Nordic Electricity Market*. Tapir Academic Press, 2007.

[40] "Desciption of balance regulation in the nordic countries," tech. rep., Nordel, 2008.

[41] S. Kraftnät, "Avtal om balansansvar för el.," tech. rep., 2010.

[42] A. J. Wood and B. F. W. ., *Power Generation Operation and Control*. John Wiley & Sons, second edition, 1996.

[43] O. Alsac and B. Stott, "Optimal load flow with steady-state security," *IEEE Transactions on Power Apparatus and Systems*, vol. PAS-93, pp. 745–751, May 1974.

[44] J. C. Smith, S. Beuning, H. Durrwachter, E. Ela, D. Hawkins, B. Kirby, W. Lasher, J. Lowell, K. Porter, K. Schuyler, and P. Sotkiewicz, "The wind at our backs," *IEEE Power and Energy Magazine*, vol. 8, pp. 63–71, Sept 2010.

[45] J. Condren and T. W. Gedra, "Expected-security-cost optimal power flow with small-signal stability constraints," *IEEE Transactions on Power Systems*, vol. 21, pp. 1736–1743, Nov 2006.

[46] J. Condren, T. W. Gedra, and P. Damrongkulkamjorn, "Optimal power flow with expected security costs," *IEEE Transactions on Power Systems*, vol. 21, pp. 541–547, May 2006.

[47] A. Schellenberg, W. Rosehart, and J. Aguado, "Cumulant-based probabilistic optimal power flow (p-opf) with gaussian and gamma distributions," *IEEE Transactions on Power Systems*, vol. 20, pp. 773–781, May 2005.

[48] G. L. Viviani and G. T. Heydt, "Stochastic optimal energy dispatch," *IEEE Transactions on Power Apparatus and Systems*, vol. PAS-100, pp. 3221–3228, July 1981.

[49] H. Zhang and P. Li, "Probabilistic analysis for optimal power flow under uncertainty," *IET Generation, Transmission Distribution*, vol. 4, pp. 553–561, May 2010.

[50] P. Zhang and S. T. Lee, "Probabilistic load flow computation using the method of combined cumulants and gram-charlier expansion," *IEEE Transactions on Power Systems*, vol. 19, pp. 676–682, Feb 2004.

[51] I. Dobson, S. Greene, R. Rajaraman, C. L. DeMarco, F. L. Alvarado, M. Glavic, J. Zhang, and R. Zimmerman, "Electric power transfer capability: Concepts, applications, sensitivity, uncertainty," Tech. Rep. Technical report 01-34, Power Systems Engineering Research Center, Nov. 2001.

[52] A. Schellenberg, W. Rosehart, and J. Aguado, "Cumulant based stochastic optimal power flow (s-opf) for variance optimization," in *IEEE Power Engineering Society General Meeting, 2005*, pp. 473–478 Vol. 1, June 2005.

[53] M. Sobierajski, "Optimal stochastic load flows," *Electric Power Systems Research*, vol. 2, no. 1, pp. 71 – 75, 1979.

[54] T. Yong and R. H. Lasseter, "Stochastic optimal power flow: formulation and solution," in *Power Engineering Society Summer Meeting, 2000. IEEE*, vol. 1, pp. 237–242 vol. 1, 2000.

[55] H. L. Durrwachter and S. K. Looney, "Integration of wind generation into the ercot market," *IEEE Transactions on Sustainable Energy*, vol. 3, pp. 862–867, Oct 2012.

[56] M. M. Begovic and A. G. Phadke, "Control of voltage stability using sensitivity analysis," *IEEE Transactions on Power Systems*, vol. 7, pp. 114–123, Feb 1992.

[57] C. A. Canizares and F. L. Alvarado, "Point of collapse and continuation methods for large ac/dc systems," *IEEE Transactions on Power Systems*, vol. 8, pp. 1–8, Feb 1993.

[58] Y. Mansour, W. Xu, F. Alvarado, and C. Rinzin, "Svc placement using critical modes of voltage instability," in *Power Industry Computer Application Conference, 1993. Conference Proceedings*, pp. 131–137, May 1993.

[59] Z. T. Faur and C. A. C. nizares, "Effect of facts devices on system loadability," in *Proceedings of the North American Power Symposium (NAPS), Bozeman, Montana, USA*, pp. 520–524, Oct. 1995.

[60] C. A. Canizares and Z. T. Faur, "Analysis of svc and tcsc controllers in voltage collapse," *IEEE Transactions on Power Systems*, vol. 14, pp. 158–165, Feb 1999.

[61] K. Zhou, J. Doyle, and K. Glover, *Robust and Optimal Control*. New Jersey: Pretice Hall, 1995.

[62] J. Birge and F. Louveaux, *Introduction to Stochastic Programming*. Berlin: Springer-Verlag, 1997.

[63] L. Abrahamsson, T. Schütte, and S. Östlund, "Use of converters for feeding of AC railways for all frequencies," *Elsevier Energy for Sustainable Development*, vol. 16, no. 3, pp. 368–378, 2012.

[64] N. Biedermann, "Criteria for the voltage in railway power supply systems (original title in Swedish: Kriterier för spänningen i banmatningsnät)," Master's thesis, Royal Institute of Technology (KTH), School of Electrical Engineering, Electrical Energy Conversion (E2C), Jan. 2010. XR-EE-EME 2010:002.

[65] W. Rosehart, C. Roman, and A. Schellenberg, "Optimal power flow with complementarity constraints," *IEEE Transactions on Power Systems*, vol. 20, pp. 813–822, May 2005.

[66] C. Roman and W. Rosehart, "Complementarity model for generator buses in opf-based maximum loading problems," *IEEE Transactions on Power Systems*, vol. 20, pp. 514–516, Feb 2005.

[67] —, "Welcome to the GAMS Home Page!," Jan. 2015. `http://www.gams.com`.

[68] R. E. Rosenthal, "GAMS – A User's Guide," 2007.

[69] B. A. McCarl, A. Meeraus, P. van der Eijk, M. Bussieck, S. Dirkse, P. Steacy, and F. Nelissen, "McCarl GAMS User Guide, Version 23.8," 2012.

[70] M. Perninge, "Approximating the loadability surface in the presence of snb–sll corner points," *Electric Power Systems Research*, vol. 96, pp. 64 – 74, 2013.

[71] M. Perninge, "Approximating the parameter-space stability boundary considering post-contingency corrective controls," *Electric Power Systems Research*, vol. 121, pp. 313 – 324, 2015.

[72] M. Perninge, "Finding points of maximal loadability considering post-contingency corrective controls," *Electric Power Systems Research*, vol. 116, pp. 187 – 200, 2014.

[73] R. D. Zimmerman, C. E. Murillo-Sanchez, and R. J. Thomas, "MATPOWER: Steady-State Operations, Planning, and Analysis Tools for Power Systems Research and Education," *Power Systems, IEEE Transactions on*, vol. 26, no. 1, pp. 12–19, 2011.

[74] L. Abrahamsson and L. Söder, "An SOS2-based moving trains, fixed nodes, railway power system simulator," in *Presented at COMPRAIL 2012*, Sept. 2012.

[75] L. Abrahamsson and L. Söder, "An electro-mechanical moving load railway power systems optimization model," *Transportation Research Part C: Emerging Technologies*, vol. 30, pp. 23–40, May 2013.

[76] J. E. Kolassa and P. McCullagh, "Edgeworth series for lattice distributions," *The Annals of Statistics*, vol. 18, no. 2, pp. 981–985, 1990.

CONSIDERING RISKS IN POWER SYSTEM OPERATION AND THE CONSEQUENCES OF DIFFERENT ACCEPTED RISK LEVELS

Energiforsk is the Swedish Energy Research Centre – an industrially owned body dedicated to meeting the common energy challenges faced by industries, authorities and society. Our vision is to be hub of Swedish energy research and our mission is to make the world of energy smarter!